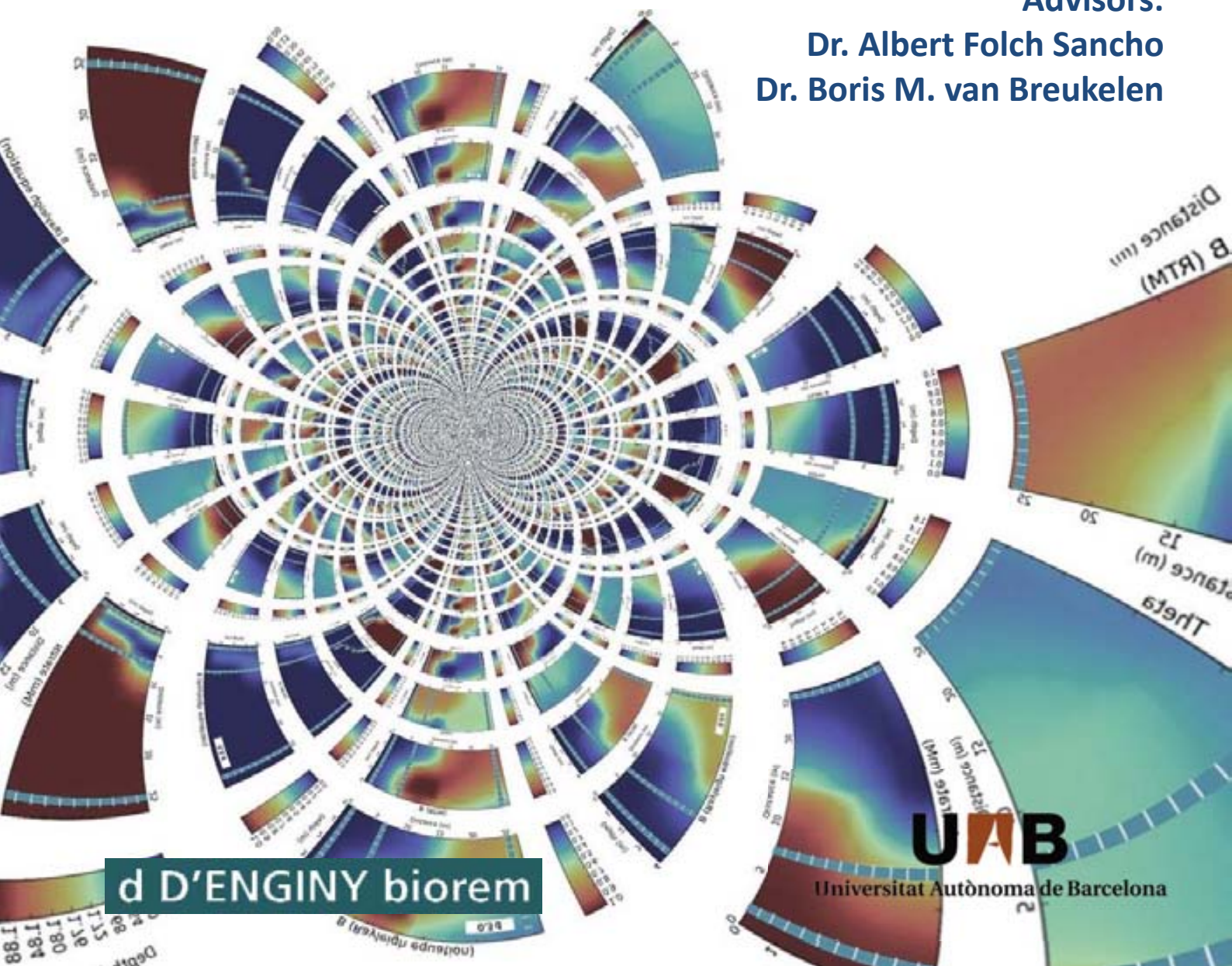# MODELING OF ENHANCED *in situ* BIODENITRIFICATION AT DIFFERENT SCALES:
Integration of microbiological, hydrogeochemical, and isotope biogeochemical processes

Paula F. Rodríguez-Escales

2014

Advisors:
Dr. Albert Folch Sancho
Dr. Boris M. van Breukelen

d D'ENGINY biorem

UAB
Universitat Autònoma de Barcelona

Modeling of Enhanced *in situ* Biodenitrification at different scales: Integration of microbiological, hydrogeochemical, and isotope biogeochemical processes

Thesis presented by:

Paula F. Rodríguez-Escales

Paula F. Rodríguez-Escales

Dr. Albert Folch
Institut de Ciència i Tecnologia Ambiental
Universitat Autònoma de Barcelona

Departament d'Enginyeria del Terreny
Universitat Politècnica de Catalunya

Dr. Boris M. van Breukelen
Department of Earth Sciences
Faculty of Earth and Life Sciences
VU University Amsterdam

Barcelona, July 2014

d D'ENGINY biorem

UAB
Universitat Autònoma de Barcelona

icta

AGRAÏMENTS

Amb aquestes línies vull donar les gràcies a tota la gent que ha confiat en mi, m'ha ajudat i m'ha acompanyat durant el doctorat. Com que he estat per aquí i per allí, aquestes línies van dedicades a força gent. A tots, moltes gràcies!

En primer lloc, moltes gràcies als meus directors: Dr. Albert Folch i Dr. Boris van Breukelen per haver-me dirigit la tesi. Albert, moltes gràcies per haver-me ajudat sempre que ho he necessitat, per confiar en mi, per donar-me la llibertat per decidir, per estar sempre disposat, per les discussions científiques, per haver-me endinsat en el món científic, per haver sabut lidiar amb la meva tossuderia... En definitiva, moltes gràcies per haver-me acompanyat durant tot el procés, ha estat un plaer. Thanks Boris for accepting my short stay in your research group and after for the co-supervision of my thesis. Also thanks for your thoroughness in corrections, I have learnt a lot with you!

Gràcies també a la Dra. Georgina Vidal-Gavilan i a d'ENGINY biorem. Georgina, moltes gràcies per confiar en mi per dur a terme la modelització dels processos de desnitrificació, per recolzar-me, per passar-me les dades dels experiments, per ensenyar-me que si les coses estan endreçades tot va millor i per endinsar-me en el món professional. També moltes gràcies a l'Eugènia i a la Caterina per acollir-me a d'ENGINY biorem.

Moltes gràcies al Dr. Albert Soler de la Universitat de Barcelona. Gràcies per acollir-me a MAIMA i per haver estat sempre disposat a donar un cop de mà i a resoldre qualsevol dubte que tingués amb els isòtops o amb qualsevol altra cosa i pels bons consells donats. Moltes gràcies també al Dr. Xavier Sánchez-Vila. Gràcies Xavi, per acollir-me al Grup d'Hidrogeologia Subterrània de la UPC, per interessar-te per la meva feina i per l'empenta final del darrer capítol. Si al principi de la meva tesi, algú m'hagués dit que acabaria parlant de transport no-Fickià amb tu, l'hagués pres per boig.

Moltes gràcies també a la Dra. Teresa Vicent del Departament d'Enginyeria Química de la Universitat Autònoma de Barcelona. Tot i no haver estat fent recerca colze a colze amb tu, sempre t'he tingut present.

A tot el grup de recerca de MAiMA. A la Dra. Neus Otero, que sempre que l'he necessitat s'ha ofert a donar-me un cop de mà o a discutir qualsevol cosa. A la Dra. Mònica Rosell amb qui he discutit la relació entre els isòtops i les rutes metabòliques i sempre ha estat disposada a donar un cop de mà amb un somriure, i a la Dra. Cristina Domènech que m'ha aclarit dubtes geoquímics. Un especial agraïment a la Dra. Clara Torrentó, per estar allí. A tot el grup de MAiMA, als recents doctors: al Raul, vam tenir grans moments al despatx; a la Carme, el teu romanticisme sempre m'aixeca un somriure; i al Roger amb qui també m'ho vaig passar molt bé compartint despatx! També moltes gràcies a la resta de membres, Alba i Diana (ara teniu el pes del relleu), Manuela, Àngels i Mercè i als satèl·lits com la Marta.

A tot el grup de recerca d'Hidrogeologia Subterrània de la UPC-CSIC. En especial, moltes gràcies al Dr. Dani Fernàndez per tots els dubtes resolts, sobretot en aquesta darrera etapa. Encara estaria modelitzant si no m'haguessis ajudat a exportar el arxius de PHT3D. Un altre especial agraïment al Dr. Carles Ayora amb qui he discutit diversos punts d'aquesta tesi, moltes gràcies pel temps i per l'interès mostrat en la meva recerca. Moltes gràcies també al Dr. Maarten Saaltink per estar disposat a respondre'm qualsevol dubte. També a la Tere per tots els tràmits. Moltes gràcies als companys i membres del grup: Albert, Genís, Carme C., Núria, Carme B., Joel, Sandra. I a tota la resta, també!

Un altre agraïment al Dr. Josep Mas-Pla, de la Universitat de Girona.

Thanks to people from Department of Earth Science of Vrije University of Amsterdam, specially to Dr. Maarten Waterloo (I greatly appreciated your warm hospitality), Stefanie, Philip, Jun and also to the others!

Gràcies al Dr. Joan Bach i al Dr. David Gómez, cap de la Unitat de Geodinàmica Externa i d'Hidrogeologia i cap del Departament de Geologia de la Universitat Autònoma de Barcelona, respectivament. També faig extensos els meus agraïments a tota la gent de l'Institut de Ciència i Tecnologia Ambiental de la Universitat Autònoma de Barcelona.

Gràcies, també, al Felip Ortuño i al Josep Fraile de l'Agència Catalana de l'Aigua.

Moltíssimes gràcies als meus amics i membres de Greenhub, per estar al meu costat, per ajudar-me quan ho he necessitat i per ser comprensius amb la tesi. Una abraçada

molt forta i sentida per a tots vosaltres.

Moltes gràcies a la meva família i a la meva parella, que m'han fet sentir especialment estimada en aquestes darreres setmanes. Va per vosaltres!

ABSTRACT

The presence of nitrate in groundwater is a worldwide problem. Intensive farming and agricultural activities that include high levels of fertilizer application and animal waste disposal are the major causes of such pollution in rural areas. Excessive nitrates and nitrites consumed with drinking water increase the risk of methemoglobinemia and stomach cancer. Consequently, a maximum drinking water nitrate concentration has been set up within the European Union of 50 mg/l. In Catalonia, 30% of the territory is polluted by nitrates, and approximately 12% of the groundwater is affected. High nitrate concentrations have decreased the availability of water for domestic uses, and many water supply wells have been abandoned as a consequence. Due to its minimal cost, the most common solution to nitrate pollution has been to mix polluted and clean groundwater. Nevertheless, this solution is highly limited by water scarcity in Mediterranean and/or (semi-)arid countries, and conditions are expected to worsen due to climate change. In this context, it is necessary to implement other solutions to improve groundwater quality.

Enhanced *in situ* biodenitrification (EIB) is a feasible technology for remediation of nitrate-polluted groundwater. The EIB process creates optimized conditions via the addition of an organic carbon source and by controlling/monitoring other environmental parameters (e.g., oxidant concentrations, pH, micro-nutrients). Similar to all *in situ* technologies, EIB interacts with other hydrogeochemical processes in the aquifer. In this way, precipitation or dissolution of carbonates can be induced leading to porosity changes. Moreover, the inclusion of stable isotopes can improve monitoring of EIB. In this context, a reactive transport model (RTM) that integrates all these processes offers a useful tool for planning, managing, monitoring, and optimizing this technology.

In this thesis, an integrated reactive transport model has therefore been developed that takes into account microbiology, geochemistry, and isotope geochemistry.

The first section of the thesis (Chapter 2) addresses the development of an isotope biogeochemical model. The goal of this chapter is the setup of the conceptual relationships among microbiology, geochemistry, and isotope geochemistry (δ^{15}N-NO_3^-, δ^{18}O-NO_3^-, δ^{13}C-DIC) during Enhanced *in situ* Biodenitrification. Thus, one of the most complete biogeochemical models in the literature of EIB has been developed. The model was validated with a batch-scale biodenitrification experiment using groundwater and sediment from a Roda de Ter (Osona, Spain) site and two different external organic carbon sources, i.e., ethanol and glucose. In both cases, the model fitted notably well the experimental data. Moreover, the developed model also incorporated the nitrite accumulation observed in the glucose experiment. Consideration of the water-rock interaction in the model determined that if ethanol is used as an organic carbon source, carbonate mineral precipitation is induced, whereas if glucose is used, carbonate mineral dissolution is observed. Moreover, nitrate isotope incorporation facilitated the determination of the extent of denitrification at the field scale. Finally, the incorporation of the carbon isotope reaction network in the model was another tool used to verify the full consistence of the model due to the central role of inorganic carbon in biodenitrification and water-rock interactions. Moreover, modeling of carbon isotope flow showed that both ethanol and glucose were inversely fractionated during EIB.

After model development and calibration to lab experimental data, the model was applied to an Enhanced *in situ* Biodenitrification application in a fractured aquifer (also Roda de Ter (Spain)). The main goal of this chapter was to extend the biogeochemical model with the simulation of groundwater flow and to validate it under complex hydrogeological conditions. It was observed that certain model parameter values from the batch experiment were applicable for field conditions (maximum consumption rate of electron donor (k_{max})) and that the other parameters (half-saturation constants (K_s) and the decay constant (b)) should be adapted, but the changes involved less than one order of magnitude. Moreover, the induced calcite precipitation caused a change of porosity of less than 3%. As a secondary goal, the use of the Rayleigh equation to determine the extent of EIB was also verified from a practical perspective. The model demonstrated that the Rayleigh equation underestimated the percentage of degradation by approximately 60-80% and increasingly at the fringes of the injection plume.

Chapter 4 focuses on modeling EIB under different injection conditions and with the formation of biofilm growth. This chapter evaluates how different feeding strategies modify the hydraulic properties of the media. It was observed in column experiments

that a weekly feeding strategy did not modify the hydraulic properties of the media, whereas daily feeding significantly enhanced the dispersivity. These changes in dispersivity implied an increase in heterogeneity and the consequent change of the conceptual model from normal to non-Fickian anomalous solute transport. This transition was well characterized using a single-rate mass transfer model. Moreover, a long-term model demonstrated that reducing the C:N ratio allowed for the optimization of ethanol injection into the system and avoided its spillage through the column outlet. Nevertheless, the results of the modelled biomass showed that these strategies were not sustainable in time because biomass was completely depleted.

Overall, the elaboration of this thesis has contributed to the knowledge of all processes involved in Enhanced *in situ* Biodenitrification and their quantification using numerical models. The developed model can allow improvement in the design, planning, monitoring and optimization of this technology at the field scale.

RESUM

La presència de nitrats a les aigües subterrànies és un dels problemes ambientals més greus a tot el món. L'ús excessiu de fertilitzants agraris, l'abocament de purins al territori i el mal manteniment de les xarxes de clavegueram són les causes més comunes de contaminació d'aigües subterrànies per nitrats. El consum de nitrats per sobre del llindar legislatiu (50 mg/l) de manera habitual pot augmentar la incidència en metahemoglobinèmia (o síndrome del nen blau) i en càncer d'estómac. A Catalunya, es quantifica que un 30% del territori i un 12% de les aigües subterrànies estan afectats per la contaminació per nitrats, la qual cosa en limita l'ús. A més a més, l'aigua als països mediterranis és un recurs limitat i es preveu que amb el canvi climàtic ho sigui més. És per aquest motiu que es requereixen solucions que siguin capaces d'eliminar els nitrats de les aigües subterrànies i retornar-los així llur qualitat.

En aquest context, sorgeix la Desnitrificació *in situ* Induïda (de l'anglès, *Enhanced in situ Biodenitrification*, d'ara endavant EIB). Aquesta tecnologia es basa en eliminar el nitrat estimulant els microorganismes desnitrificants de l'aqüífer que utilitzen el nitrat com a acceptor d'electrons dins del seu metabolisme en condicions anòxiques. Per tal d'accelerar el procés, l'EIB crea les condicions òptimes per al creixement d'aquests microorganismes afegint un donador d'electrons i controlant els paràmetres ambientals. Com en tota tecnologia *in situ*, els processos induïts per l'EIB influeixen a la geoquímica de l'aqüífer. En aquest sentit, poden induir precipitacions/dissolucions de carbonats. A més a més, l'ús dels isòtops estables com a eina de monitorització del procés, facilita llur gestió. L'obtenció d'un model de transport reactiu (de l'anglès *Reactive Transport Model*, d'ara endavant RTM) que permeti la predicció del comportament dels compostos que intervenen en l'EIB així com la interrelació entre els diferents processos (microbiològics, geoquímics i isotòpics) permetrà facilitar la implementació, la gestió, la monitorització i l'optimització d'aquesta tecnologia al territori.

En aquesta tesi s'ha desenvolupat un model de transport reactiu que integra tots els processos principals i secundaris que afecten la desnitrificació *in situ* induïda a diferents escales de treball. Així, l'eina obtinguda relaciona els processos biològics induïts quan s'afegeix un donador d'electrons a l'aqüífer amb els processos geoquímics (interacció aigua-roca) i la geoquímica dels isòtops.

A la primera part de la tesi (Capítol 2) és on s'ha desenvolupat el model conceptual i on s'han establert les relacions que existeixen entre la microbiologia i la geoquímica prèvia de l'aqüífer a escala de *batch.* D'altra banda, també s'ha desenvolupat el model conceptual de tota la geoquímica isotòpica associada al procés ($\delta^{15}N\text{-}NO_3^-$; $\delta^{18}O\text{-}NO_3^-$ i $\delta^{13}C\text{-}DIC$ incorporant tota la geoquímica del $\delta^{13}C$). En aquest sentit, s'ha desenvolupat un dels models biogeoquímics més complets de la literatura relacionats amb la desnitrificació *in situ* induïda. El model s'ha calibrat emprant dos experiments a escala de *batch* realitzats amb etanol i glucosa com a fonts de carboni externa. En tots dos casos, s'han obtingut molt bons ajustos amb les dades experimentals. A més, el model també incorpora l'acumulació de nitrit en el cas de l'experiment de la glucosa. L'avaluació dels processos geoquímics induïts per l'EIB ha posat de manifest que en funció de la font de carboni s'indueixen processos de precipitació (en el cas de l'etanol) i processos de dissolució de carbonats (en el cas de la glucosa). Aquests dos processos poden alterar la velocitat de l'aigua i crear importants problemes operacionals durant l'EIB. També s'han incorporat els processos de fraccionament isotòpic del nitrat millorant l'avaluació de l'abast de la desnitrificació en els models a escala de camp. Finalment, el model desenvolupat incorpora tota la geoquímica dels isòtops associats al cicle del carboni dins de la desnitrificació. Els paràmetres obtinguts posen de manifest que va existir un fraccionament invers de l'etanol.

Un cop elaborat el model biogeoquímic que estableix el model conceptual que quantifica les interaccions entre els diferents processos que hi intervenen, el model s'ha escalat a un cas de desnitrificació induïda a escala de camp en un aqüífer fracturat (Roda de Ter (Osona, Espanya)). En aquest apartat de la tesi (Capítol 3), s'ha perseguit avaluar quin era l'impacte del canvi d'escala en els paràmetres biogeoquímics. A més a més, també s'ha determinat el canvi de porositat induïda per la precipitació de calcita. Finalment, la incorporació dels isòtops al RTM ha permès comparar qualitativament i quantitativament l'extensió dels processos de desnitrificació calculats pel RTM i per l'equació de Rayleigh. Els resultats demostren que l'equació de Rayleigh descriu bé, en termes qualitatius, l'extensió de la desnitrificació, però en general la subestima entre un 60 i un 80%.

Finalment, un cop avaluada l'aplicabilitat del model tant a escala de *batch* com a l'escala de camp, s'ha desenvolupat un model que reprodueix diferents escenaris d'injeccions de carboni orgànic en un experiment de columna de llarga durada considerant els canvis sobre les propietats hidràuliques produïts pel creixement microbià. Així, s'ha determinat que el creixement del biofilm va augmentar set cops la dispersivitat, augmentant, per tant, la heterogeneïtat del sistema i, conseqüentment, es va produir un canvi del model conceptual del flux i del transport del transport normal al transport no-Fickià. Aquesta transició es va caracteritzar emprant un model de transferència simple de massa. A més a més, el model de llarga durada ha permès determinar que freqüències d'injecció més espaiades en el temps produeixen un impacte menor en les propietats hidràuliques del medi. A més a més, les estratègies d'injecció amb la relació Carboni:Nitrogen per sota de l'estequiomètrica es poden emprar per a minimitzar el risc de *bioclogging* mantenint les taxes de degradació, sempre i quan hi hagi una població important de microorganismes.

En aquesta tesi s'ha desenvolupat un model que integra tots els processos relacionats amb l'EIB. Aquest model ha estat validat a diferents escales de treball. El model desenvolupat millora amb escreix els prèviament existents de la literatura i facilitarà l'àmplia implementació de l'EIB pel territori tot millorant-ne la seva gestió, planificació, monitorització i optimització.

RESUMEN

La presencia de nitratos en las aguas subterráneas es uno de los problemas ambientales más graves de todo el mundo. El uso excesivo de fertilizantes agrarios, el vertido de purines en el territorio y el mal mantenimiento de las redes de alcantarillado son las causas más comunes de contaminación de aguas subterráneas por nitratos. El consumo de nitratos de manera habitual por encima del umbral legislativo (50 mg/l) puede aumentar la incidencia en metahemoglobinemia (o síndrome del niño azul) y en cáncer de estómago. En Cataluña, se cuantifica que un 30% del territorio y un 12% de las aguas subterráneas están afectados por nitratos, limitando el uso de las aguas. Además, en los países mediterráneos el agua es un recurso limitado y se prevé que, con la llegada del cambio climático, lo sea más. Es por este motivo que se requieren soluciones de emergencia que sean capaces de eliminar los nitratos de las aguas subterráneas y devolverlas a su calidad.

En este contexto, surge la Desnitrificación *in situ* Inducida (del inglés, *Enhanced in situ Biodenitrification*, en adelante EIB). Esta tecnología se basa en la eliminación del nitrato estimulando los microorganismos denitrificantes del acuífero que utilizan el nitrato como aceptor de electrones dentro de su metabolismo en condiciones anóxicas. Para acelerar el proceso, la EIB crea las condiciones óptimas para el crecimiento de estos microorganismos añadiendo un donador de electrones y controlando los parámetros ambientales. Como toda tecnología *in situ*, los procesos inducidos por la EIB coexisten con la geoquímica previa del acuífero. En este sentido, inducen precipitaciones/disoluciones de carbonatos. Además, el uso de los isótopos estables como herramienta de monitorización del proceso, facilita su gestión. La obtención de un modelo de transporte reactivo (del inglés *Reactive Transporte Models*, en adelante RTM) que permita la predicción del comportamiento de los compuestos que intervienen en la EIB así como la interrelación entre los diferentes

procesos (microbiológicos, geoquímicos e isotópicos) permitirá facilitar la implementación, la gestión, la monitorización y la optimización de esta tecnología por el territorio.

En esta tesis se ha desarrollado un modelo de transporte reactivo que integra todos los procesos principales y secundarios que afectan a la desnitrificación *in situ* inducida a distintas escalas de trabajo. Así, la herramienta obtenida relaciona los procesos biológicos inducidos cuando se añade un donador de electrones en el acuífero con los procesos geoquímicos (interacción agua-roca) y la geoquímica de los isótopos.

En la primera parte de la tesis (Capítulo 2) es donde se ha desarrollado el modelo conceptual y donde se han establecido las relaciones que existen entre la microbiología y la geoquímica previa del acuífero a escala de *batch*. Por otra parte, también se ha desarrollado el modelo conceptual de toda la geoquímica isotópica asociada al proceso (δ^{15}N-NO$_3^-$; δ^{18}O-NO$_3^-$ y δ^{13}C-DIC incorporando toda la geoquímica de δ^{13}C). En este sentido, se ha desarrollado uno de los modelos biogeoquímicos más completos de la literatura relacionados con la desnitrificación *in situ* inducida. El modelo se ha validado empleando dos experimentos a escala de *batch* realizados con etanol y glucosa como fuentes de carbono externa. En ambos casos, se han obtenido muy buenos ajustes con los datos experimentales. Además, el modelo también incorpora la acumulación de nitrito en el caso del experimento de la glucosa. La evaluación de los procesos geoquímicos inducidos por la EIB ha demostrado que en función de la fuente de carbono se inducen procesos de precipitación (en el caso del etanol) y procesos de disolución de carbonatos (en el caso de la glucosa). Estos dos procesos pueden alterar la velocidad del agua y crear importantes problemas operacionales durante la implementación de la tecnología. Además, la incorporación de los procesos de fraccionamiento isotópico del nitrato permite la evaluación del alcance de la desnitrificación en los modelos a escala de campo. Finalmente, el modelo desarrollado incorpora toda la geoquímica de los isótopos asociados al ciclo del carbono dentro de la desnitrificación. Los parámetros obtenidos demuestran que existió un fraccionamiento inverso del etanol.

Una vez elaborado el modelo biogeoquímico que establece todas las relaciones conceptuales, el modelo se ha escalado a un caso de desnitrificación inducida a escala de campo en un acuífero fracturado (en el emplazamiento de Roda de Ter (Osona, España). En este apartado de la tesis (Capítulo 3), se ha evaluado cuál era el impacto del cambio de escala en los parámetros biogeoquímicos. Además, también se ha determinado el cambio de porosidad inducida por la precipitación de calcita.

Finalmente, la incorporación de los isótopos en el RTM ha permitido comparar cualitativamente y cuantitativamente la extensión de los procesos de desnitrificación calculados por RTM y por la ecuación de Rayleigh. Los resultados demuestran que la ecuación de Rayleigh describe bien, en términos cualitativos, la extensión de la desnitrificación pero en general la subestima entre un 60 i un 80%.

Una vez evaluada la aplicabilidad del modelo tanto a escala de *batch* como la escala de campo, se ha desarrollado un modelo que reproduce diferentes escenarios de inyecciones de carbono orgánico en un experimento de columna de larga duración. El objetivo de este capítulo (Capítulo 4) ha sido desarrollar un modelo que permita optimizar las inyecciones de carbono orgánico: minimizando el uso de carbono orgánico y el riesgo de *bioclogging*. En este capítulo se determinó que el crecimiento del biofilm produce un cambio del modelo conceptual del transporte reactivo y modifica el transporte de normal a no-Fickiano. El modelo ha demostrado que frecuencias de inyección más espaciadas en el tiempo producen un impacto menor en las propiedades hidráulicas del medio. Además, las estrategias de inyección con la relación Carbono:Nitrógeno por debajo de la estequiometria pueden ser una buena solución para minimizar el riesgo de *bioclogging;* siempre y cuando haya una población importante de microorganismos previa.

En esta tesis se ha desarrollado un modelo que integra todos los procesos relacionados con el EIB. Este modelo ha sido validado en diferentes escalas de trabajo. El modelo desarrollado mejora creces los de la literatura y facilitará la amplia implementación de la EIB por el territorio, mejorando su gestión, planificación, monitorización y optimización.

CONTENTS

LIST OF FIGURES

LIST OF TABLES

CHAPTER 1

Introduction

Increasing world population has resulted in higher food and energy demands and consumption over the past half century (UN, 1996). Human activities have greatly accelerated and enlarged the natural cycles of nutrients in the soil, water, and atmosphere. One of the most important nutrients in this context is nitrogen. However, although this element is an essential nutrient that plays important roles in increasing crop yields and quality, it is also a major pollutant in aquatic systems (Baker, 2003; Oenema et al., 1998; Schepers et al., 1995). Excess nitrogen from fertilization has disturbed the biogeochemical nitrogen cycle of natural ecosystems, resulting in water quality degradation associated with nitrate leaching from agricultural soils (Galloway, 1998; Galloway, 2000; Galloway et al., 1995). Another consequence of the increasing world population has resulted in large population concentrations in cities. For the first time in history, more than half of all human beings live in cities (UN, 2004). Wastewater disposal and poor maintenance of septic tanks and sewage systems (MacQuarrie et al., 2001) also drive nitrate pollution of groundwater after reduced nitrogen compounds are oxidized (Wakida and Lerner, 2005). These two main reasons have resulted in nitrates becoming one of the most common chemical contaminants in the world's groundwater aquifers (Figure 1.1A)

(European Environment Agency, 2007; Organisation for Economic Co-operation and Development, 2008; Spalding and Exner, 1993).

From a human health perspective, excessive nitrates and nitrites consumed with drinking water (nitrate is converted to nitrite in the human body) increase the risk of methemoglobinemia (H Bosch et al., 1950; Walton, 1951). Related to carcinogenic risk, nitrate and nitrite are listed in Group 2A of the IARC list (WHO, 2010). Certain authors even note that nitrogen compounds can act as human stomach cancer promoters (Volkmer et al., 2005; Ward et al., 2005). Moreover, nitrate has an impact on the environment by contributing to the eutrophication of surface water bodies (Rivett et al., 2008). Consequently, maximum drinking nitrate and nitrite concentrations in water have been established: 50 mg/l for nitrate and 0.1 mg/l for nitrite within the European Union and 10 mg/l for nitrate (measured as nitrogen) and 1 mg/l for nitrite (measured as nitrogen) within the USA.

The severity of the nitrate problem is illustrated by European Environment Agency (EEA) data on groundwater nitrate concentrations across the European Union (Figure 1.1B) (European Environment Agency, 2007). The proportion of groundwater bodies with a high risk for nitrate pollution (with a mean nitrate concentration above 25 mg/l) was reported as 80% in Spain, 50% in the UK, 36% in Germany, 34% in France, and 32% in Italy.

The aquifers most polluted by nitrate in Spain lie along the Mediterranean coast, especially in the Maresme and Osona regions (Barcelona), in the large plains of Castelló, and in the Andalucia region. Significant pollution is also found in the archipelago of Canarias, where nitrate concentrations exceed 100 mg/l. Inland, in the plain of Castilla la Mancha, the alluvial aquifer of the Ebro river and certain areas of the Guadalquivir valley are the most affected by nitrate pollution, and nitrate concentrations range from 50 mg/l to 100 mg/l (IGME, 2009).

The occurrence of nitrate is also the most important groundwater pollution problem in Catalonia (Figure 1.1C). A total of 17 out of 53 groundwater bodies are classified as "at risk" of not meeting the good quality status in 2015 required by the Water Directive Framework (Directive 2000/60) due to nitrate pollution (ACA, 2007). According to the Health Department of the Catalan Government, 7% of the groundwater supply wells in Catalonia have nitrate contents above 50 mg/l and primarily affect small municipalities.

Various regulations have been developed to minimize this problem within the European Union. The most important regulations are the Nitrate Directives (Directive 1991/676 and Directive 1998/83), which aim to identify zones vulnerable to nitrate pollution (Figure 1.1B) and to protect water quality across Europe. These directives are also intended to prevent nitrates from agricultural sources from polluting ground- and surface water and to promote the use of good farming practices. The transposition of the European Directive to Spanish (Real Decreto 261/1996) and the Catalan Legislation (Decret 283/1998, Decret 476/2004, and Acord GOV/128/2009) has allowed the determination of zones vulnerable to nitrate pollution and the establishment of codes of good agricultural practices (Figure 1.1C). Nevertheless, these good practices do not appear to be sufficient, and nitrate pollution is still the most important problem in Spanish and Catalan groundwater.
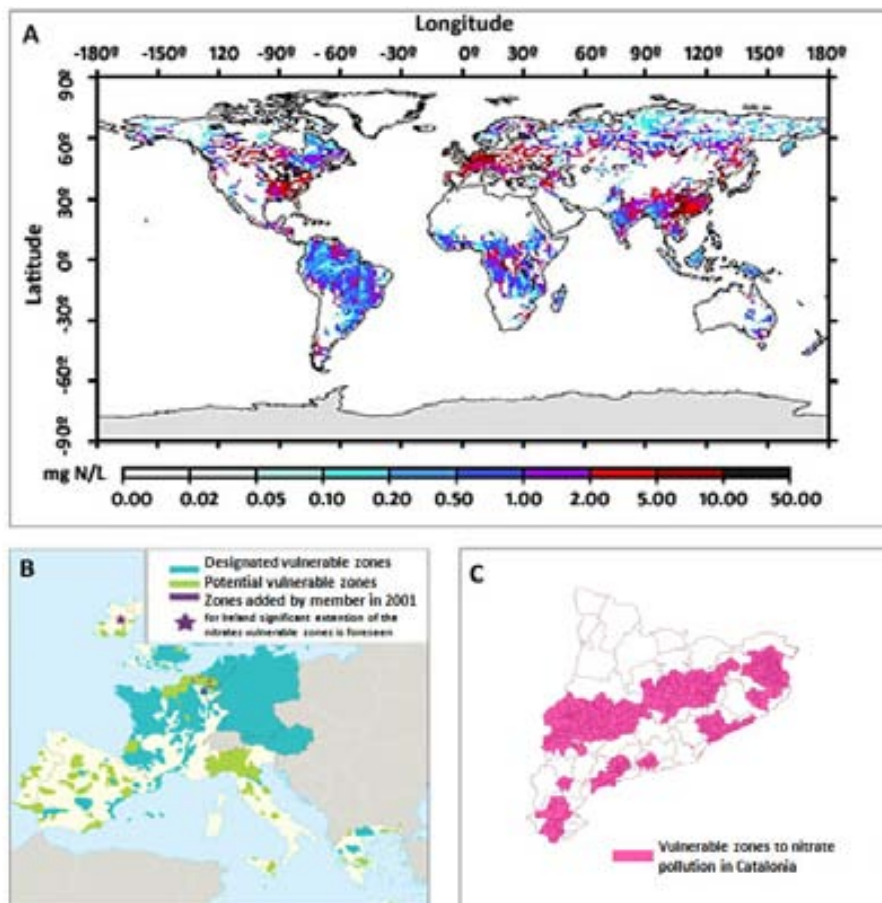
Figure 1.1 A) Presence of nitrate in rivers (modified from He et al. (2011)); B) Nitrate vulnerable zones in the European Union (except for Scandinavian countries) (map from United Nations Environment Programme); C) Map of zones vulnerable to nitrate pollution in Catalonia.

Consequently, many water supply wells have been closed, and due to its minimal cost, the most common solution has been to mix nitrate-polluted groundwater with clean drinking water. Nevertheless, this solution is limited by water scarcity in Mediterranean and/or dry countries, a situation that is expected to worsen due to climate change (IPCC, 2007). Even in countries with no water shortage problems, there is often no source of clean water with which to mix and dilute high-nitrate groundwater (Stuart et al., 2011; Veraart et al., 2014). In this context, it is necessary to implement other solutions that allow supply of groundwater and recovery of its quality.

1.1   Technologies available

Different technologies are available for treating nitrate in groundwater and can be divided between physical treatments (i.e., ion exchange, electrodialysis, and reverse osmosis) and biological treatment, (i.e., biological denitrification) (McAdam and Judd, 2007; Ricardo et al., 2012; Schnobrich et al., 2007).

Ion exchange is the most common physical technology (Richard, 1989; Shahbazi et al., 2010) and involves the exchange of ions in solution with a chemically equivalent number of ions associated with the exchange material (i.e., resin). The mechanism involved is typically the replacement of these ions with chloride ions as groundwater passes through the resin. The ion-exchange process for the replacement of nitrate uses either a strongly basic or weakly basic anion exchanger. Membrane separation techniques in nitrate treatment, such as electrodialysis (Elmidaoui et al., 2003; Hell et al., 1998; Menkouchi Sahli et al., 2006) and reverse osmosis (e.g., (Bohdziewicz et al., 1999; Schoeman and Steyn, 2003), can be used for nitrate removal but are up to eight times more expensive to operate than ion exchange processes and are not selective for nitrate ion removal (Reddy and Lin, 2000). The principle of electrodialysis is the removal of ionic components from aqueous solutions through ion exchange membranes using the driving force of an electric field. The water to be treated is pumped through a membrane stack, which consists of alternately placed anionic and cationic selective membranes. Separated by gasket framers and spacers, the membranes are fixed between two plates, which contain the electrodes that produce the electric field. Reverse osmosis is based on forcing water flow through a semi-permeable membrane under pressure such that water passes through and the contaminants are impeded by the membrane.

Most of these technologies are focused on *ex situ* treatments, which are inherently more expensive than *in situ* treatments due to energy consumption and the interference with surface activity and land uses (construction of a treatment plant) (Della Rocca et al., 2007).

However, biological denitrification uses the reduction of nitrate-enhancing microorganisms that use nitrate as an electron acceptor under anoxic conditions. This technology has been used in both *ex situ* and *in situ* conditions (Khan and Spalding, 2004; Richard, 1989; Vidal-Gavilan et al., 2013). Biological *in situ* biodenitrification, known as Enhanced *in situ* Biodenitrification (EIB), exhibits an environmental and economic advantage over the other methods because it is simple, selective for nitrate, and cost effective (Smith et al., 2001).

Finally, a new technology that combines biological reduction with electrochemical systems is under development (Tong and He, 2013; Zhang and Angelidaki, 2013). Nevertheless, at this moment, field implementation is not proven, and the combined method remains the subject of additional basic research.

1.2 Enhanced *in situ* Biodenitrification

Biodenitrification is the reduction of nitrate to dinitrogen gas via anaerobic facultative bacteria that use nitrate as an electron acceptor. This redox process can be promoted by heterotrophic or autotrophic bacteria. The first type uses organic carbon as an electron donor (Reaction 1.1), whereas the second uses inorganic compounds as an electron donor (e.g., FeS_2, H_2) (Beller, 2005; Straub et al., 1996; Zumft, 1997) (Reaction 1.2 and 1.3).

$$5CH_2O + 4NO_3^- \rightarrow 2N_2 + 5HCO_3^- + 1H^+ + 2H_2O \qquad \text{(Reaction 1.1)}$$

$$5FeS_2 + 14\ NO_3^- + 4H^+ \rightarrow 7N_2 + 10SO_4^{2-} + 5Fe^{+2} + 2H_2O \qquad \text{(Reaction 1.2)}$$

$$5H_2 + 2\ NO_3^- + 2H^+ \rightarrow N_2 + 6H_2O \qquad \text{(Reaction 1.3)}$$
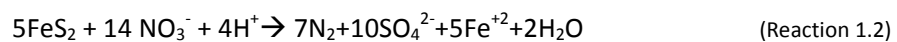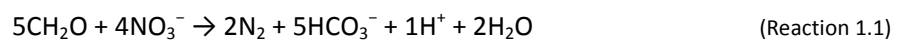
The nitrogen of nitrate is increasingly reduced, eventually arriving at harmless dinitrogen gas (Reaction 1.4). However, if optimal conditions do not exist (e.g., inadequate supply of the electron donor or the presence of oxygen), intermediate nitrogen compounds can temporally accumulate. Nitrite is significantly more toxic than nitrate, and this toxicity is reflected in its considerably lower standard of 0.1 mg/l

(Fan and Steinberg, 1996). Moreover, $NO_{(g)}$ and $N_2O_{(g)}$ accumulation should also be avoided because they are considered greenhouse gases.

$$NO_3^- \rightarrow NO_2^- \rightarrow NO_{(g)} \rightarrow N_2O_{(g)} \rightarrow N_{2(g)}$$ (Reaction 1.4)
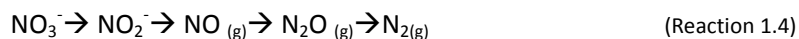
Aquifers vary widely in their denitrifying capacities, but biodenitrification appears to be possible anywhere bacteria thrive, electron donors are present, and oxygen levels are low (Korom, 1992). Nevertheless, under natural aquifer conditions, a major limiting factor for biodenitrification to occur is the lack of electron donors to provide energy to microorganisms. To solve this problem, Enhanced *in situ* Biodenitrification (EIB) creates optimized conditions through the addition of an electron donor to the aquifer and by controlling/monitoring other environmental parameters (e.g., oxidant concentrations, pH, micro-nutrients).

For successful biodenitrification, the aquifer environmental parameters must be controlled. Denitrification is thermodynamically less favorable than the reduction of dissolved oxygen, and therefore, oxygen will be preferred over nitrate as an electron acceptor. Denitrification will occur when the dissolved oxygen concentrations are less than 1-2 mg/l (Cey et al., 1999; Korom, 1992). Denitrifiers are not particularly pH sensitive, exhibiting an optimal pH range between 5.5 and 8.0 (Rust et al., 2000). The metabolic requirements for nitrogen can be met through the direct assimilation of nitrate (Rittmann and McCarty, 2001; Rivett et al., 2008). This process also requires phosphorous, sulfur, and other micronutrients (i.e., B, Cu, Fe, Mn, Mo, Zn, and Co) for effective metabolism. Most groundwater contains these necessary elements at concentrations adequate for supporting microbial growth (Champ et al., 1979). However, phosphorus availability can be a limiting factor (Rivett et al., 2008) due to its low mobility in groundwater; therefore, it is sometimes added as an external nutrient in EIB (Vidal-Gavilan et al., 2013; Zhang et al., 2014).

The EIB method can be focused on both heterotrophic and autotrophic metabolisms. Most of the current experience is centered on heterotrophic bacteria because nitrate reduction rates are higher than in autotrophic biodenitrification (Torrentó et al., 2011). Nevertheless, this high rate facilitates the risk of clogging due to excessive growth of biofilms (bioclogging) and potential dinitrogen gas accumulation (Soares et al., 1989), which can imply post-treatment disinfection. Bioclogging results in changes in soil hydraulic properties such as porosity, hydraulic conductivity, and dispersivity (Taylor and Jaffé, 1990; Taylor et al., 1990; Thullner et al., 2008) and is considered as one of the most important problems in all bioremediation applications (Dupin and McCarty, 2000). Moreover, if the optimal conditions do not exist for denitrification,

nitrite can accumulate. These two important disadvantages (risk of bioclogging and nitrite accumulation) are minimized in autotrophic biodenitrification (Torrentó et al., 2011). Nevertheless, hydrogen safety concerns (due to the high inflammability of hydrogen) in the case of hydrogenotrophic biodenitrification (Reaction 1.3) (Haugen et al., 2002; Karanasios et al., 2010) and the production of sulfate when sulfur is used (Reaction 1.2) limit the wide application of autotrophic denitrification at the field scale. Moreover, autotrophic sulfide biodenitrification is limited to the presence of sulfide minerals (e.g., pyrite). In this manner, heterotrophic biodenitrification appears to be an easier and more feasible technology for wide introduction. Nevertheless, the risks of clogging and nitrite production remain a concern.

In heterotrophic biodenitrification, both risks can be minimized with the type of external organic carbon source and control of its availability to the denitrifier biomass (Gomez et al., 2003; Gómez et al., 2000; van Rijn et al., 1996). The most common carbon sources used in EIB have been acetate (André et al., 2011; Calderer et al., 2010a; Gierczak et al., 2007; Khan and Spalding, 2004; Mastrocicco et al., 2011), alcohol (i.e., methanol and ethanol) (Vidal-Gavilan et al., 2013), and sugars (i.e., sucrose or glucose) (Calderer et al., 2010a; Vidal-Gavilan et al., 2013). van Rijn et al. (1996) correlated nitrite accumulation with the oxidation state of the carbon source and found that greater extracellular nitrite accumulated if highly oxidized carbon sources were used. Gómez et al. (2000) also observed a higher nitrite concentration in column experiments when sucrose (oxidation state 0) was used instead of ethanol or methanol (oxidation state -2). Lower biofilm growth was observed when alcohols were used as an external organic carbon source (Gómez et al., 2000). This result was achieved due to better yields for N removal compared to, for example, sucrose. In other words, a lower concentration of carbonaceous compound was required for equal yields of N removal when alcohols were used instead of sugars, primarily in the case of ethanol. Comparing sucrose, ethanol, and methanol, Gómez et al. (2000) concluded that ethanol was a reasonably good option due to its lower nitrite production and biofilm growth compared with sucrose and better safety compared with methanol.

In addition to these two technical issues, other important factors to consider when selecting organic carbon sources are related to safety and price fluctuations. Safety is a highly important issue for carbon source selection and is primarily related to the flammability of certain organic carbon sources (e.g., methanol, acetic acid, and ethanol). Additionally, the levels of flammability associated with the carbon source selected will have an impact on the cost of the system. Also, the hazards associated

with handling these products will require consideration. The price fluctuations are mainly related to origin from fuel fossils of a lot of organic carbon sources (methanol, ethanol and acetic acid). These markets can have a huge impact on the prices of these sources. Agriculturally derived carbon sources such as sugars tend to have more predictable and less volatile price profiles (USEPA, 2013).

Different applications have been developed to assess the feasibility of *in situ* denitrification at specific sites at field scale (Boisson et al., 2013; Tartakovsky et al., 2002). These projects are aimed at the study of *in situ* geochemical and microbial reactions at the field scale (Istok et al., 1997). The common single-well system test operates by simply pumping a solution of election donors and nutrients into the nitrate-contaminated aquifer, allowing denitrification to take place, and extracting the treated water from the same well at a later time (Boisson et al., 2013; Mercado et al., 1988; Vandenbohede et al., 2008). Usually, a conservative tracer test is added to the injection solution (Vandenbohede et al., 2008). Next, from comparison of the concentrations of reactants and reaction products with the concentration of the non-reactive tracer, it is possible to identify the geochemical or microbiological reactions. A more sophisticated system is the dual well systems, which use an injection-withdrawal well pair to introduce the required nutrients and electron donors to the aquifer.

If the objective is the recuperation of a groundwater supply well, the daisy-well system is the best option. A daisy-well system is generated by combining multiple injection wells with a single central extraction well. The distance between the injection and extraction wells is calculated by considering the capture zone of the latter, the groundwater velocity, and the residence time necessary to degrade the nitrate. In general, a residence time of two days is sufficient for complete denitrification (Bates and Spalding, 1998). The daisy arrangement of wells is favored for full-scale treatment operations. An active zone of denitrification entirely surrounding the pumping well is created, thus ensuring a high percentage of nitrate removal from the water that is captured and pumped. Several studies have been reported in which the daisy-well system was successful in pilot and full-scale applications (Table 1.1). In virtually all cases, these tests performed best when the electron donor supply was introduced to the aquifer in discrete pulses as opposed to continuous injections (Gierczak et al., 2007). In particular, the advantage of pulsing was a reduction in clogging of the aquifers and well screens due to biomass.
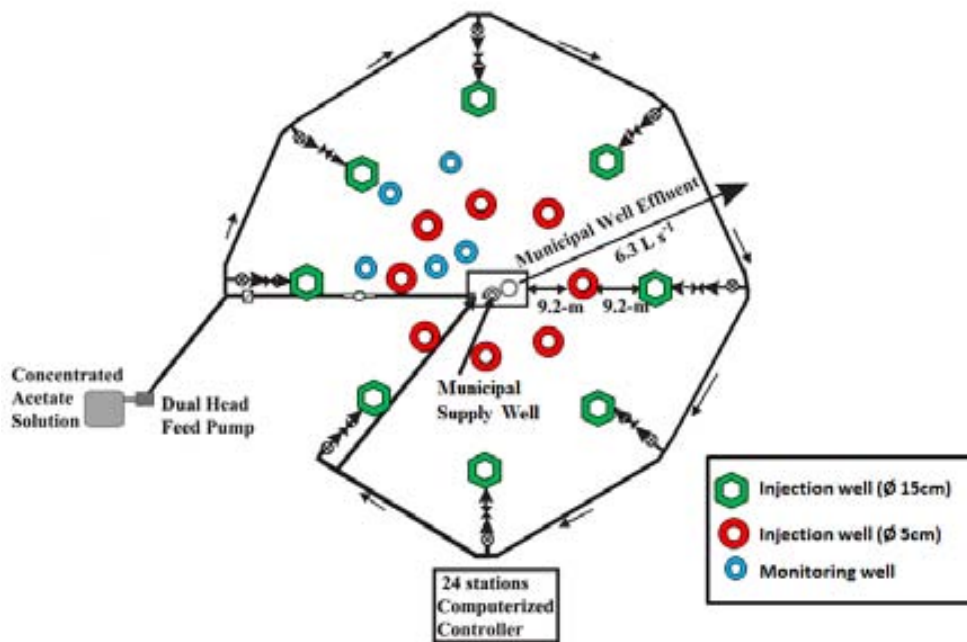
Figure 1.2 Example of a daisy well infrastructure. Modified from Khan and Spalding (2004).

Another option used to remediate nitrate from aquifers through EIB is the application of Permeable Reactive Barriers (PRBs) (Gierczak et al., 2007). These systems are classified as passive remediation technologies because after their installation, the maintenance and operation requires less effort. The PRBs are based on the flow of polluted groundwater through a reactive material that enhances denitrification. The reactive materials tested for denitrification have generally consisted of complex sources of carbon, i.e., cotton (Volokita et al., 1996), newspaper (Volokita et al., 1996), sawdust (Schipper and Vojvodić-Vuković, 2000), wood chips (Robertson and Cherry, 1997), and cellulose (Soares, 2000). Two long-term tests (Robertson et al., 2000; Schipper and Vojvodic-Vukovic, 2001) showed that PRBs continue to operate passively for at least five years. The main inconveniences of PRBs are related to the short residence time of groundwater in the structures to ensure complete reactions and their limitation to shallower aquifers. Maintaining adequate hydraulic conductivity is also a design challenge, but this has generally been possible to achieve in field tests (McMahon et al., 1999; Schipper et al., 2004).

—9—

Table 1.1 Summary of daisy-well *in situ* biodenitrification tests with carbon substrate injections. Modified from Gierczak et al. (2007). NR is not reported value; NA is not applicable, and ND is not detected.

Source	Location	Aquifer type	Saturated zone (m)	Aquifer depth (m)	Number of injection wells	Pumping rate (m³/d)	Retention time (h)	Initial NO_3^- (mg/l)	% NO_3^- reduction claimed	NO_2^- (mg/l)	Electron donor	C:N	Substrate pulsing interval (h on/ h off)
Hamon and Fustec (1991)	Carbonne, France	Alluvium, sand and gravel	7	7	30	30	22.8	98	70%	0.5	Ethanol	1.02	NA
Janda et al. (1988)	Vsetaty, Czechoslovakia	Fine gravel and sand	17	17	4	18-22	24-48	90-120	45%	0.09-0.44	95% Ethanol, 5% methanol	0.83	NA
Mercado et al. (1988)	RishonLezion Municipality, Israel	Sandy loam containing clay layers	51	100	3	50-60	NR	62	10%	NR	Sucrose	1.3	NA
Khan and Spalding (2004)	Municipality of Wahoo Nebraska, USA	Sand and gravel	22	25	8	24	96	53	20%	<1	Acetate	1.2	1/23 per injection well, pump on 6 h every 24 h
						19	NR						1.5/22.5 per injection well, pump on 6 h every 24 h
Khan and Spalding (2003)	Merrick County, Nebraska, USA	Fluvial sand and gravel	9.8	12.2	8	9.1	42-240	177	100%	ND	Ethanol	1.5	NA
									100%		Ethanol	1.5	1/23 per injection well, pump on 6 h every 24 h
									72%		Acetate	10	1/23 per injection well, pump on 6 h every 24 h
Jechlinger et al. (1998)	Bisemberg, Austria	Highly permeable	8.5	13	49	216	NR	60	66%		Ethanol	12-35	3.5/20.5 per injection well, pump on 6 h every 24 h

1.3   Biogeochemical interactions and isotope geochemistry

1.3.1   Water rock interaction

When an aquifer is disturbed, as with injection of organic carbon in EIB and the subsequent reactions involved, the complete hydrogeochemistry of the aquifer is affected. In general, biological reactions consume protons and produce gases such as CO_2, CH_4, and H_2S. All these components will disturb the initial geochemical equilibrium and this may generate secondary processes that might need to be controlled to minimize potential operational problems during EIB. The most typical secondary processes are related to acidification or basification of the systems, which can lead to mineral precipitation or dissolution or can produce inhibition processes to microorganisms.

A few studies have investigated the change in geochemistry due to active remediation, and one of the most complete works is that of Kouznetsova et al. (2010). This group studied all the secondary reactions involved in an enhanced reductive dechlorination of chlorination solvents. Moreover, the researchers incorporated all these reactions into a biogeochemical model that integrated both geochemical and microbiological reactions and described how each dechlorination step produces an hydrogen and chloride ion, giving rise to hydrochloric acid production and promoting the acidification of groundwater. Van Breukelen et al. (2004) also developed a complete study involving microbiological processes and geochemical interactions for a natural attenuation study of a landfill leachate pollution plume in the Netherlands.

Furthermore, mineral precipitation or dissolution can modify the hydraulic properties of the media. Consequently, these issues together with their role in pH regulation should be evaluated together with bioclogging in any EIB application. The velocity of groundwater is a key parameter in the design of all enhanced applications because it is used to calculate, considering a target abstraction rate, the minimum residence time of solutes in groundwater to facilitate the target reactions (biodenitrification). Therefore, the minimum distance between the injection points and the extraction well (see Figure 1.2) can be determined (in the cases of PRBs, the minimum thickness of a permeable barrier). Thus, any change of velocity (modification of hydraulic conductivity, porosity of the media or abstraction rate) should be evaluated accurately.

Because of inorganic carbon production (in heterotrophic metabolism) and proton consumption, acidification or basification of the system can also be induced. These

processes enhance mineral precipitation or dissolution and can cause inhibition of selected biodegradation reactions (Kouznetsova et al., 2010).

1.3.2   Isotope geochemistry

Much uncertainty is associated with subsurface pollution. At times, subsurface pollution characterization is difficult, the cost of monitoring well installation is expensive, and chemical data are often not conclusive due to difficulty in closing the hydrochemistry mass balance (Elsner, 2010). In this context, the use of stable isotopes is another tool that allows improvement of the characterization of subsurface processes.

Because chemical bonds are typically broken more easily if they contain a light rather than a heavy isotope (Melander and Saunders, 1980), contaminant molecules with heavy isotopes are degraded more slowly and tend to accumulate in the fraction of molecules that remain as degradation transformation occurs. This process is known as kinetic isotope fractionation. If a contaminant sample downgradient of a suspected source shows such isotopic enrichment, there is strong evidence that degradation occurs, even if the mass balances cannot be closed and metabolites are not detected (Elsner, 2010). In this context, it is often assumed that processes of a physical nature (i.e., diffusion, sorption, or volatilization) are associated with a much smaller isotope fractionation effects and therefore can be generally neglected.

This kinetic effect offers the possibility of quantifying the degradation occurrence using the Rayleigh equation. This equation relates the change in the isotope ratio of an element in a molecule to the fraction of molecule remaining (f) via the kinetic isotope fractionation factor (α) and the degradation process (Equation 1.1):

$$R = R_0 \, f^{(\alpha-1)} \tag{1.1}$$

where R is the stable isotope ratio of the fraction of molecules f remaining at time t, $R_{s,0}$ is the initial isotopic composition of the molecule, and α is the kinetic isotopic fractionation factor of the transformation process (in a closed system with perfect mixing), which is often represented as the kinetic isotopic enrichment factor ε (in permil, ‰), where $\varepsilon = (\alpha-1)$. Isotopes are typically expressed using delta notation (Equation 1.2):

$$\delta(‰) = \left(\frac{R}{R_{std}} - 1\right) \times 1000 \tag{1.2}$$

where R is the ratio between the heavy isotope and light isotope concentration, and R_{std} is the ratio of the international standard.

In recent years, it was shown that Rayleigh application is essentially restricted to closed systems, although its application to the field scale generally results in underestimating the extent of biodegradation (Abe and Hunkeler, 2006; van Breukelen, 2007; van Breukelen and Prommer, 2008). This underestimation is associated with recently observed fractionation of such physical processes as hydrodynamic dispersion (van Breukelen and Rolle, 2012). Validation of the Rayleigh equation has been evaluated in different studies (e.g., van Breukelen et al. 2008, Lutz et al. 2014), these studies always have been centered on natural attenuation processes. Nevertheless, no studies are available that evaluate the validity of the Rayleigh equation in an Enhanced *in situ* Biodenitrification, which is an active remediation strategy.

On the other hand, isotopes are also used to distinguish among contamination sources (Hosono et al., 2014; Hunkeler et al., 2004) through the isotopic characterization of different potential nitrate sources (fertilizer, wastewater/pig manure).

In EIB applications, two types of isotopes are traditionally used: nitrogen but also oxygen isotopes of nitrate molecules and carbon isotopes of the different carbon compounds involved in biodenitrification. Typically, when nitrate is consumed, residual NO_3^- becomes enriched in the heavy isotopes ^{15}N and ^{18}O, with respect to the light isotopes ^{14}N and ^{16}O, respectively. Monitoring of nitrate isotopes during EIB is useful for the following:

1) ***Identifying the nitrate source*** (Mengis et al., 2001; Puig et al., 2013; Vitoria et al., 2004). In addition to attributing liabilities to pollution, identification of the source is useful to understand the annual dynamics of nitrate in the groundwater. For example, nitrate pollution associated with agriculture can be influenced by the fertilization periods of crops or by rainy periods that facilitate the lixiviation of nitrate from the unsaturated zone to the groundwater. If nitrate inputs to an aquifer and their evolution with the EIB application are controlled, carbon and nutrient injection can be optimized to minimize clogging risks and save costs. Moreover, knowing the source of

nitrate allows identification of the initial isotopic ratio, which subsequently facilitates the quantification of degradation.

2) **_Ensuring that target processes are enhanced_** (Aravena and Robertson, 1998). For example, nitrate degradation processes other than heterotrophic denitrification can be identified, such as autotrophic denitrification or dissimilatory nitrate reduction to ammonia (DNRA or ammonification) (Carrey et al., 2013; Otero et al., 2009).

3) **_Evaluating the extent of biodenitrification_** (Cey et al., 1999; Grischek et al., 1998; Mengis et al., 1999). Because of dilution (e.g. recharge periods, hydrodynamic dispersion), a decrease in nitrate concentration cannot always be attributed to degradation. Monitoring the changes in the nitrogen and oxygen isotope ratios of nitrate (δ^{15}N-NO$_3^-$ and δ^{18}O-NO$_3^-$) allows nitrate transformation and dilution to be distinguished.

Carbon flow in biodenitrification is primarily focused to the oxidation of an organic carbon source to inorganic carbon and its incorporation into biomass. During this process, the carbonate equilibrium could be simultaneously modified with potential occurrence of volatilization (CO$_2$ formation) and/or precipitation/dissolution of CaCO$_3$. Therefore, inorganic carbon plays a central role in the overall network of biodenitrification, and it is necessary to monitor ^{13}C isotopes to understand these secondary processes induced by EIB.

1.4 Modeling of Enhanced _in situ_ Biodenitrification

In this context, field-scale reactive transport modeling of EIB that integrates hydrology, microbiology, geochemistry, and isotope fractionation can provide significant benefits for planning, characterization, monitoring, and optimization of this technology in field applications. Reactive transport models permit quantitative analysis of the interactions between transport and reaction processes (Steefel et al., 2005) and provide a framework to integrate all the reactive processes involved in EIB, i.e., microbiological respiration, water-rock interaction, and isotopic fractionation.

Various studies have been conducted to evaluate biodenitrification using numerical models at different scales, including batch (Calderer et al., 2010b; Killingstad et al., 2002; Kornaros and Lyberatos, 1998; Mastrocicco et al., 2011), column (André et al.,

2011; Clement et al., 1997), and field (Chen and MacQuarrie, 2004; Killingstad et al., 2002; Kinzelbach et al., 1991; Lee et al., 2009) (Table 1.2).

Certain models are focused on EIB applications (André et al., 2011; Calderer et al., 2010b; Mastrocicco et al., 2011), whereas most aim to simulate natural denitrification in groundwater. All of the published enhanced biodenitrification models focused on field applications, and all were applied to EIB in non-fractured sedimentary aquifers (Table 1.2).

All previous works have modeled nitrate degradation coupled to biomass growth by following the double Monod kinetics. This kinetic model is focused on application of the Monod kinetic model (Equation 1.3) to both electron donors and electron acceptors.

$$\frac{dS}{dt} = -v_m \frac{S}{K_s + S} \qquad (1.3)$$

where S is the substrate concentration [M], v_m is the substrate utilization rate [T^{-1}], and k_s is the half-saturation constant [M]. Other biodegradation kinetics (such as first- and zero-order approximations) are not widely used in denitrification because they are less applicable. The choice of biodegradation kinetics should address the life stage of the biomass (lag phase, exponential growth, stationary phase, or decay) and nutrient availability. Monod or Michaelis-Menten expressions address different scenarios. When biomass grows exponentially, substrate concentration (organic carbon and nitrate) is much lower than the saturation constant, and Monod kinetics can be linearized to first-order kinetics with respect to substrate (Bekins et al., 1998; Horan, 1990). In contrast, when biomass is in the stationary phase, and there are no nutrient limitations, the Monod expression can be transformed to zero-order because the substrate concentration is much higher at this point than the saturation constant (Bekins et al., 1998; Horan, 1990). Appendix 1 presents a table with a list of different kinetic parameters used in denitrification models.

Related to geochemical interactions, only certain studies have examined the effects of water-rock interactions during biodenitrification within the aquifer matrices (Chen and MacQuarrie, 2004; Mastrocicco et al., 2011), and only a few have explored the potential use of isotope fractionation for monitoring of biodenitrification (Chen and MacQuarrie, 2004).

As observed in Table 1.2, no model is available that integrates all the processes (microbiology, water-rock interaction, and isotope fractionation) involved in enhanced biodenitrification at any scale.

Table 1.2. Different processes considered in selected models of denitrification.

	Source	Aquifer type	Type of biodenitrification and electron donor used	Biological processes considered	Geochemical interaction	Isotope fractionation
BATCH	Calderer (2010b)	-	Enhanced (glucose)	Aerobic respiration Nitrate respiration Microbial growth and decay	No	No
	Mastrocicco (2011)	-	Enhanced (acetate)	Nitrate respiration Microbial growth and decay	Yes (carbonate equilibrium)	No
	Killingstad et al. (2002)	-	Natural attenuation (natural organic matter)		No	No
	Kornaros and Lyberatos (1998)	-	Enhanced (glutamate)	Aerobic respiration Nitrate respiration Microbial growth and decay	No	No
COLUMN	Clement et al. (1997)	-	Enhanced (acetate)	Nitrate respiration Microbial growth and decay	No	No
	André et al. (2011)	-	Enhanced (acetate)	Nitrate respiration Microbial growth and decay	No	No
FIELD	Killingstad et al. (2002)	Sedimentary			No	No
	Lee et al. (2009)	Sedimentary	Natural attenuation (natural organic matter)	Nitrate respiration Microbial growth and decay	No	No
	Chen and MacQuarrie (2004)	Sedimentary	Natural attenuation (natural organic matter)	Nitrate respiration Geochemical interaction Isotope geochemistry	Yes (carbonate equilibrium)	Yes (^{15}N-NO_3^-)
	Kinzelbach et al. (1991)	Sedimentary	Enhanced (hydrocarbon, aliphatic and aromatic)	Nitrate respiration Microbial growth and decay	No	No
	Boisson et al. (2013)	Fractured	Natural attenuation (pyrite)	Nitrate respiration	No	No

1.5 Motivation and objectives

The framework of this dissertation represents a component of a Research and Technological Development project developed between a private company (d D'ENGINY biorem S.L.) and various universities (Autonomous University of Barcelona and University of Barcelona). The main goal of the project is the development of Enhanced *in situ* Biodenitrification for wider application of this technology to reduce nitrate pollution in groundwater. This goal is based on three different objectives: (1) to demonstrate the feasibility of this technology in reducing nitrate in groundwater in complex aquifer (e.g. fractured aquifer), (2) to demonstrate the feasibility of this technology in recuperating a water supply well by achieving cleaned groundwater in continuous flow, and (3) to develop a reactive transport model as a tool for planning, managing, monitoring and optimizing Enhanced *in situ* Biodenitrification.

This dissertation focused on the third objective, modeling of Enhanced *in situ* Biodenitrification at different scales.

> **Therefore, the main objective of this thesis is to develop a reactive transport model that incorporates all processes involved in Enhanced *in situ* Biodenitrification (microbiological, geochemical, and isotopic fractionation) as a tool for planning, managing, monitoring, and optimizing this technology.**

To accomplish this objective, specific goals have been considered:

1- To develop a numerical model that integrates all processes involved in Enhanced *in situ* Biodenitrification, i.e., microbiological processes, geochemistry, and isotope geochemistry;

2- To evaluate the model at different scales (from batch to field scale) and in complex hydrogeology (fractured aquifers);

3- To evaluate the behavior of the model parameters at different scales;

4- To evaluate whether the Rayleigh equation can be used from a practical point of view in the determination of the extent of EIB based on isotope data;

5- To evaluate the model performance in a long-term denitrification experiment to assess ideal injection strategies; and,

6- To consider the changes in hydrogeological properties due to biofilm growth and geochemical interaction as well as how they can be considered in the numerical model.

1.6 Outline

This dissertation is organized into five main chapters.

In addition to this introduction (Chapter 1), Chapter 2 addresses the development of the isotope biogeochemical model. The goal of this chapter is to define the conceptual relationships among microbiology, geochemistry, and isotope geochemistry during Enhanced *in situ* Biodenitrification. The model is validated with batch-scale biodenitrification experiments using groundwater and sediment from an experimental site (Roda de Ter in Osona region, Spain) and two different external organic carbon sources, namely, ethanol and glucose. The code used to develop the model is PHREEQC-2.

In Chapter 3, the integrated model developed in Chapter 2 is validated in an Enhanced *in situ* Biodenitrification application at the field scale in fractured media (also at the site of Roda de Ter) under natural groundwater flow conditions. The main goal of this chapter is to incorporate the groundwater flow equations into the biogeochemical model and validate it under complex hydrogeological conditions (fractured media). As a secondary goal, the use of the Rayleigh equation to determine the extent of EIB is also evaluated from a practical perspective. The code used to develop the model is PHAST, which couples the PHREEQC-2 code (the isotope biogeochemical model) to the 3-D groundwater flow model HST3D.

Chapter 4 is focused on modeling EIB at the column scale that reproduces the system under different injection strategies and under conditions of significant biofilm growth. This chapter aims to evaluate how different feeding strategies modify the hydraulic properties of the porous medium. Moreover, a reactive transport model of a long-term column experiment was developed. The code used to develop this model was PHT3D which couples PHREEQC-2 to the 3-D groundwater flow and solute transport model MODFLOW/MT3DMS. .

Finally, Chapter 5 presents the conclusions of the performed research. Suggestions for future research in modeling of EIB are also provided.

The Appendix includes three main sections. The first section includes 1) a summary table of different parameters and their values used in the published models of biodenitrification (Appendix 1), 2) other papers developed during the PhD training period (Appendix 2.1 - 2.3), and 3) other scientific communications (Appendix 3). The second section includes a) a paper based on a natural nitrate attenuation experiment in which the bottom sediments of a lake were used as source of electron donor

(Appendix 2.1) and b) two papers based on experiments carried out during my master thesis aimed at evaluating the desorption and biodegradation of a Polycyclic Aromatic Hydrocarbons mixture using different surfactants and the *Trametes versicolor* (white rot fungi) (Appendix 2.2 and 2.3). Finally, the third section includes a list of other scientific communications (abstract and proceeding conferences) performed during the PhD training period.

CHAPTER 2

Integrated modeling of biogeochemical reactions and associated isotope fractionations at batch scale: a tool to monitor enhanced biodenitrification applications[*]

2.1   Introduction

In groundwater, biodenitrification is predominantly restricted by the availability of electron donors to provide energy to heterotrophic microorganisms (Knowles, 1982). To solve this problem, Enhanced *in situ* Biodenitrification (EIB) creates optimized conditions through the addition of organic carbon sources and by controlling/monitoring other environmental parameters (e.g., oxidant concentrations, pH, micro-nutrients). EIB is thus a potential technology for cleaning nitrate-polluted groundwater and achieving drinking water standards (Khan and Spalding, 2004; Matějů et al., 1992; Vidal-Gavilan et al., 2013).

Bioreduction of nitrate proceeds through different intermediate nitrogen compounds (Reaction 1.4, Chapter 1). The nitrogen of nitrate is increasingly reduced, eventually

---

arriving at dinitrogen gas. Notably, if optimal conditions do not exist (e.g., inadequate supply of organic carbon or the presence of oxygen), intermediate nitrogen compounds such as nitrite can temporally accumulate. Nitrite is significantly more toxic than nitrate, and this toxicity is reflected in its considerably lower standard of 0.1 mg/l (Fan and Steinberg, 1996).

Geochemical interactions can occur between the biodenitrification reactants and the porous geologic medium in response to biodegradation reactions. These interactions may play a critical role in EIB implementation. Because of inorganic carbon production and pH alteration, carbonate mineral dissolution/precipitation is induced by heterotrophic biodenitrification.

Another important factor when monitoring EIB in the field is dilution resulting from hydrodynamic dispersion, mixing, or other processes. Because of dilution, a decrease in nitrate concentration cannot always be attributed to degradation. Monitoring the changes in the nitrogen and oxygen isotope ratios of nitrate (δ^{15}N-NO$_3^-$ and δ^{18}O-NO$_3^-$) allows nitrate transformation and dilution to be distinguished (e.g., van Breukelen, 2007). As NO$_3^-$ is consumed, the residual NO$_3$- becomes enriched in the heavy isotopes ^{15}N and ^{18}O, and the denitrification reaction follows a Rayleigh distillation process (Chapter 1).

The inclusion of dissolved inorganic carbon isotopes (δ^{13}C-DIC), which are involved in both direct (oxidation of organic carbon) and indirect (carbonate mineral interaction) processes of enhanced biodenitrification, in the biogeochemical model is expected to better allow the evaluation of the overall model consistency due to the central role of δ^{13}C-DIC in the reaction network.

To control the direct and indirect processes that are associated with enhanced biodenitrification, complete models that consider all interactions (i.e., microbiological, geochemical, and isotopic) need to be developed. Nevertheless, there is a lack of models that integrates microbiological, geochemical, and isotope geochemistry in EIB (Chapter 1 and Appendix 1). Consequently, in this chapter it is developed an integrated model for enhanced biodenitrification which considers all these mentioned processes. This model was calibrated and validated with batch scale experimental data obtained from Vidal-Gavilan et al. (2013), who used either ethanol or glucose as external carbon sources. This biogeochemical model represents a key step towards simulating EIB at the field scale as a core of reactive transport models (RTMs). The model considered: 1) microbiological processes – exogenous and endogenous respiration; 2) geochemical processes – calcite precipitation and dissolution; and 3)

isotopic fractionation – δ^{15}N-NO$_3^-$, δ^{18}O-NO$_3^-$, and δ^{13}C-DIC, while considering full δ^{13}C isotope geochemistry. This is the first model that simulates all relevance processes during EIB including also isotopes (Table 1.2 and Appendix 1)

2.2 Model construction

2.2.1 Model code

The Phreeqc-2 model code (Parkhurst and Appelo, 1999) was used to simulate the evolution of groundwater chemistry and isotopic composition during enhanced biodenitrification. The model was calibrated using the parameter estimation software PEST (Doherty, 2005). Previously, this approach has been successful in calibrating reactive transport models (Karlsen et al., 2012; van Breukelen et al., 2004). PEST adjusts model parameters until a fit between model outputs and data observations (in this study: nitrate, ethanol, biomass, calcium, DIC, δ^{13}C-DIC) is obtained through the method of weighted least squares. Weights were applied as in Karlsen et al. (2012) and Matott and Rabideau (2008). These researchers used the inverse of the standard deviation, considering the concentration measurement errors as 5%. For δ^{13}C-DIC, it was considered the measurement errors to be 0.2‰. PEST uses a nonlinear estimation technique known as the Gauss-Marquardt-Levenberg method.

2.2.2 Batch experiments and initial conditions

The experimental data used to validate the developed model were obtained from Vidal-Gavilan et al. (2013). The experiments lasted 7 days and were executed at aquifer temperature (15ºC) using core material and groundwater obtained from an experimental site. The experimental site was located in Roda de Ter (442270, 4647255 UTM31/ETR89) in the central part of the Osona region, which is recognized as an area that is vulnerable to nitrate pollution. This region is located 100 km north of Barcelona (Spain). The aquifer at the site was characterized by subvertical fracture networks and horizontal bedding joint surfaces. The aquifer behaved as unconfined (Vidal-Gavilan et al., 2013). Groundwater was obtained the day of the experiment set-up and purged with argon to remove dissolved oxygen (2.5 mg/l). Core fragments were added to all batch reactors to provide solid material from the site. They were obtained from different boreholes carried out in the site; the sediment was from saturated zones. Glass balloon reactors (6.5 l) were filled with 5.5 l of groundwater and 1.2 kg of sediment and sealed anaerobically under an argon atmosphere. Control batch reactors were also run to verify that no natural attenuation occurred during the experiment. The water chemistry and initial conditions of the batch experiments and of the model simulations are specified in Table 2.1. Nitrate was the primary electron

acceptor present in the water, and heterotrophic biodenitrification due to external organic carbon was the only nitrate reduction process in the batch experiments. The amount of carbon added was calculated using the stoichiometry between ethanol and nitrate described by Vidal-Gavilan et al. (2013). Thus, there was no external organic carbon left for the reduction of other electron acceptors present (e.g., sulfate). To determine denitrifying biomass content, the microbial population was quantified by the most-probable-number method published by Saitoh et al. (2003) and converted to moles using a denitrifier cell weight of 10^{-9} mg (Alvarez et al., 1994). Additionally, cores from the site had been fragmented and kept dry in the lab. X-ray diffraction indicated that the core fragments were composed primarily of calcite (27.2 wt.%), muscovite ($KAl_2(AlSi_3O_{10})(OH)_2$, 26.2 wt.%), and quartz (23.1 wt.%), with small amounts of albite ($NaAlSi_3O_8$, 10.3 wt.%), dolomite (7.7 wt.%), sudoite ($Mg_2(Al; Fe^{3+})_3Si_3AlO_{10}(OH)_8$, 4.9 wt.%), and pyrite (0.6 wt.%) (Torrentó et al., 2011).

Most of the analytical methods are described in detail in Vidal-Gavilan et al. (2013). The initial isotopic characterization of δ^{13}C-ethanol was performed using a Trace GC Ultra coupled with a combustion interface to an isotope ratio mass spectrometer. Initial δ^{13}C-glucose isotopic composition was determined by an elemental analyzer (EA, Carlo Erba Flash 1112) coupled to an isotope ratio mass spectrometer (Finnigan Delta C IRMS). Carbon isotope ratios are reported relative to an international standard (V-PDB, Vienna Peedee Belemnite (0.011237)) using the delta notation (Equation 1.2, Chapter 1). All the measurements were run in duplicate. The standard deviations of the δ^{13}C in ethanol values were below ±0.5‰ whereas the standard deviations of the δ^{13}C in glucose values were below ±0.2‰.

Table 2.1 Initial conditions of batch experiments (ethanol and glucose). (*) Denitrifying population was enumerated by the most-probable-number and converted to moles using denitrifier cell weight of 10^{-9}mg (Alvarez et al., 1994). (**) Estimated from literature. (***) Calculated.

Parameter	Unit	Ethanol case Value	Glucose case Value
Ethanol	mM	3.23	
Glucose	mM		1.98
Nitrate	mM	3.40	3.05
DIC	mM	7.40	7.20
Denitrifying biomass*	mM	5.19×10^{-6}	3.89×10^{-8}
pH		7.23	7.20
Temperature	ºC	15	15
Chloride	mM	1.43	1.67
Sulfate	mM	1.35	1.43
Calcium	mM	5.89	3.22
Sodium	mM	2.25	1.32
Magnesium	mM	1.38	0.97
Potassium	mM	2.41	0.14
Phosphate	mM	1.77	1.77
δ^{15}N-NO3	‰	12.7	13.0
δ^{18}O-NO3	‰	3.97	4.30
δ^{13}C-DIC	‰	-15.9	-12.9
δ^{13}C-Ethanol	‰	-30.5	
δ^{13}C-Glucose	‰		-21.0
δ^{13}C-Biomass**	‰	-20	-20
δ^{13}C-CaCO$_3$***	‰	-11.3	-11.3

2.2.3 Enhanced biodenitrification model

Biodenitrification was modeled considering exogenous and endogenous respiration. The model was run over a total of 7.5 days with a time step of 0.05 days. Exogenous nitrate respiration was modeled using a multiple-Monod expression (Equation 2.1-2.3), one of the most common expressions used in biodenitrification models (Calderer et al., 2010b; Chen and MacQuarrie, 2004; Lee et al., 2006; MacQuarrie and Sudicky, 2001; Rittmann and McCarty, 2001). This multiple-Monod expression was divided into three main equations: one for the electron donor (organic carbon, Equation 2.1), one for the electron acceptor (nitrate, Equation 2.2), and one for the biomass (Equation 2.3). Biomass always refers to denitrifying populations. When significant nitrite accumulated (only in the case of glucose addition), biodenitrification was simulated as a two-step redox reaction employing multiple-Monod expressions: the reduction from nitrate to nitrite and the reduction from nitrite to dinitrogen gas. However, the presence of nitrate limits the reduction of nitrite (Almeida et al., 1995). An inhibition

factor (Equation 2.4), therefore, was added to Equation 2.1 for the nitrate to nitrite step.

$$r_{ED} = -k_{max} \frac{[ED]}{[ED] + K_{S,ED}} \frac{[EA]}{[EA] + K_{S,EA}} [X]$$

(2.1)

$$r_{EA} = Q r_{ED}$$

(2.2)

$$r_X = -Y_h r_{ED} - b[X]$$

(2.3)

$$F_{inh} = \frac{K_{Inh}}{[EA] + K_{Inh}}$$

(2.4)

where [ED] is the concentration [M_{ED} L^{-3}] of the electron donor (ethanol or glucose). [EA] is the concentration of the electron acceptor (nitrate or nitrite, [M_{EA} L^{-3}]), and [X] is the biomass concentration [M_X L^{-3}]. Y_h (microbial yield) and Q are stoichiometrical parameters [$M_X M_{ED}^{-1}$]; [M_{EA} M_{ED}^{-1}]. k_{max} [T^{-1}], $K_{s\,ED}$ [M_{ED} L^{-3}], $K_{s\,EA}$ [M_{EA} L^{-3}], and b [T^{-1}] are kinetics parameters. The stoichiometrical parameters define the reaction stoichiometry of certain components: Y_h relates the biomass production to electron donor consumption as part of the microbiological synthesis; Q defines the proportion of electron acceptor to electron donor consumption. k_{max} is the maximum consumption rate of electron donor. The half saturation constants $K_{s\,EA}$ and $K_{s\,ED}$ are equal to the electron acceptor and electron donor concentrations, respectively, at which the biomass growth rate is half of its potential maximum growth rate. Finally, b is the endogenous decay, which is related to cell self-oxidation to meet maintenance-energy needs (Rittmann and McCarty, 2001).

The derivation of the stoichiometric overall reactions for biodenitrification was accomplished using thermodynamic and bioenergetic principles described by McCarty (1975). A full stoichiometry derivation allowed the determination of the stoichiometric parameters, such as Y_h. Moreover, knowledge of the complete stoichiometry is useful in predicting the amount of organic carbon needed for full nitrate removal (VanBriesen, 2002). McCarty's method required three semi-reactions: one for the electron donor (R_d), one for the electron acceptor (R_a), and one for cell synthesis (R_c). The resulting overall reaction (R) was then obtained from:

$$R = R_d - f_e R_a - f_s R_c$$

(2.5)

When microorganisms use an electron-donor substrate for cellular synthesis, a fraction of its electrons (f_e) is initially transferred to the electron acceptor to provide energy for conversion of the remaining fraction of electrons (f_s; $f_s + f_e = 1$) into the microbial cells (McCarty, 1975). f_s is predicted by calculating the energy required to convert the carbon source to pyruvate and pyruvate to cellular carbon. One important feature of denitrifying bacteria is that they often use NO_3^- as the N source for cell synthesis (Rittmann and McCarty, 2001; Rivett et al., 2008). The calculations were performed following the protocol of Rittmann and McCarty (2001). For glucose, nitrite accumulation was observed in the experiments, and thus the redox process was divided into two steps: the reduction of nitrate to nitrite and the subsequent reduction of nitrite to dinitrogen gas. After determining the electron fractions, f_s (Equation 2.5), reactions 2.1-2.2.2 were obtained. The electron fractions were 0.682 for ethanol and 0.727 and 0.812, respectively, for each of the two glucose redox steps.

$$0.083\ C_2H_6O + 0.088\ NO_3^- + 0.043\ H^+ \rightarrow 0.024\ C_5H_7O_2N + 0.032\ N_2 + 0.045\ HCO_3^- + 0.164\ H_2O$$

<div align="right">Reaction 2.1</div>

$$0.042\ C_6H_{12}O_6 + 0.162\ NO_3^- \rightarrow 0.026\ C_5H_7O_2N + 0.136\ NO_2^- + 0.098\ H^+ + 0.120\ HCO_3^- + 0.052\ H_2O$$

<div align="right">Reaction 2.2.1</div>

$$0.042\ C_6H_{12}O_6 + 0.063\ NO_2^- + 0.029\ NO_3^- \rightarrow 0.029\ C_5H_7O_2N + 0.031\ N_2 + 0.018\ H^+ + 0.105\ HCO_3^- + 0.089\ H_2O$$
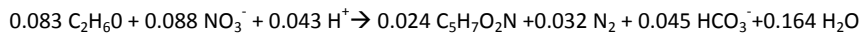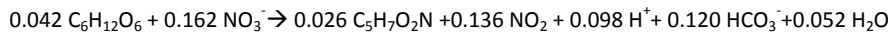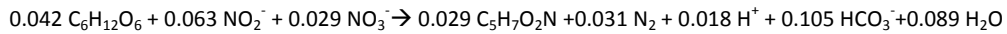
<div align="right">Reaction 2.2.2</div>

Kinetic parameters (K_{max}, $K_{s,ED}$, $K_{s,EA}$, and b) were determined using the calibration program PEST.

Endogenous respiration occurs when cells oxidize themselves to meet energy needs. In the model, endogenous respiration was included and coupled with exogenous nitrate respiration. Endogenous respiration is slower than exogenous respiration; however, endogenous respiration does not depend on the organic substrate availability (Orozco et al., 2010). Endogenous respiration, therefore, may continue biodenitrification after organic carbon sources become exhausted. Taking these facts into account in the model, the total nitrate-reduction rate ($r_{EA,EXO}$, [$M_{EA}\ L^{-3}T^{-1}$]) was the sum of biodenitrification via exogenous respiration (ethanol or glucose in this case) and endogenous respiration (using their own biomass, Equation 2.6):

$$r_{EA,total} = Qr_{ED,EXO} + Sr_{ED,ENDO}$$

<div align="right">(2.6)</div>

where $r_{ED,EXO}$ is the rate of external organic carbon consumption [$M_{ED,EXO}$ $L^{-3}T^{-1}$] and $r_{ED,ENDO}$ is the rate of endogenous organic carbon consumption [$M_{ED,ENDO}$ $L^{-3}T^{-1}$], which is related to biomass decay (Equation 2.3). Q and S [M_{EA} $M_{ED,END}^{-1}$] are the stoichiometric factors for both reactions; their units are moles nitrate (nitrite)/moles organic carbon. In the model, endogenous respiration was defined as the use of decayed cells as electron donors.

2.2.4   Water-rock interaction model: calcite equilibrium model

Both calcite precipitation and dissolution were modeled as kinetic reactions. Observed changes in the calcite saturation index indicated that microbial reactions in these batch experiments changed the solution pH and alkalinity. These changes modified the water saturation state with respect to calcite faster than the calcite mineral-water interaction process could respond. The rate of precipitation (Equation 2.7) was modeled as the observed rate constant (K_{obs}; [M L^{-3} T^{-1}]) times the saturation state minus 1 (Busenberg and Plummer, 1982; van Breukelen et al., 2004):

$$r_{min,prep} = K_{obs}(\Omega - 1) \tag{2.7}$$

with

$$\Omega = \frac{IAP}{K} \tag{2.8}$$

where Ω is the saturation state, IAP is the ion activity product, and K is the thermodynamic equilibrium constant at 15°C. The saturation index (logarithm of saturation state) is 0 at thermodynamic equilibrium. The water is supersaturated with respect to a particular mineral when the saturation index is positive and under saturated when negative. The equilibrium constant of calcite was obtained from the Phreeqc database. The calcite precipitation rate constant, K_{obs}, was determined using PEST optimization.

The rate of calcite dissolution ($r_{min,d}$) was modeled as an active surface time dissolution constant at 25ºC, corrected by the Arrhenius term times the saturation state minus 1. This expression was obtained from (Palandri and Kharaka, 2004):

$$r_{min,d} = SAK(\Omega - 1)^n \tag{2.9}$$

with

$$A = e^{\left[\frac{-E}{R}\left(T^{-1} - 298.15^{-1}\right)\right]}$$

(2.10)

where S is the reactive surface area $[L^2]$; A is the Arrhenius term; K is dissolution constant at 25º $[M\ L^2\ T^{-1}] - 10^{-5.81}$ mol m^{-2} s^{-1} (Palandri and Kharaka, 2004); parameter n is empirical and dimensionless and equal to unity by default (Palandri and Kharaka, 2004); E is an Arrhenius constant (2.35×10^4 J mol^{-1}); R is gas constant; and T (K) is the temperature of the experiment. The initial reactive mineral surface area was estimated (9.64×10^{-2} m^2) considering the total mass of dry sediment used (1.2 kg), the specific weight of calcite (2.71 kg L^{-1}) and an assumed circular shape with an average diameter of 0.75 cm. The reactive surface area in the model was normalized per liter of water.

2.2.5   Stable isotope geochemistry model
Modeling of δ^{15}N-NO$_3$- and δ^{18}O-NO$_3^-$ isotope geochemistry

Assuming Monod degradation kinetics, the disappearance rate of heavy (NO$_3^-$,h; ^{15}N-NO$_3^-$ and ^{18}O- NO$_3^-$) and light (NO$_3^-$, l; ^{14}N- NO$_3^-$ and ^{16}O- NO$_3^-$) isotopes from the batch experiment was described as follows (van Breukelen and Prommer, 2008):

$$r_{NO_{3,l}^-} = r_{EA,total} \frac{[NO_{3,l}^-]}{[NO_{3,l}^-] + [NO_{3,h}^-]}$$

(2.11)

$$r_{NO_{3,h}^-} = r_{EA,total} \frac{[NO_{3,h}^-]}{[NO_{3,l}^-] + [NO_{3,h}^-]} (\varepsilon + 1)$$

(2.12)

where ε is the isotopic enrichment factor; $[NO_{3,h}^-]$ is the concentration of the heavy nitrogen/oxygen isotopes of nitrate $[M\ L^{-3}]$; and $[NO_{3,l}^-]$ is the concentration of light isotopes $[M\ L^{-3}]$. The kinetic isotope enrichment factors (ε) were obtained from Vidal-Gavilan et al. (2013), who determined these factors using the Rayleigh equation (-12.9‰ and -8.8‰ for nitrogen and oxygen of nitrate, respectively, for their ethanol experiment and -17.2‰ and -15.1‰, respectively, for their glucose experiment). In the model, ε_N and ε_O were taken to be equal for the reduction of nitrate to dinitrogen gas and for the reduction of nitrate to nitrite in both the ethanol and glucose cases. Note that the total nitrate-reduction rate includes both nitrate consumed by exogenous respiration and nitrate consumed by endogenous respiration; equal isotope enrichment factors were assumed for both processes. The predicted isotopic

signatures were calculated after the model simulations using Equation 2.2 and international standards (V-SMOW for $\delta^{18}O$ (0.0020052), Atmospheric N_2 for $\delta^{15}N$ (0.003677)).

Modeling of $\delta^{13}C$ isotope geochemistry

The stable carbon isotope geochemistry is affected by respiration processes and calcite-water interactions. Carbon isotope geochemistry was simulated by adding "^{12}C" and "^{13}C" of each carbon species (ethanol/glucose, dissolved inorganic carbon (DIC), biomass, and calcite) as separate imaginary solutes to the model. The exact concentration of both isotopes was calculated from the groundwater's carbon isotope signature (Table 2.1). The $\delta^{13}C$ contents of heterotrophic biomasses in other studies fell within -10.3 to -25.4‰ for *Pseudomonas aeruginosa* (Blair et al., 1985; Coffin et al., 1990). For both experiments, -20‰ was considered the input in the model as the initial $\delta^{13}C$-biomass.

The carbon isotope fractionation of the organic carbon source was modeled using the following expression:

$$r_{ED,h} = r_{ED}\frac{[ED_h]}{[ED_l]+[ED_h]}(\varepsilon+1)$$

$$(2.13)$$

where ε is the isotopic enrichment factor of organic carbon; $[ED_h]$ is the concentration of the heavy carbon isotopes of the organic carbon $[M\ L^{-3}]$; and $[ED_l]$ is the concentration of the light isotopes $[M\ L^{-3}]$. Heavy inorganic carbon ($r_{13C\text{-}DIC,rex}$) and heavy biomass production ($r_{13C\text{-}X,rex}$) from organic carbon source oxidation (exogenous respiration) were modeled by the following equations:

$$r_{^{13}C\text{-}DIC,r_{ex}} = Pr_{ED}\frac{[ED_h]}{[ED_l]+[ED_h]}(\varepsilon+1)$$

$$(2.14)$$

$$r_{^{13}C-X,r_{ex}} = Y_h r_{ED}\frac{[ED_h]}{[ED_l]+[ED_h]}(\varepsilon+1)$$

$$(2.15)$$

where P is the stoichiometric relation between organic and inorganic carbon production of exogenous respiration (in mol DIC/mol organic carbon); Y_h is the microbial yield (defined in Equation 2.3); r_{ED} is the electron donor rate (defined in Equation 2.1); and ε is the isotopic enrichment factor of organic carbon. ε was determined using PEST optimization.

The isotopic effect in the organic carbon can be observed in the first step of microbial metabolism; however, the isotopic effect manifested in its end products (biomass and carbon dioxide) results from different fractionations in each step of metabolism. Because of this complexity, the model was simplified by considering only one isotopic fractionation factor as representative of the overall metabolism. Additionally, the same value for the three rates was used (Equations 2.13-2.15). This simplification was employed in the recent work of Vavilin (2013). He used, in a different model, the identical isotopic fractionation factor for the fractionation of organic carbon and its end products. Note that the addition of Equations 2.14 and 2.15 yields Equation 2.13.

The biomass produced also decays and contributes to inorganic carbon production (endogenous respiration). To model this process, it was assumed: 1) endogenous respiration only contributed to the generation of inorganic carbon (i.e., not to new biomass); and 2) carbon isotope fractionation between the decayed biomass and the produced inorganic carbon did not occur. Using these assumptions, the inorganic carbon isotope flow was simulated according to the following expression:

$$r_{^{13}C-DIC, r_{end}} = R\,X_h\,b$$

(2.16)

Where X_h is the fraction of biomass $[ML^{-3}]$ containing heavy carbon and is related to Equation 2.15; b is the endogenous decay constant (Equation 2.3); and R is the stoichiometric factor of endogenous decay to inorganic carbon production $[M_{DIC,END}\,M_{ED,END}^{-1}]$, which is internally calculated by Phreeqc.

Finally, carbon isotope flow resulting from calcite precipitation and dissolution was included in the model. For calcite precipitation, the $\delta^{13}C$-DIC modification was calculated following the procedure of Van Breukelen et al. (2004). They calculated ^{13}C-CaCO$_3$ precipitation by applying the equilibrium fractionation factors to the different inorganic carbon species and calcite (as defined by Mook (2000)). At 15ºC, $^{13}\varepsilon_{a/b}$ was -10.12‰, $^{13}\varepsilon_{c/b}$ was -0.49, and $^{13}\varepsilon_{s/b}$ was +0.41, where a is the dissolved CO_2, b is the dissolved HCO_3^-, c the dissolved CO_3^{-2}, and s is the solid calcite. Considering these fractionation factors and initial $\delta^{13}C$-DIC, the calculated initial value of $\delta^{13}C$-CaCO$_3$was -11.32‰. This value was in the range described by Mook (2000), and the value is consistent with values presented by Appelo and Postma (2005). For calcite dissolution, isotope fractionation between calcite and produced DIC was assumed to be negligible. Therefore, the $\delta^{13}C$-DIC produced was calculated by multiplying the calcite dissolution rate by the actual carbon-13 fraction in calcite:

$$r_{^{13}C-DIC,CC_d} = r_{CC_d} \frac{[cc_h]}{[cc_l]+[cc_h]}$$

(2.17)

where $[cc_h]$ is the concentration $[ML^{-3}]$ of the heavy carbon isotope of calcite and $[cc_l]$ is the concentration $[ML^{-3}]$ of the light isotopes. Predicted carbon isotopic signatures were calculated after the model simulations using Equation 1.2 and an international standard (V-PDB). Figure 2.1 summarizes all processes considered in the $\delta^{13}C$ isotope geochemistry of the EIB.
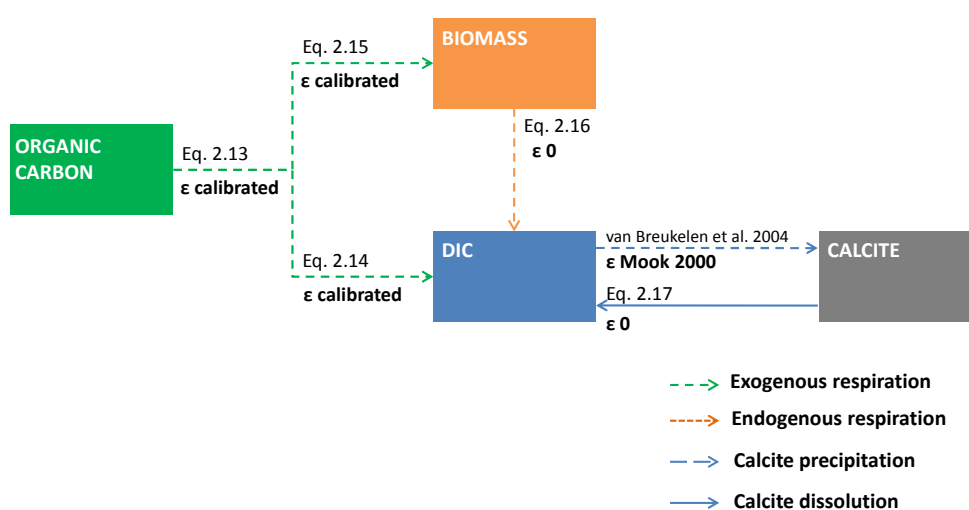
Figure 2.1 Processes involved in $\delta^{13}C$ isotope geochemistry.

2.3   Results and discussion

2.3.1   Enhanced biodenitrification model

The model results of both the ethanol and glucose experiments matched the experimental data well (Figure 2.2) when the calibrated parameters listed in Table 2.2 were applied, including the best-fit kinetic parameters from the PEST calibration. Initial values of kinetic parameters (k_{max}, k_{sat} and b) were obtained from Calderer et al. (2010), who performed similar experiments with indigenous biomass from aquifers and used glucose as the organic carbon source. The microbial yield coefficients (Y_h, moles C-cell / moles C-organic carbon) were 0.731 for ethanol and 0.520 and 0.580, respectively, for each of the two redox steps.

Table 2.2 Kinetic parameters optimized in the model

Parameter	Units	Initial value (Calderer et al. 2010)	Calibrated value	
			Ethanol experiment	Glucose experiment
$k_{max, NO3}$	mol OCmol C-biomass^{-1} d^{-1}	1.7	53.95	12.25
$k_{max, NO2}$	mol OC mol C-biomass^{-1} L^{-1}	-	-	8.78
$K_{sat, organic carbon}$	M	1.03×10^{-4}	7.28×10^{-2}	6.04×10^{-3}
$K_{sat, NO3-}$	M	3.56×10^{-5}	1.86×10^{-4}	1.55×10^{-3}
b	d^{-1}	8.3×10^{-1}	1.50×10^{-1}	8.79×10^{-2}
$K_{sat, NO2-}$	M	-	-	5.06×10^{-3}
K_{inh}	M	-	-	8.51×10^{-5}

The fitted parameters differed substantially from the initial values of Calderer et al. (2010), most likely because of dissolved oxygen in the media of their experiments. Nitrate depletion was achieved after two days in the ethanol experiments and after only one day in the glucose experiments. In both cases, a small depletion of biomass from endogenous respiration was simulated when the nitrate and organic carbon was consumed. Furthermore, in the model can be observed how this decayed biomass was oxidized to inorganic carbon by the reduction of sulfate since nitrate was completely depleted (note the small increase of DIC after day 5 for ethanol and after day 4 for glucose).
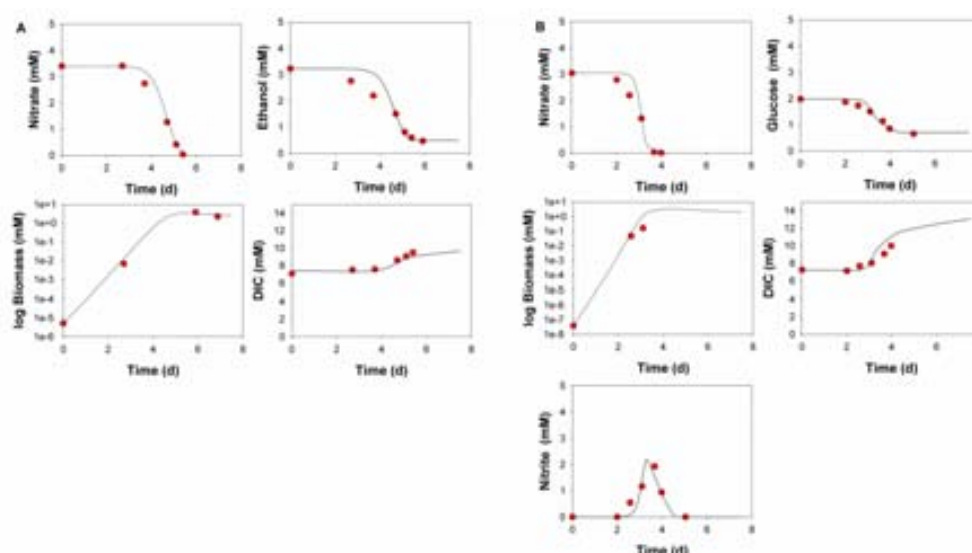
Figure 2.2 Modeling results (lines−) versus experimental data (●) for the carbon source, nitrate, biomass, and total inorganic carbon using ethanol (A) and glucose (B). The experimental data were taken from Vidal-Gavilan et al. (2013).

In the model it was considered the inhibitory character of nitrate to nitrite reduction. This inhibition is considered noncompetitive, and it has been widely considered by different authors (Killingstad et al., 2002; Smith et al., 2001). In this type of noncompetitive inhibition, nitrate binds with the degradative enzyme (nitrite reductase) at a site different than the active site, altering the enzyme's conformation in a manner that slows substrate (nitrite) utilization (Rittmann and McCarty, 2001).

Endogenous respiration occurs when denitrifiers oxidize their own cellular mass instead of external organic matter. The stoichiometric parameter (S, Equation 2.8), internally calculated by Phreeqc, was 0.92 moles NO_3^-/moles $C_{org-end}$ for the ethanol experiment and 2.78 moles NO_3^-/moles $C_{org-end}$ for the glucose experiment. These parameters were based on modeling results, although they are similar to the experimental parameters determined by Dawes and Ribbons (1964) (between 0.83 and 3.27), who obtained these experimental relationships from the consumption of nitrate and endogenous carbon from PHB (poly-β-hydroxybutyrate, microbial storage compounds). The importance of endogenous respiration is illustrated in Figures 2.3A and 2.3B. In both the ethanol and glucose experiments, exogenous respiration was the most important process in nitrate reduction (90% of flux). When nitrate levels dwindled, the relative importance of endogenous respiration increased. Although endogenous respiration increased, it did not constitute a significant portion of the nitrate reduction rates.
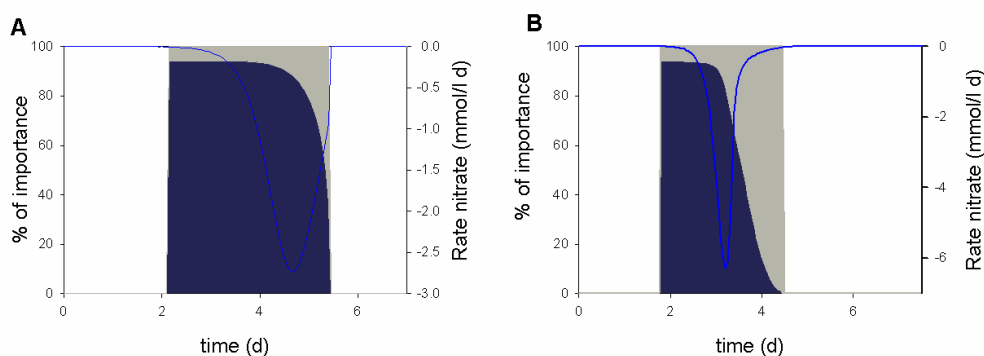
Figure 2.3 Relative contributions of exogenous (dark grey) and endogenous (grey) respiration to the rate of nitrate-reduction using ethanol (A) and glucose (B).

2.3.2   Water-rock interaction: the calcite equilibrium model

Biological reactions induced by EIB may trigger geochemical reactions in the aquifer. Because of pH alteration and HCO_3^- production during nitrate reduction (Reactions 2.1-

2.2.2.), one of the most affected geochemical reactions is the dissolution/precipitation of carbonates. Depending on which process (proton consumption or CO_2 production) is more important, biodenitrification will tend to basify or acidify the aquifer. The relative importance of each process will depend on the organic carbon source.

The model results matched the experimental data well (Figure 2.4). With ethanol, the system was basified (pH increased from 7.2 to 8.1; Figure 2.4A), and an increase in the calcite saturation index was observed (from 0.45 to 1.15; Figure 2.4A). Because the amount of calcium in solution decreased, the kinetic precipitation of calcite was added to the model (Figure 2.4A). The precipitation rate constant (Equation 2.8) fitted was 9×10^{-6} M calcite /d and was consistent with values determined by others (e.g., van Breukelen et al., 2004). The model predicted a total calcite precipitation of 3.72×10^{-1} mM. Some authors have reported calcite precipitation in biodenitrification experiments where acetate was used as the organic carbon source (Mastrocicco et al. 2011). Additionally, Fernández-Nava et al. (2008) observed calcite precipitation during biodenitrification in high-calcium wastewaters. Barbieri et al. (2011) described an increase in the calcite saturation index and induced carbonate mineral precipitation in systems using acetate and methanol as the organic carbon sources.

In contrast, for glucose, a slight decrease in pH was observed (from 7.2 to 7.1). The calcite saturation index dropped to zero, and calcium increased in solution until all glucose was consumed, suggesting that calcite dissolution occurred (Figure 2.4B). The precipitation rate constant was identical to the precipitation rate constant in the ethanol experiment (9×10^{-6} M calcite/d), predicting a total calcite dissolution of 2.69×10^{-1} mM and a calcite precipitation of 3.61×10^{-2} mM for the glucose experiment.
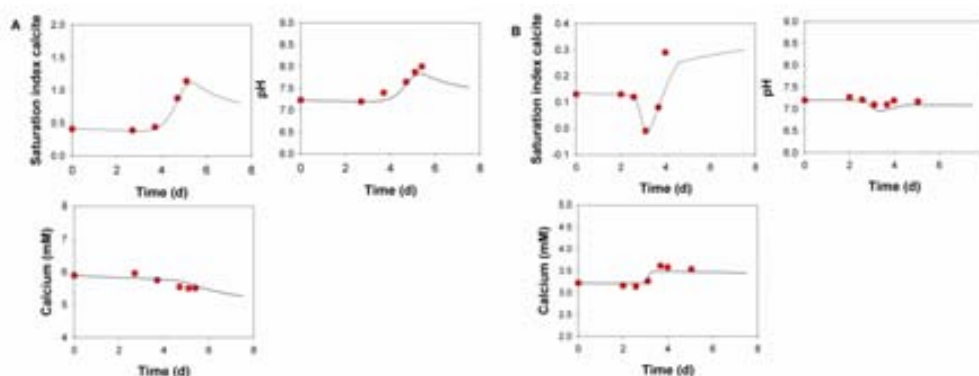
Figure 2.4 Modeling results (lines—) *versus* experimental data (●) of the saturation index of calcite, calcium, and pH using ethanol (A) and glucose (B). The experimental data were taken from Vidal-Gavilan et al. (2013).

2.3.3 Stable isotope geochemistry model

Modeling of δ^{15}N-NO$_3^-$ and δ^{18}O-NO$_3^-$ isotope geochemistry

In the isotope fractionation model (Equation 2.11 and 2.12) the total nitrate consumption rate was the sum of the exogenous and endogenous respiration rates (Equation 2.6). This overall rate was linked to the reaction rate of the individual nitrate isotopes (Equation 2.11 and 2.12) by the assumption of equal isotope fractionation factors for both types of respiration.

The modeling results fit the observation data well (Figure 2.5). In both cases, δ^{15}N-NO$_3^-$ and δ^{18}O-NO$_3^-$ increased between days 4 and 6, and this increase occurred simultaneously with nitrate reductions (Figure 2.2), indicating denitrification. The incorporation of isotope fractionation processes into the numerical biogeochemical model overcomes the limitations of the Rayleigh equation when the model is extended to a reactive transport model and applied at the field scale. Because the Raleigh equation was developed for a closed system, it does not account for hydrodynamic dispersion and other physical processes that occasionally contribute to isotopic variations (Abe and Hunkeler, 2006; van Breukelen, 2007; van Breukelen and Prommer, 2008; van Breukelen and Rolle, 2012). Van Breukelen and Prommer (2008) solved these limitations by simulating isotope fractionation processes in reactive transport models.
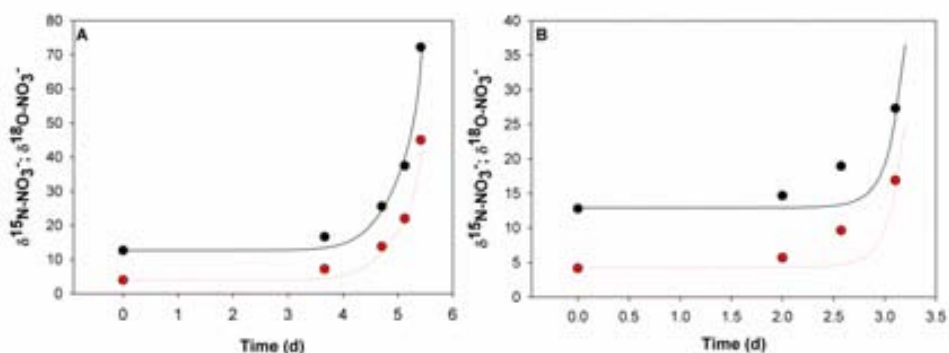
Figure 2.5 Evolution of experimental values δ^{15}N-NO$_3^-$ (●), δ^{18}O-NO$_3^-$ (●) over time with ethanol (A) and glucose (B) as carbon source versus modeled values (dotted red lines ···). The experimental data were taken from Vidal-Gavilan et al. (2013).

Modeling of δ^{13}C isotope geochemistry

All processes affecting δ^{13}C-DIC production were introduced into the model – the two types of respiration and calcite precipitation and/or dissolution. Figure 2.6 provides

the carbon network relationships between all species involved in the modification of δ^{13}C-DIC in the ethanol and glucose experiments. The incorporation of δ^{13}C-DIC into the model provided another parameter for checking validity.

The model fitted experimental data well for both the ethanol and glucose experiments (Figure 2.7). The stoichiometric relationships between organic and inorganic carbon (P parameters from Equation 2.14) were 0.538 moles ethanol/moles inorganic carbon and 2.881 and 3.119 moles glucose/moles inorganic carbon. The first glucose value relates to the reduction of nitrate to nitrite, whereas the second value relates to the reduction of nitrite to dinitrogen gas. These values were calculated considering the stoichiometry from reactions 2.1 to 2.2.2. Each model was verified by the δ^{13}C mass balance of all components remaining constant over the experiment (Figure 2.7).

In the ethanol experiment (Figure 2.7A), the calibrated fractionation factor for ethanol degradation ($\varepsilon_{DIC/Eth}$) was +8‰. This value implied that the initially produced δ^{13}C-DIC was enriched with ^{13}C relative to the organic substrate. However, a decrease in δ^{13}C-DIC was observed in the model (from -15.9 to -18.3‰). This phenomenon occurred because the ethanol was initially depleted in ^{13}C (δ^{13}C value -30.53‰) compared with initial δ^{13}C-DIC (-15.9‰) and the mixing effect was therefore more important than inverse fractionation. The ethanol δ^{13}C decreased to -39.7‰. Similarly, the δ^{13}C-biomass decreased from -20‰ until -29.7‰ ($\varepsilon_{biomass/Eth}$ was also +8‰). The majority of the carbon in the final biomass originated from ethanol. Consequently, at the end of the reaction, the biomass had a similar isotopic composition to the initial ethanol. The final value of δ^{13}C-biomass was not identical because the ethanol was not completely consumed (Figure 2.2).
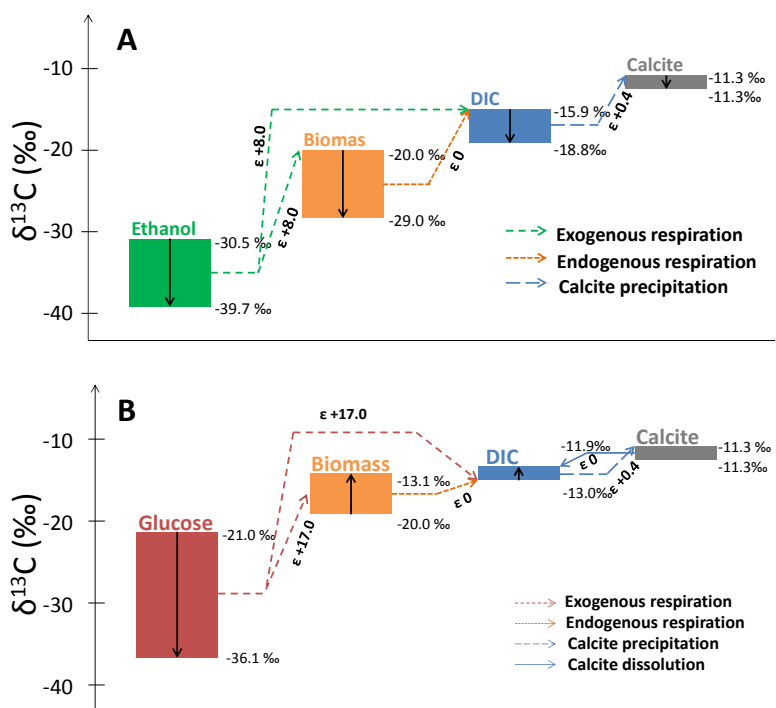
Figure 2.6 Reaction network of carbon isotope flow during biodenitrification in the ethanol (A) and the glucose experiments (B).

The model also considered the effect of calcite precipitation and its induced δ^{13}C-DIC depletion. Depletion of δ^{13}C-DIC due to calcite precipitation was also observed by Carrey et al. (2013) and van Breukelen et al. (2004). Calcite precipitation, however, was not as important as other processes. Most of the DIC changes resulted from different oxidation reactions (ethanol or glucose oxidation and decayed biomass oxidation). Therefore, the contribution of precipitation to changing δ^{13}C-DIC was minor.

In contrast, in the glucose experiments, the δ^{13}C-DIC slowly enriched until day 4, decreased until day 5, and finally increased again (Figure 2.7B). In this case, the calibrated carbon isotope fractionation factor for glucose degradation was +17‰. This large fractionation factor coupled with the initial glucose δ^{13}C, which was enriched relative to ethanol (-21‰), contributed to the initial enrichment of δ^{13}C-DIC and δ^{13}C-biomass. Between day 4 and the complete consumption of glucose (day 5), δ^{13}C-DIC decreased because the difference between δ^{13}C-glucose and δ^{13}C-DIC factored more importantly than inverse fractionation. Between day 5 and day 7.5, δ^{13}C-DIC enriched again because of endogenous decay and calcite dissolution (δ^{13}C-biomass and δ^{13}C-calcite were more enriched than δ^{13}C-DIC). The biomass behavior in the glucose

experiment was different from the biomass behavior in the ethanol experiment. Hall et al. (1999) observed a similar behavior of δ^{13}C-biomass in the degradation of phenol by *Rhodococcus* sp.

Furthermore, δ^{13}C-DIC was affected by both calcite dissolution and precipitation. Although these processes had only minor effects because they altered the DIC pool less than organic substrate degradation, calcite dissolution contributed to the initial and final enrichment of δ^{13}C-DIC because of the relatively heavy carbon isotope ratio of calcite (-11.3‰). Calcite precipitation exhibited the opposite behavior (as explained in the ethanol case), but its effect was also minor.

Both calibrated enrichment factors (+8‰ for ethanol and +17‰ for glucose) indicated an inverse fractionation (where the heavy isotope reacts faster than the light isotope existed) for both organic carbon sources. Both the modeled and experimental DIC results showed that denitrifiers preferred consuming the heavier ^{13}C in both organic carbon sources. It was also determined the model outcome without fractionation and with a normal fractionation effect (Figure 2.7). In both cases, the model results did not fit the experimental data. Goevert and Conrad (2008) found inverse fractionation of acetate was linked to sulfate reduction. They compared the metabolic pathways of different sulfate-reducing bacteria and concluded that if acetate was oxidized via the Acetyl-CoA pathway then a normal acetate fractionation existed. Conversely, if acetate was oxidized via the TCA-cycle, then an inverse acetate fractionation existed. The results could indicate that the denitrifiers used the TCA cycle for oxidation. However, although carbon isotope fractionation in sulfate reduction has been studied, little research has been conducted on this type of fractionation during denitrification. To draw conclusions, additional experiments would be necessary to corroborate the modeled results and to study how different metabolic pathways in denitrifiers might influence the carbon isotopic fractionation of the organic substrates.

Figure 2.7 Evolution of experimental values (●) versus modeled values (lines --) of δ^{13}C-DIC and modeled values of δ^{13}C-species. The experimental data were taken from Vidal-Gavilan et al. (2013).

Both calibrated enrichment factors (+8‰ for ethanol and +17‰ for glucose) indicated an inverse fractionation (where the heavy isotope reacts faster than the light isotope existed) for both organic carbon sources. Both the modeled and experimental DIC results showed that denitrifiers preferred consuming the heavier ^{13}C in both organic carbon sources. It was also determined the model outcome without fractionation and with a normal fractionation effect (Figure 2.7). In both cases, the model results did not fit the experimental data. Goevert and Conrad (2008) found inverse fractionation of acetate was linked to sulfate reduction. They compared the metabolic pathways of different sulfate-reducing bacteria and concluded that if acetate was oxidized via the Acetyl-CoA pathway then a normal acetate fractionation existed. Conversely, if

acetate was oxidized via the TCA-cycle, then an inverse acetate fractionation existed. The results could indicate that the denitrifiers used the TCA cycle for oxidation. However, although carbon isotope fractionation in sulfate reduction has been studied, little research has been conducted on this type of fractionation during denitrification. To draw conclusions, additional experiments would be necessary to corroborate the modeled results and to study how different metabolic pathways in denitrifiers might influence the carbon isotopic fractionation of the organic substrates.

2.3.4 Considerations for extending the biogeochemical model to a reactive transport model for Enhanced *in situ* Biodenitrification applications

The integrated biogeochemical model presented here was intended to be a key step in an integrated EIB reactive transport model at the field scale. Because this model was calibrated and validated at the batch scale, some issues should be considered before applying it at the field scale: (i) nutrient bioavailability, (ii) biomass distribution over the aqueous and solid phases, and (iii) effects of biomass clogging and carbonate mineral interaction, as discussed below.

First, the bioavailability of the main nutrients (nitrate, organic substrates and micronutrients) will vary spatially at the field scale, in contrast to the batch scale. For example, injected substrates and biomass may not mix well with the nitrate polluted groundwater, which can cause large spatial variations in the EIB rates. The applied RTM should thus describe these reaction fronts well. Second, the batch scale model did not distinguish between aqueous and solid-phase biomass. A RTM of EIB may therefore need to include this distribution and include the mobility/sorption of the denitrifying biomass.

Third, biomass growth and carbonate mineral interactions during EIB may affect hydrogeological parameters such as porosity and hydraulic conductivity. The biomass should therefore be monitored at EIB sites, and its interaction with groundwater flow must be considered in RTMs of EIB. Furthermore, geochemical modeling has shown that the type of carbon source and the interaction with carbonate minerals needs to be evaluated during field applications. As shown, carbon sources induce either carbonate precipitation or dissolution. Precipitation and dissolution of minerals in aquifers may generate significant changes in the hydraulic properties (hydraulic conductivity and porosity) over extended periods of time, which in turn can cause considerable operational problems and even obstruct further implementation (Li et al., 2006; Noiriel et al., 2012).

Moreover, carbonate precipitation linked to bioclogging can cause significant operational problems for EIB implementation. The injection of carbon sources that induce calcite dissolution could solve problems related to decreases in hydraulic conductivity. Further modeling and/or experiments are necessary to evaluate how hydraulic conductivity changes with different combinations of organic carbon sources.

2.4 Conclusions

An integrated numerical model accounting for isotope fractionation was developed to predict the water chemistry during batch-scale enhanced biodenitrification experiments. The model's results fitted well with the experimental data. The model improved on existing biodenitrification models by considering both the geochemical interactions induced by enhanced biodenitrification itself and the stable isotope behavior associated with all processes. Moreover, the model also considered the accumulation of nitrite in a glucose experiment. Because of the imbalanced proton consumption and CO_2 production resulting from denitrification, carbonate mineral (calcite) dissolution/precipitation was found to be an important associated process that must be investigated before and during field applications.

The incorporation of isotope fractionation in the model allows for accounting of hydrogeological processes, such as dilution and dispersion, in a reactive transport model version on EIB field applications. The EIB model extension with simulation of $\delta^{13}C$-DIC is significant as this isotope parameter is affected by all main EIB processes, thereby enabling an overall check of model consistency.

Both calibrated enrichment factors (+8‰ for ethanol and +17‰ for glucose) indicated that the heavy isotope reacted faster than the light isotope (inverse fractionation). More experiments are necessary to corroborate the modeled results and to study how different metabolic pathways could influence the carbon isotopic fractionation of the organic substrates.
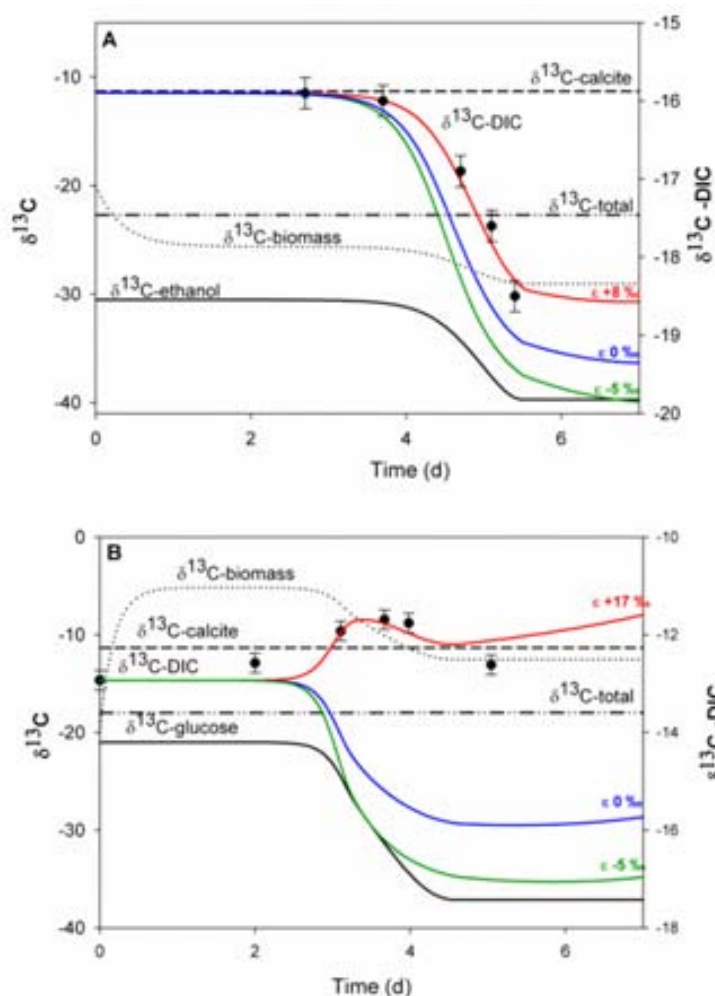
This model provides the basis for incorporating isotopic fractionation processes into numerical EIB field models. For example, the presented Phreeqc model can be implemented in PHAST (Parkhurst et al., 2010) and PHT3D (Prommer and Post, 2010). Both PHAST and PHT3D couples Phreeqc to a 3-D groundwater flow and solute transport model, enabling 2D/3D simulations at field scale and thereby accounting for other hydrogeological processes (e.g., dilution).

CHAPTER 3

Modeling biogeochemical processes and isotope fractionation of Enhanced *in situ* Biodenitrification in a fractured aquifer[*]

3.1   Introduction

Many technologies are available for treating nitrate from groundwater, such as reverse osmosis, ion exchange, electrodialysis, and chemical and biological denitrification (McAdam and Judd, 2007; Ricardo et al., 2012; Schnobrich et al., 2007). Most of these technologies focus on *ex situ* treatments, which are inherently more expensive than *in situ* treatments due to energy consumption and the interference with surface activities (e.g., building a treatment plant) (Della Rocca et al., 2007). Biological denitrification, which is known as Enhanced *In situ* Biodenitrification (EIB), has environmental and economic advantages over other methods because it is simple, selective, and cost effective (Smith et al., 2001).

Geochemical interactions occur between the biodenitrification reactants and the porous geological medium in response to biodegradation reactions. These interactions may play a critical role in the implementation of EIB. Because of inorganic carbon

[*]Chapter based on Rodríguez-Escales, P., Folch, A., Vidal-Gavilan, G., van Breukelen, B.M. 2014. Modeling biogeochemical processes and isotope fractionation of enhanced *in situ* biodenitrification in a fractured aquifer.Submitted to Water Research.

production and pH alteration, carbonate mineral dissolution/precipitation is induced by changes in the initial hydrogeological properties of the aquifer by heterotrophic biodenitrification (see Chapter 2). These changes can modify the hydrogeological characteristics of the aquifer and modify the efficiency of the groundwater treatment (Li et al., 2006; Noiriel et al., 2012).

Another important factor when monitoring EIB in the field is dilution caused by hydrodynamic dispersion, mixing (with recharge) or other processes. Because of dilution, a decrease in nitrate concentration cannot always be attributed to degradation. Monitoring the changes in the nitrogen and oxygen isotope ratios of nitrate (δ^{15}N-NO$_3^-$ and δ^{18}O-NO$_3^-$) allows degradation to be identified (Carrey et al., 2013; Otero et al., 2009; Puig et al., 2013) and nitrate transformation and dilution to be distinguished. In EIB applications, this distinction improves the characterization of the clean groundwater plume and allows nutrient injection to be optimized, which reduces treatment costs.

Despite the many studies that have characterized isotopic processes associated with biodenitrification using the Rayleigh equation, recent studies have shown that this equation does not always give accurate results at the field scale (Abe and Hunkeler, 2006; van Breukelen, 2007; van Breukelen and Prommer, 2008; van Breukelen and Rolle, 2012). This is because the Rayleigh equation was developed for a closed system (van Breukelen, 2007) and does not account for hydrodynamic dispersion and other physical processes that occasionally contribute to isotopic variations. These limitations have been addressed by incorporating isotope fractionation processes into numerical or analytical reactive transport models (van Breukelen and Prommer, 2008).

In addition to nitrate isotopes, several other isotopes are involved in EIB and help to quantify the reaction network (biological reactions and geochemical interactions). The inclusion of dissolved inorganic carbon isotopes (δ^{13}C-DIC) in the biogeochemical model, which are involved in both direct (oxidation of organic carbon) and indirect processes (carbonate mineral interaction) of enhanced biodenitrification, is expected to allow better evaluations of the consistency of the model due the central role thatδ^{13}C-DIC plays in the overall reaction network.

In this context, RTMs allow quantitative analyses of the interactions between transport and reaction processes (Steefel et al., 2005) and provide a framework to integrate the different reactive processes involved in EIB, such as microbiological respiration, water-rock interactions and isotope fractionation.

Several studies have evaluated biodenitrification using numerical models at different scales (see Chapter 1 and Appendix 1). Nevertheless, there is a lack of models that integrates microbiological, geochemical and isotope geochemistry in one RTM at field scale. Because of this lack of knowledge, the aim of this chapter is to develop a reactive transport model that considers microbiological processes, geochemical interactions, and complete isotope geochemistry during EIB in a fractured media at the field scale. In fractured aquifers, hydrogeological parameters such as heterogeneity, connectivity between the fracture networks, flow dynamics, and porosity differ notably from those in more extensively tested alluvial aquifers and may pose difficulty for the modeling of *in situ* technologies. The model focuses on microbiological processes, such as exogenous and endogenous nitrate and sulfate respiration coupled with microbial growth and decay, geochemical processes, such as the precipitation of calcite, nitrate isotopic fractionation, including δ^{15}N-NO$_3^-$ and δ^{18}O-NO$_3^-$, and carbon isotope interactions. In addition, once the model was constructed, the extent of biodenitrification using nitrate isotopes was also evaluated with the Rayleigh equation to assess its use from a practical perspective.

3.2   Materials and Methods

3.2.1   Field Site

The experimental data used in this chapter were obtained from Vidal-Gavilan et al. (2013). The site was located in Roda de Ter (442270, 4647255 UTM31/ETR89) in the central part of the Osona region (100 km north of Barcelona, Spain) (Figure 3.1). The area is recognized as being vulnerable to nitrate pollution due to the large amount of pig farming. Nitrate levels in the groundwater have reached 200 mg/l or more for the last 10-20 years (Otero et al., 2009).
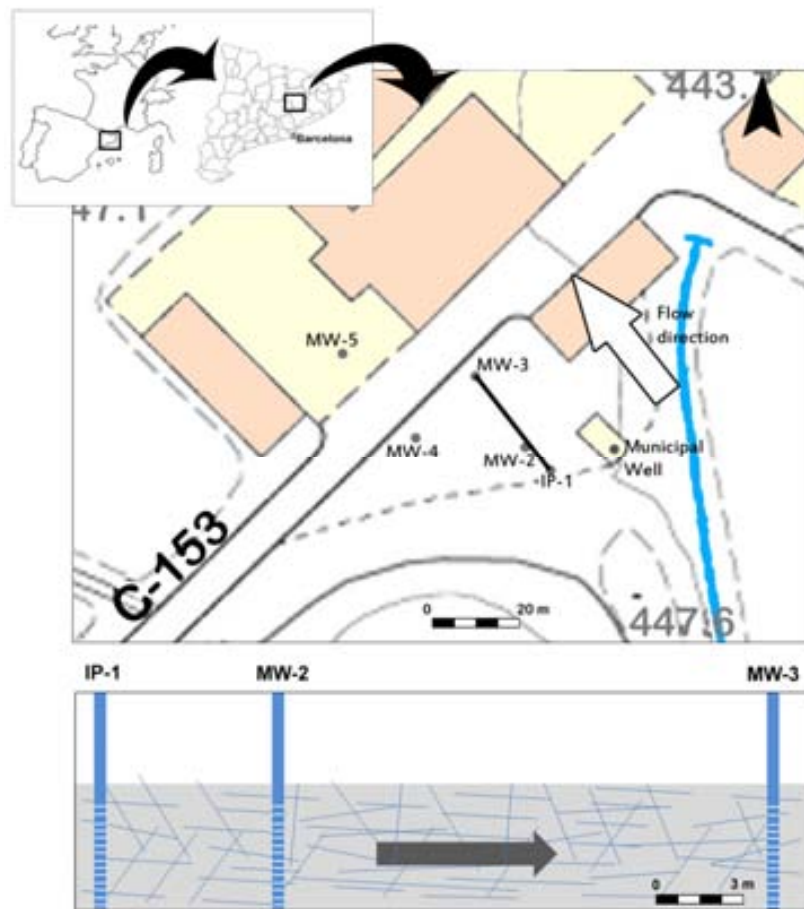
Figure 3.1 Pilot test layout and cross section considered in the model. IP means Injection Point, and MW means Monitoring Well. The model simulates the effect of ethanol injection between the IP and MW-3. Modified from Vidal-Gavilan (2013).

The aquifer in the area is composed of marls with a subvertical fracture network (NW–SE and NNE–SSW) and horizontal bedding joint surfaces. Groundwater flow occurs due to the fracture-related secondary porosity, and the main groundwater flow direction is SE to NW. The groundwater level was at a depth of 8.5–9 m.b.s. (Meters below surface) and has an average temperature of 15°C.Due to the good connection between the subvertical and horizontal fractures, the formation behaves as an unconfined aquifer at shallow levels. The experimental site covers an area of approximately 1000 $m^2$and was monitored with six piezometers with an average depth of 12.5 m.b.s. (432.5 m a.s.l.). The screening levels covered the aquifer thickness (4-5 m) (Vidal-Gavilan et al. 2013).

Before application of EIB, pumping and bromide-tracer tests were carried out to characterize the hydrogeological parameters and flow conditions. The pumping test was performed using MW-2 as the pumping well (due to its central location at the site; see Figure 3.1) and other monitoring wells (IP, MW-1, MW-3, MW-4 and MW-5) as observation points. The pumping test indicated good connectivity between the boreholes despite being in a fractured aquifer. It also indicated a relatively homogeneous effective permeability of approximately 5 m/day. This value was determined using the analytical model of Copper-Jacob (Copper and Jacob, 1946), which is a good approximation for the transmissivity in heterogeneous media (Meier et al., 1998).

To determine the flow velocity and dispersivity, a tracer test was performed with bromide under natural flow conditions. IP-1 was used as the injection point of the bromide, and MW-2 and MW-3 were used as observation wells. Bromide was monitored at three depths (11 m.b.s., 12m.b.s., 13m.b.s.), which covers the full depth of the piezometers. The different tracer arrivals in the monitoring wells indicated a preferential flow path at depth (13 m.b.s.) between IP and MW-2. These depth differences in bromide concentrations were not observed in MW-3, indicating a homogenization of the bromide transport along the flow line. The average groundwater flow velocity was approximately 30 m/d. Based on the calculated hydraulic conductivity, the effective porosity was between 10^{-3} and 10^{-4}. Using the analytical model (Sauty, 1980), the longitudinal dispersivity coefficient was calculated as 1 m between IP and MW-2 and 5 m between IP and MW-3. The vertical dispersivity coefficient was assumed to be 10% of the longitudinal dispersivity.

EIB was applied using the installed piezometers and an abandoned municipal supply well. One piezometer was used as an injection point (IP), and five monitoring wells (MW-num.) located downgradient were used as observation wells. Groundwater flowed in the direction from IP to MW-3 (Figure 3.1). The municipal well (located upgradient from the injection point) was used as the extraction point for the groundwater used for injection and as a reference to characterize the nitrate concentration in the aquifer before EIB treatment.

Biodenitrification activity was stimulated and sustained by the regular addition of ethanol as an organic carbon source and disodium hydrogen phosphate as a phosphate source. A 1 m^3 tank of groundwater from the extraction point (with the hydrochemical properties shown in Table 3.1) with concentrations of 630 mg/l of ethanol and 10 mg/l of disodium hydrogen phosphate were added regularly every

72h. The amended water was then injected by gravity. The injection events lasted for 50 min. Dilution of the nitrate in the groundwater due to injection was avoided because the injected solution was prepared with a groundwater solution.

Table 3.1 Hydrochemistry of the aquifer and the injection solution from Vidal-Gavilan et al. (2013).

Parameter	Unit	Aquifer solution Value	Injected solution Value
Ethanol	mM		13.69
Nitrate	mM	1.9	1.9
DIC	mM	9.53	9.53
pH		6.7	6.7
Temperature	ºC	15	15
Chloride	mM	1.43	1.43
Sulfate	mM	1.03	1.03
Calcium	mM	4.6	4.6
Sodium	mM	2.25	2.25
Magnesium	mM	1.38	1.38
Potassium	mM	2.41	2.41
δ^{15}N-NO$_3^-$	‰	12.31	12.31
δ^{18}O-NO$_3^-$	‰	2.91	2.91
δ^{13}C-DIC	‰	-11.31	-11.31
δ^{13}C-Ethanol	‰		-30.51

Two types of experiments were performed. The first experiment was performed for five months and was aimed at evaluating the feasibility of the technology in the fractured media. The second experiment focused on a slug injection of ethanol after the system had stopped and when the nitrate background had recovered for two weeks. The aim of the second experiment was to evaluate the recovery of the system after injection stopped. *In situ* biodenitrification was followed by sampling events every 8 h for 48 h to determine the environmental conditions (conductivity, pH, Eh, dissolved O$_2$ and temperature) and the chemical (anions, cations, NH$_4$, alkalinity, remaining C source, dissolved organic and dissolved inorganic carbon(DOC and DIC)) and isotopic parameters (δ^{15}N-NO$_3^-$, δ^{18}O-NO$_3^-$, and δ^{13}C-DIC). Samples were obtained from the middle part of the screened interval in the saturated zone (between 434 and 435 m a.s.l.) by bailer sampling (1 l volume) (Figure 3.1). The reactive transport model was focused on the slug injection event for constant groundwater flow conditions (no effect of recharge or pumping).

3.3   Modeling

A multicomponent reactive transport model was developed with PHAST (Parkhurst et al., 2010) and was used to perform two dimensional cross-sectional simulations of

transport, degradation reactions, geochemical interactions, and corresponding isotopic changes. The model focused on the slug injection of ethanol and its subsequent monitoring for the two days of injection. The model simulated the cross section between the injection point (IP) and monitoring well 3 (MW-3) (located 26.5 m from the IP) along the groundwater flow direction and considered a saturated thickness of 4 m (see Figure 3.1). The model was run for a two day period at a time step of 0.005 days. The model domain was 26.5 m long, 4 m deep, and used a uniform 0.5 x 0.1 m grid. Both the time step and the cell size values were calculated according to the Peclet (Equation 3.1) and Courant (Equation 3.2) numbers.

$$\frac{\Delta l}{\alpha} < 2 \qquad\qquad (3.1)$$

$$\frac{v\Delta t}{\Delta l} < 1 \qquad\qquad (3.2)$$

where Δl is the size of the cell (length and height) [L], α is the dispersivity coefficient (longitudinal or vertical) [L], v is the groundwater velocity [LT^{-1}], and Δt is the time step [T].

The aquifer was treated as unconfined with constant heads and concentrations on the upstream and downstream boundaries. Constant head values were assigned to simulate the gradient observed during the field experiments. Because no changes in flow were observed during the slug injection (no rainfall or pumping), zero flux conditions were assigned to the lateral and bottom boundaries.

First, a conservative transport model was used to determine the hydrogeological parameters (hydraulic conductivity, porosity, and dispersivity) and their distributions in the model domain. The model was developed in PHAST (a numerical model) instead of using an analytical model because PHAST enables to account for the different flow velocities observed in the field tests. Next, the reactive transport model was developed using the hydraulic parameters from the conservative transport model.

3.3.1   Conservative transport

The conservative transport model was constructed based on the bromide (conservative ion) tracer test. The main aim of this step was to adjust the hydrogeological parameters, including hydraulic conductivity, porosity, and dispersivity coefficient and their variations through the model domain. The model was a transient model because it considered the injection of bromide at the IP. The model

was calibrated with the bromide observations from the tracer test under natural flow conditions at three depths in piezometers MW-2 and MW-3.

3.3.2 Biogeochemical reactive transport model

The model simulated the injection of an ethanol solution (previously mixed at the surface with groundwater from the aquifer) at the injection point (IP) and its evolution downgradient over two days. The model was run in transient conditions considering the initial heads measured before the biodenitrification started. The model was calibrated with the observations in MW-2 and MW-3.

The reactive transport model involved microbiological processes (exogenous and endogenous respiration with nitrate and sulfate coupled to microbial growth and decay) and geochemical processes (calcite precipitation). Aerobic degradation was neglected because the oxygen concentration of the groundwater was less than 1 mg/l. Denitrification can occur when the dissolved oxygen concentrations are less than 1-2 mg/l (Cey et al., 1999; Korom, 1992). Moreover, ethanol degradation due to oxygen consumption was negligible at these concentrations. Changes in iron were not observed; therefore, iron reduction was not considered.

Microbiological processes

Both nitrate and sulfate respiration coupled to microbial growth were modeled using double Monod kinetics considering the thermodynamic limitations of the Monod equations described in Jin and Bethke (2003). The model assumed three main expressions: one for the electron donor (ethanol; Equation 3.3), one for the electron acceptor (nitrate or sulfate; Equation 3.4) and one for biomass (denitrifier or sulfate reducer biomass; Equation 3.5).

$$r_{ED} = -k_{max} \frac{[ED]}{[ED]+K_{S,ED}} \frac{[EA]}{[EA]+K_{S,EA}} [X] \, F_T \qquad (3.3)$$

$$r_{EA} = Qr_{ED} - Sb_d X_d - Sb_s X_s \qquad (3.4)$$

$$r_X = -Y_h r_{ED} - b[X] \qquad (3.5)$$

where [ED] is the concentration [M L^{-3}] of the electron donor (ethanol), [EA] is the concentration of the electron acceptor (nitrate or sulfate; [M L^{-3}]), [X] is the biomass

concentration (denitrifier (X_d) or sulfate reducer (X_s); [M L^{-3}]), k_{max}[T^{-1}] is the maximum consumption rate of the electron donor, $K_{s\ ED}$ [M L^{-3}] and $K_{s\ EA}$ [M L^{-3}] are the half-saturation constants of the electron donor and electron acceptor, respectively, b [T^{-1}] is the decay constant (b_d is referred to denitrifier biomass and b_s to sulfate reducer), F_T is referred to as the thermodynamic factor, and Y_h (microbial yields), Q, S and T are stoichiometric parameters ([M$_X$M$_{ED}^{-1}$];[M$_{EA}$ M$_{ED}^{-1}$]) that relate the electron donor consumption to biomass growth and the electron donor to the electron acceptor, respectively.

The stoichiometric relationships are based on Reactions 3.1 (Chapter 2) and 3.2, which summarize the redox respiration reaction in nitrate and sulfate reduction coupled with microbial growth. In those reactions, the biomass was considered to have an average chemical composition of $C_5H_7O_2N$ (Porges et al., 1956). The portions of the substrate's electrons used for cell synthesis during these anoxic processes were assumed to be 0.682 and 0.882 moles C-biomass/moles C-ethanol for denitrification and sulfate-reduction, respectively, based on the calculations described in McCarty (1975). S is a stoichiometric parameter that relates the endogenous electron donor consumption from denitrification and sulfate reduction to nitrate consumption. This value is internally calculated by Phreeqc and its value is 0.92 molC$_{endogenous}$/mol Nitrate (Chapter 2).

0.083 C_2H_5OH + 0.088 NO_3^- + 0.043 H^+= 0.024 $C_5H_7O_2N$ +0.032 N_2 + 0.045 HCO_3^- +0.164 H_2O

Reaction 3.1

0.083 C_2H_5OH + 0.0221 SO_4^{2-} + 0.029 NO_3^- + 0.0539 H^+ = 0.0221 H_2S + 0.0294 $C_5H_7O_2N$ +0.0196 HCO_3^- + 0.1422H_2O
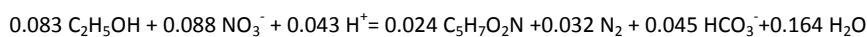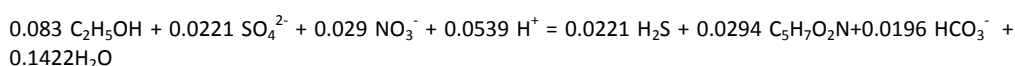
Reaction 3.2

The Monod equations do not take into account that microbial metabolism in natural environments is subject to significant thermodynamic control. Jin and Bethke (2003) proposed the incorporation of a thermodynamic factor in the Monod equation (F_T; Equation 3.6).

$$F_T = 1 - e^{\left(\frac{f}{\chi RT}\right)}$$

(3.6)

where f is the net thermodynamic driving force for microbial respiration, which is related to the change in free energy of the redox reaction (ΔG) and the phosphorylation potential (ΔG$_p$) (which is assumed to be 50 kJ/mol under typical physiological conditions (White, 2000)), χ is the average stoichiometric number, R is

the gas ideal constant, and T is the temperature. When the system has sufficient energy, the thermodynamic factor is equal to one, and the Monod expressions can be used by themselves. Nevertheless, when there is a lack of energy, the thermodynamic factor is less than one, and the thermodynamic factor should be considered.

The model incorporated two types of biomass: the denitrifier and the sulfate reducing biomass. Both types of biomasses were assumed to remain attached to the sediment. Because the model was focused on a system with mature biofilm, the initial value of the denitrifier biomass was taken as the maximum value of the biomass simulated in a previous batch model using the same groundwater composition of field site and following the equations developed in Chapter 2. The initial value was 9×10^{-4} M, and the same initial concentration was applied for both types of biomass. This approach was also followed by Tang et al. (2013), who used the same initial value for different populations (denitrifiers, Fe reducers, sulfate reducers, fermenters and methanogens) in amodel of uranium redox transformation.

Geochemical processes

The main abiotic geochemical process considered was calcite precipitation. In previous chapter was observed that depending on the carbon source, calcite precipitation or dissolution could be induced. When ethanol was the external carbon source, calcite precipitation was induced due to the imbalanced proton consumption and CO_2 production (Reaction 3.1). The expressions of calcite precipitation are described in previous chapter. Potential changes in porosity were calculated using the Equation 3.7 and initial porosity.

$$\phi = \frac{V_o - \rho_{cc} M_{cc}}{V_t} \tag{3.7}$$

where ϕ is the porosity [-], V_o is the initial void volume [L^3], ρ_{cc} is the calcite density [$M L^{-3}$] (2.71 g cm^{-3}) and V_t is total volume.

3.3.3 Stable isotope geochemistry model

The isotopic fractionation of nitrogen and oxygen in nitrate and of carbon compounds was included in the model. The isotopic fractionation modeling of nitrate was based on model described in Chapter 2. The kinetic isotope enrichment factors (ε) were obtained from the batch experiments of Vidal-Gavilan et al. (2013), who determined the factors via application of the Rayleigh equation (-12.9 ‰ and -8.8 ‰ for the nitrogen and oxygen of nitrate, respectively). The batch experiments were performed

with the groundwater and the sediment of the field site and using ethanol as the external organic carbon source.

The carbon isotope network was based on model described in Chapter 2, which was an extended model of van Breukelen et al. (2004). The model considered the carbon isotopes of ethanol (δ^{13}C-ethanol), inorganic carbon (δ^{13}C-DIC), denitrifier biomass (δ^{13}C-denitrifier biomass), sulfate reducer biomass (δ^{13}C-sulfate-reducer biomass), and calcite (δ^{13}C-calcite). Compared to the batch models of previous chapter, it also included the oxidation of ethanol due to sulfate reduction and the decay of sulfate-reducing biomass. To simplify the model and because degassing is not quantitatively important, the contribution of degassing to ^{13}C-DIC was assumed to be negligible. The complete carbon isotope network for this field experiment is outlined in Figure 3.2. The model was calibrated with the δ^{13}C-DIC observations.
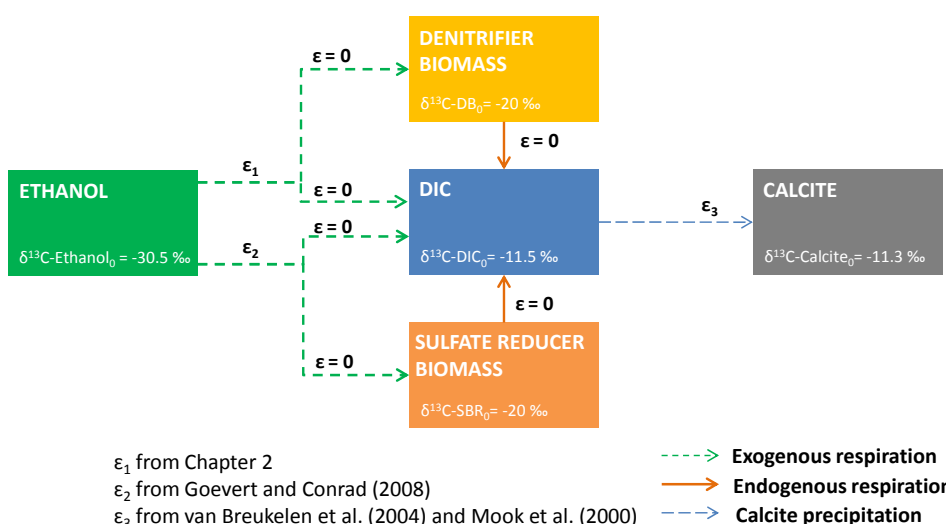
Figure 3.2 Carbon isotope reaction network for the field experiment with different isotope fractionations and initial conditions.

The carbon isotope fractionation of ethanol during denitrification was taken from previous chapter (ε =+8 ‰). However, it was not determined the fractionation factors for the oxidation of ethanol associated with to sulfate reduction. Consequently, both fractionation factor determined by Goevert and Conrad (2008) were used for the oxidation of acetate by heterotrophic sulfate-reducers (ε=+1.8‰ and -19.1 ‰) because acetate is a metabolite of ethanol in many sulfate reduction metabolisms

(Nagpal et al., 2000). The large difference between the fractionation factors observed by Goevert and Conrad (2008) occurred because the sulfate reducers used different metabolic pathways to reduce the acetate. These authors attributed normal fractionation (ε=-19.1‰) to the sulfate reducers that oxidized acetate via the Acetyl-Coa pathway and inverse fractionation (ε=+1.8‰) when acetate was oxidized via the TCA-cycle.

The $\delta^{13}C$ contents of heterotrophic biomass for *Pseudomonas aeruginosa* have been found to vary from -10.3 to -25.4 ‰ (Blair et al., 1985; Coffin et al., 1990). It was adopted -20 ‰ for both the denitrifiers and sulfate-reducers. For calcite precipitation, the $\delta^{13}C$-DIC modification was calculated following the procedure of van Breukelen et al. (2004) and described in Chapter 2.

3.3.4   Evaluation of the extent of Enhanced *in situ* Biodenitrification: RTM *versus* Rayleigh equation

In order to evaluate the use of Rayleigh equation to determine the extent of biodenitrification from a practical perspective, results using RTM and Rayleigh equation were compared. In general, the extent of biodegradation (B%) is related to the fraction of degradation of target pollutant, in this case nitrate (Equation 3.8).

$$B\ (\%) = (1 - f_{deg})x100 \tag{3.8}$$

where f_{deg} is the remaining fraction of the target compound (C/C_0). To facilitate the comparison of the extent of EIB, nitrate reduction was only related to ethanol degradation, and the biomass decay was assumed to be zero.

For the case where the extent of biodegradation is calculated using the Rayleigh equation, $B_{Rayleigh}$ (%), the degradation fraction ($f_{deg,\ Rayleigh}$) was related to the isotope signals (Equation 3.9) (van Breukelen, 2007).

$$f_{deg,\ Rayleigh}\ = e^{\Delta/\varepsilon} \tag{3.9}$$

where Δ (‰) represents the isotopic shift of a sample with respect to the source, and ε represents the kinetic isotopic enrichment factor. The extent of biodegradation calculated using the RTM, B_{RTM} (%), was calculated by adding a tracer test at the same concentration of ethanol in the injected water of the model and relating the degradation of ethanol to nitrate using a stoichiometric relation (Equations 3.10, 3.11, and 3.12).

$$\Delta_{Eth,deg} = C_{tracer} - C_{eth} \tag{3.10}$$

$$\Delta_{Nit,deg} = \Delta_{Eth,deg}Q \tag{3.11}$$

where $\Delta_{Eth,deg}$ represents the degraded ethanol [ML^{-3}], C_{tracer} represents the tracer concentration [ML^{-3}], C_{eth} represents the ethanol concentration [ML^{-3}], $\Delta_{Nit,deg}$ represents the total degraded nitrate [ML^{-3}], Q represents a stoichiometric factor between ethanol and nitrate (1.06 mol nitrate mol ethanol^{-1}). A degradation factor ($f_{deg, RTM}$) was then calculated using Equation 3.12, and B_{RTM} (%) was calculated using Equation 3.8.

$$f_{deg,RTM} = \frac{C_0 - \Delta_{Nit,deg}}{C_0} \tag{3.12}$$

where C_o represents the initial nitrate concentration in the aquifer [ML^{-3}]. The difference between the extents of EIB calculated by the Rayleigh equation and the RTM is evaluated by the theta value (Equation 3.13). When Ө values are lower than 100, Rayleigh equation underestimates the extent of degradation, whereas for higher values overestimates. This approach has been used in several studies (Abe and Hunkeler, 2006; van Breukelen and Prommer, 2008).

$$\theta = \left(1 - \frac{Inf_{deg,Rayleigh}}{Inf_{deg,RTM}}\right)x100 \tag{3.13}$$

3.4 Results and discussion

3.4.1 Conservative transport model

Before the buildup of the RTM, a model that only considered conservative transport was run and validated using the tracer test results with bromide (Figure 3.3). To avoid scaling problems with the hydrogeological parameters (e.g., extrapolation of parameters from the laboratory to the field or from the regional to the local scale), the tracer test was carried out in the same domain as where EIB occurred. Scale dependence has been identified for several transport parameters, such as diffusion (Liu et al., 2008; Zhou et al., 2007), transmissivity (Sánchez-Vila et al., 1996), and dispersivity (Fernàndez-Garcia et al., 2005).
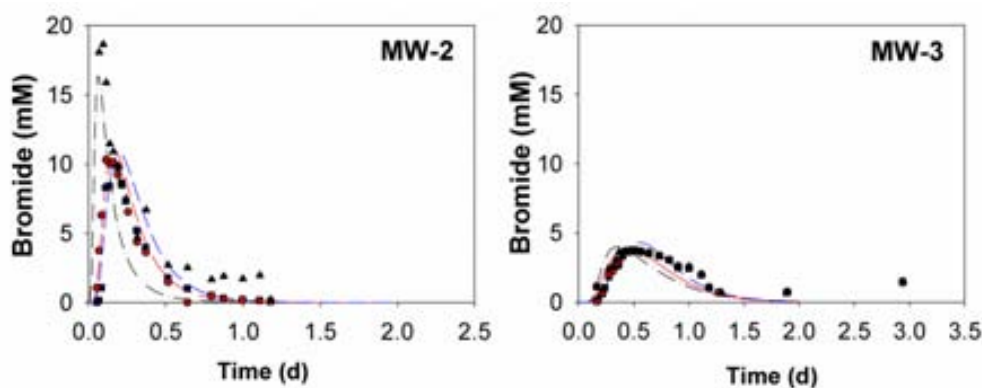
Figure 3.3 Observations (data points: Δ, 434 m.a.s.l.; ● , 435 .a.s.l. m; □, 436 m.a.s.l.) *versus* modeling results (lines) (dotted line, 434m.a.s.l., --435 m.a.s.l., — 436m.a.s.l.).

Multilevel monitoring indicated an earlier arrival and higher concentrations of bromide in the deeper part of MW-2 (Figure 3.3). These depth differences in bromide concentration were not observed in MW-3, which indicates a homogenization of bromide transport along the flow line. Therefore, this fractured aquifer was assumed as an equivalent porous medium (same values of hydraulic conductivity and porosity) with faster flow at depth between the injection point (IP) and MW-2, which was characterized in the model with higher hydraulic conductivity. Because the tracer test was performed at the same site as the EIB and at the same scale, the hydraulic parameters determined in the field were directly extrapolated to the EIB model.

The calibrated value of hydraulic conductivity was 7.5 m/d, which was similar to the value in the analytical model (5m/d). The faster flow at depth was modelled as a zone of permeability of 32 m/d. The porosity (effective porosity) was considered to be homogenous and having a value of $7x10^{-4}$, which was in the range of the porosities determined in the field (between $1x10^{-3}$ and $1x10^{-4}$). This porosity was only related to the secondary porosity because groundwater flow occurs mainly through fractures (Vidal-Gavilan et al., 2013). The model was calibrated using two dispersivity coefficients depending on the distance to the injection point (1.4 m from 0 to 12.5 m in the domain and 6.5 m from 12.5 to 26.5 m). The obtained values are consistent with the scale of the biodenitrification application (Gelhar et al., 1992; Xu and Eckstein, 1995). Traditionally, dispersivity is a transport parameter that varies with scale (Fernàndez-Garcia et al., 2005; Gelhar, 1986).

Note the small increase of bromide in MW-3 after day two (Figure 3.3). This increase was ascribed to a slower groundwater flow component as part of the fracture network

with lower hydraulic conductivity or due to effects of the injection. Nevertheless, because the biodenitrification model extended for only two days, this flow component was not quantitatively important and was not included in the model.

3.4.2 Biogeochemical Reactive Transport Model
Microbiological processes

Once the conservative model was calibrated, the RTM was constructed and calibrated. The modeling was performed taking the hydrogeological parameters determined in the conservative transport model with refreshed head constants. In this case, the head levels differed from the tracer test and the hydraulic gradient was higher; consequently, the flow velocity increased. The flow velocity during the slug injection in most of the domain was approximately 50 m/d. All of the hydrogeological parameters were assumed to be constant with time because the model only ran for two days, and potential changes due to bioclogging, flow conditions, and/or mineral interactions were negligible.

Prior to the reactive transport model, the thermodynamic factor in the system was evaluated. The results indicated that the thermodynamic factor was equal to one in the biodenitrification process and very close to one in the sulfate reduction (higher than 0.98) (Figure 3.3). Thus, it was simplified that both thermodynamic factors were equal to one, and it was used the double Monod equations without further considering thermodynamic limitations. Several authors have found that the thermodynamic factor for nitrate respiration is equal to one (André et al., 2011; Jin and Bethke, 2005). Nitrate respiration is characterized by a strong thermodynamic driving force. In such cases, the thermodynamic control can be ignored (Jin and Bethke, 2005). For respiration that utilizes less powerful thermodynamic driving forces, such as sulfate reduction, the thermodynamic control of the respiration rate can be dominant; however, in this case, it is close to one and was ignored.
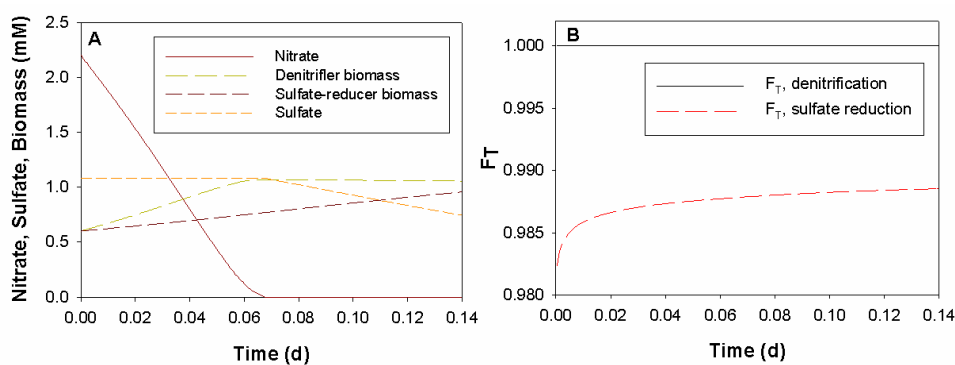
Figure 3.4 Modeling results of previous batch models used to evaluate the thermodynamic factor.

Figure 3.5A shows the results of the 2D RTM for the upper and lower ends of wells MW-2 and MW-3 using the parameters in Table 3.2. In general, the model fits well, and the modeled values matched the observations. Both MW-2 and MW-3 showed decreasing nitrate concentrations until non-detectable levels were present in less than 0.2 days. This rapid reduction in concentration can be attributed to the high activity of biomass that was stimulated during the previous five months. The modeled nitrate concentration at MW-3 began to increase after less than one day, while the observed concentrations stayed at zero. The later breakthrough of nitrate observed in the field was attributed to the slower flow described in the tracer test (see section 3.1.1) that was not taken into account in the model (Figure 3.3).

Although the amount of organic carbon injected during the field test was calculated using the stoichiometric relationship determined from biodenitrification reactions (Vidal-Gavilan et al., 2013), sulfate reduction was observed. Sulfate decreased over time in both MW-2 and MW-3 (Figure 3.5), indicating that there was another source of organic carbon. Biomass by itself was attributed as another organic carbon source. Through endogenous decay, biomass used itself as an electron donor; consequently, the redox system did not stop with nitrate arriving at sulfate-reduction (in this system, the iron and manganese concentrations were not important, and the redox system passes directly to sulfate reduction). Endogenous decay has been observed to act as an extra organic carbon donor in other studies, such as in tetrachloroethylene biodegradation (Béranger et al., 2006).
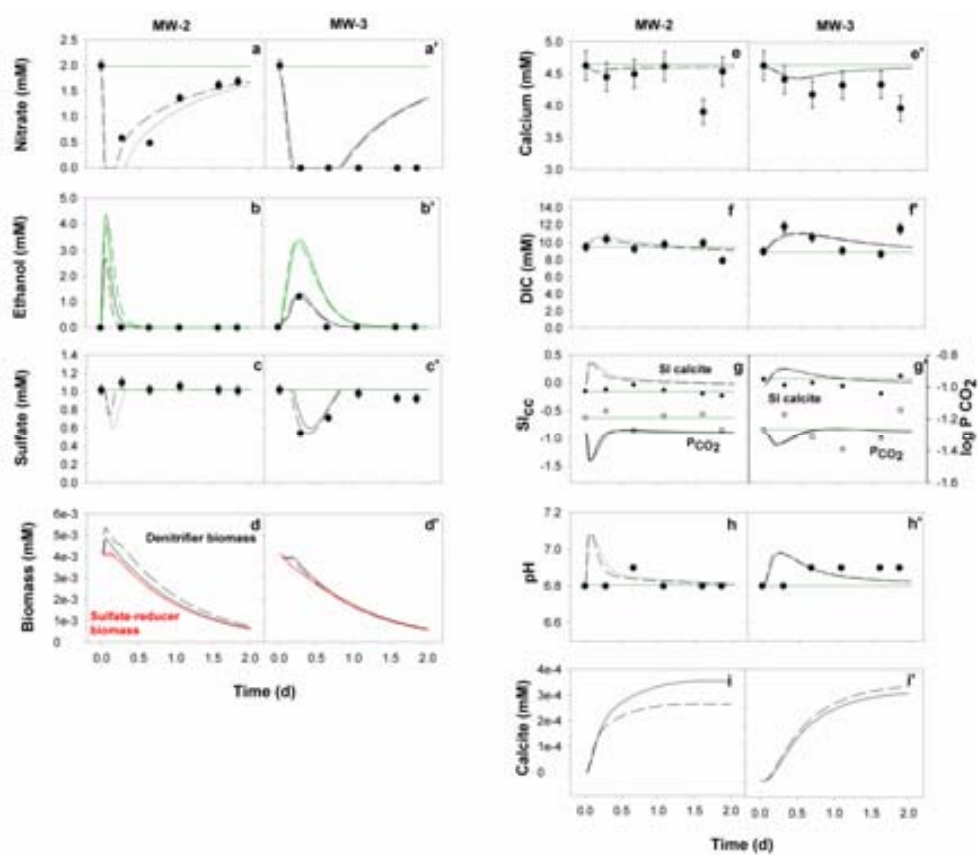
Figure 3.5 Modeling results (lines) versus observations (●) in MW-2 and MW-3. Solid lines correspond to 434 m a.s.l., whereas dashed lines correspond to 435 m a.s.l. Red lines correspond to sulfate-reducer biomass, and green lines represent the results of the conservative transport model.

The initial parameters for biodenitrification were taken from previous batch models (Chapter 2). For the sulfate reduction process, the initial values were taken from Nagpal et al. (2000), who modeled sulfate reduction by using ethanol as an organic carbon source in a batch system. During the upscaling process, these parameters were adjusted by considering the difference between the bioavailability of nutrients at the batch and field scales (based on the half-saturation constants) and the adaptation of microbial metabolism to the environment (based on decay constants) (Jin et al., 2012).

The availability of nutrients at the field scale is significantly different from that at the batch scale (Jin et al., 2012). The half-saturation constants are related to the adaptation of organisms to their environmental conditions (Button et al., 2004). Hence, applying half-saturation constants determined by laboratory experiments should consider how microorganisms adapt to different field availability of nutrients.

Table 3.2 shows that the differences in the half-saturation parameters between the batch and field experiments are all less than one order of magnitude, except for the half-saturation of nitrate during denitrification.

Table 3.2 Comparison of microbial parameters between the batch scale and the field scale. (1) From Chapter 2 (2) (Nagpal et al., 2000).

	DENITRIFICATION		SULFATE-REDUCTION	
	Batch scale[1]	Field scale	Batch scale[2]	Field scale
Y_h (mol C-biomass/mol C-ethanol)	0.73	0.73	0.88	0.88
K_{max} (mol ethanol/mol biomass s)	3.1×10^{-3}	3.1×10^{-3}	1.5×10^{-3}	1.5×10^{-3}
K_{sat} ethanol (M)	7.3×10^{-2}	6.5×10^{-2}	4.5×10^{-3}	6.5×10^{-2}
K_{sat} nitrate (M)	1.9×10^{-4}	1.4×10^{-5}		
K_{sat} sulfate (M)			8.5×10^{-3}	5×10^{-3}
b (s^{-1})	1.7×10^{-6}	1.1×10^{-5}	-	1.1×10^{-5}

The decay constant (b) is related to the energy consumed due to maintenance of the cell. The amount of energy used for maintenance is related to several cellular processes, such as cell locomotion, osmoregulation, homeostasis, cellular defenses or regenerating dysfunctional cellular components (Pirt, 1965). Because most laboratory experiments are carried out under optimal physical and chemical conditions for microbial growth, direct extrapolation of this parameter to the field scale cannot reproduce the results obtained in the field. The decay constant in the field was higher than that in the lab (Table 3.2) because the biomass used in the batch experiments was younger (seven days) than that used at the field scale (five months).

In contrast, the specific growth yields (Y_h) and the maximum rate constant (k_{max}) can be directly transferred from the lab to the field scale (Jin et al., 2012). Table 3.2 shows how these parameters have the same values at both scales. Both parameters are related to the properties of enzymes and pathways of metabolic reactions that are the same in the laboratory and in the field. Thus, these values can be directly extrapolated from the laboratory scale to the field scale.

Geochemical processes

Calcite precipitation was confirmed by the decrease of calcium in solution and the increase of the saturation index of calcite (Figure 3.5). The saturation index of calcite began at negative values but became positive when inorganic carbon was added to

the system (due to ethanol oxidation). In Chapter 2 was described that when ethanol was used as a source of organic carbon in biodenitrification, calcite precipitation was induced. In this case, the precipitation rate constant differed between batch scale (1×10^{-10} M s^{-1}) and field scale (5×10^{-9} M s^{-1}). The value in the field was unexpectedly fifty times higher than that in the lab experiments. This difference may have been caused by sediment being deposited in the reactor in the batch experiment, which limited the growth of calcite from the standing solution to the crystals in the sediment. In the field there was more contact between the groundwater and the solid matrix due to the transport of groundwater through microfractures. The field precipitation rate constant is consistent with the large range of values from the literature (1.0×10^{-7}, 1.2×10^{-7}, 7.0×10^{-10}, and 2.3×10^{-10} M s^{-1} from Inskeep and Bloom (1985), Busenberg and Plummer (1982), Jensen et al. (2002) and van Breukelen et al. (2004), respectively).

The pH increased from 6.8 before injection to 7.1 after injection (Figure 3.5). The timing of this increase matched that of the increase of the calcite saturation index. After 0.5 days, it recovered to the previous value of 6.8. Note that whereas pH increased, the calcite precipitated and partial pressure of CO_2 also increased. The occurrence of both phenomena can be related to the slower rate of calcite precipitation compared to the rate of CO_2 production by the chemical evolution of denitrification.

Biofilm growth, microbial-induced mineral precipitation or dissolution and bubble formation can modify the hydrologic properties of the media (e.g., hydraulic conductivity, dispersivity and porosity) (Soares et al., 1991; Soares et al., 1989; Thullner, 2010). In this model, the hydrologic properties of the media were constant due to the short duration of the field test (two days).

In this case, the amount of biomass did not change significantly and remained at the same order of magnitude (Figure 3.5) (bioclogging can be assumed negligible). The maximum change of porosity due to calcite precipitation (Figure 3.6) at the end of the model (2 days) was less than 3% across the entire model domain. This change was calculated using Equation 3.7. Then, calcite precipitation did not significantly modify the hydraulic properties.
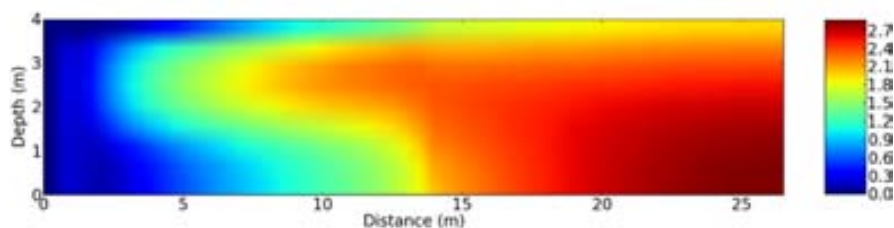
Figure 3.6 Decreasing of porosity after two days due to calcite precipitation.

The two flow velocities modified the porosity differently. The shallower part of the aquifer (with a homogenous flow velocity) experienced constant calcite precipitation along the distance. In contrast, the change of hydraulic conductivity (i.e., velocity) in the deeper layer modified the change in porosity due to calcite precipitation and was more significant at greater distances from the injection point. This may have occurred because calcite did not have enough time to precipitate due to the high velocity flow in depth.

Finally, the formation of gas bubbles can also modify the hydraulic properties. Nevertheless, because complete degassing was assumed due to the media being well connected (the total porosity and effective porosity were equal), its effect was not further considered.

3.4.3 Stable isotope geochemistry model

The nitrate isotope fractionation matches the observation data reasonably well in MW-2 (Figure 3.7). The delta values are only shown for nitrate concentrations that exceed 1 mg/l (where Compound Specific Isotope Analysis is possible). In MW-2, the $\delta^{15}N$-NO_3^- and $\delta^{18}O$-NO_3^- values increased between days 0.1 and 0.3 at the same time as nitrate decreased (Figure 3.5). On the other hand, when the nitrate concentrations increased to the background values of the aquifer, the isotopic values also decreased to their initial values.
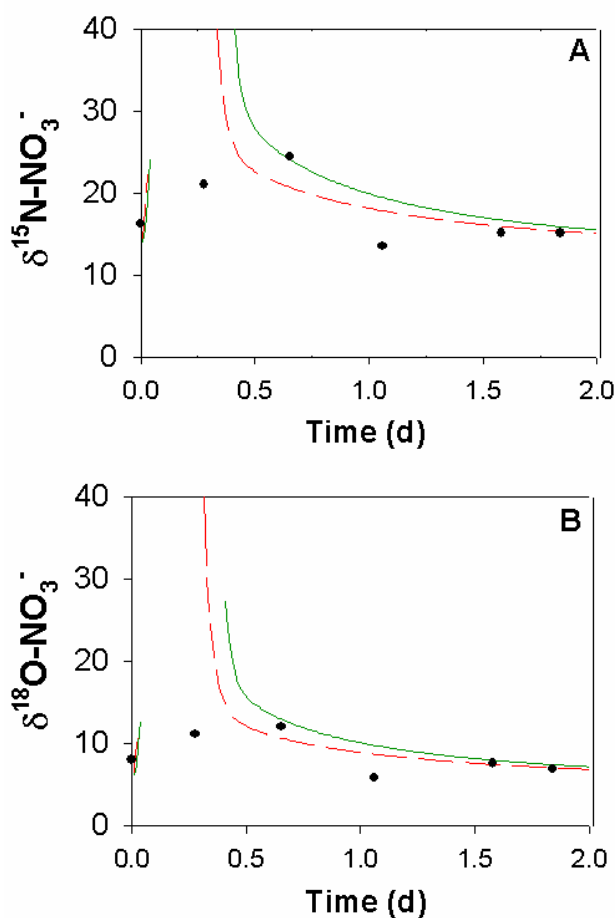
Figure 3.7 Modeling results (lines) versus observations in MW-2. Solid lines correspond to 434 m a.s.l., whereas dashed lines correspond to 435 m a.s.l. The observations are from Vidal-Gavilan et al. (2013).

Variations of $\delta^{13}C_{DIC}$ are controlled by the sources of carbon oxidation, including physical (e.g., CO_2 degassing, source mixing, carbonate precipitation or dissolution) and biochemical processes (e.g., microbial respiration). Thus, all of the processes that affect the δ^{13}C-DIC signal were included in the model, including the two types of respiration (exogenous and endogenous) for both nitrate and sulfate reduction and calcite precipitation. Although the modeled values of δ^{13}C-DIC do not follow the general trend of the experimental field values, they indicate the main processes that affect their variation (Figure 3.8). Despite the important fractionation due to the oxidation of ethanol and independent of the fractionation factor of ethanol used in sulfate reduction, the δ^{13}C-DIC values did not change considerably (maximum

variation of 2 ‰) (Figure 3.8, which only shows results of $\varepsilon_{eth/sulf}$=+1.8‰). The differences between the field and modeled δ^{13}C-DIC changes are attributed to the natural variations of this isotope in groundwater (the δ^{13}C-DIC values in the municipal well, which represent the natural background, oscillated from -11 ‰ to -8 ‰ during the slug injection test).
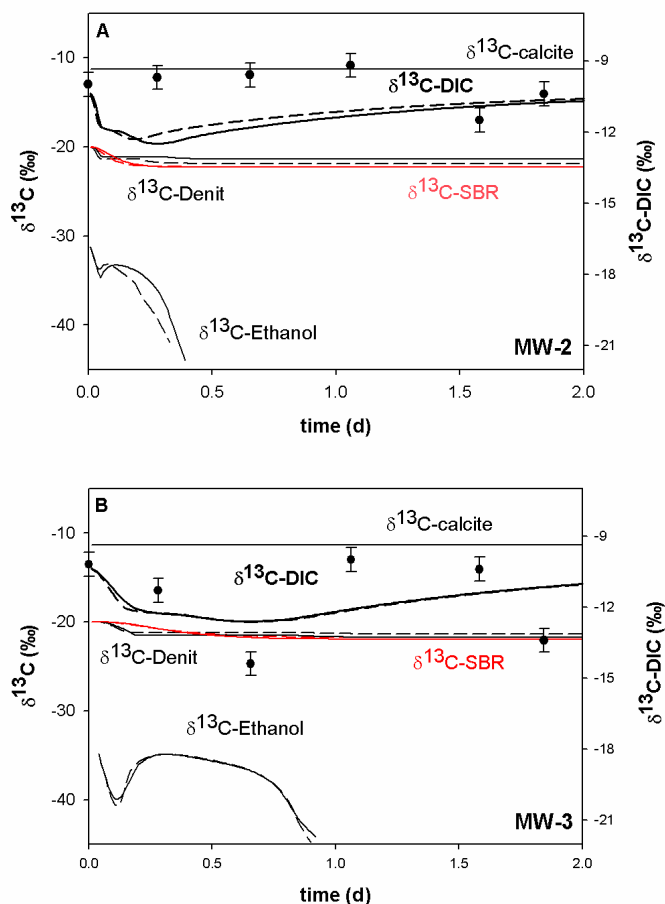
Figure 3.8 Modeling results (lines) versus observations of δ^{13}C-DIC at MW-2 and MW-3. Solid lines correspond to 434 m a.s.l., whereas the dashed lines correspond to 435 m a.s.l.. The plots correspond to different fractionation factors of ethanol due to sulfate reduction; A and B correspond to +1.8‰, and C and D correspond to -19.1‰. The observations are from Vidal-Gavilan et al. (2013).

3.4.4 Evaluation of the extent of Enhanced *in situ* Biodenitrification: RTM *versus* Rayleigh equation

The Rayleigh equation describes the redistribution of the isotopes of an element in a molecule that is undergoing degradation in a fully mixed and closed reservoir. Groundwater systems, however, represent open systems in which the concentrations

and isotope ratio gradients develop as a result of both transport and degradation processes. Several authors have observed that the extent of biodegradation is underestimated by using the Rayleigh equation instead of RTM (Abe and Hunkeler, 2006; Lutz et al., 2013; van Breukelen and Prommer, 2008). In the studied case, the Rayleigh equation also underestimates the extent of Enhanced *in situ* Biodenitrification compared with the RTM simulations. However, the extent of biodenitrification was qualitatively similar in RTM and Rayleigh equation scenarios (Figure 3.9). This indicates that from a practical point of view and considering its conservative behavior, i.e., underestimation of degradation, the Rayleigh equation can be applied to develop an initial estimate of the extent of EIB because of its ease of use.
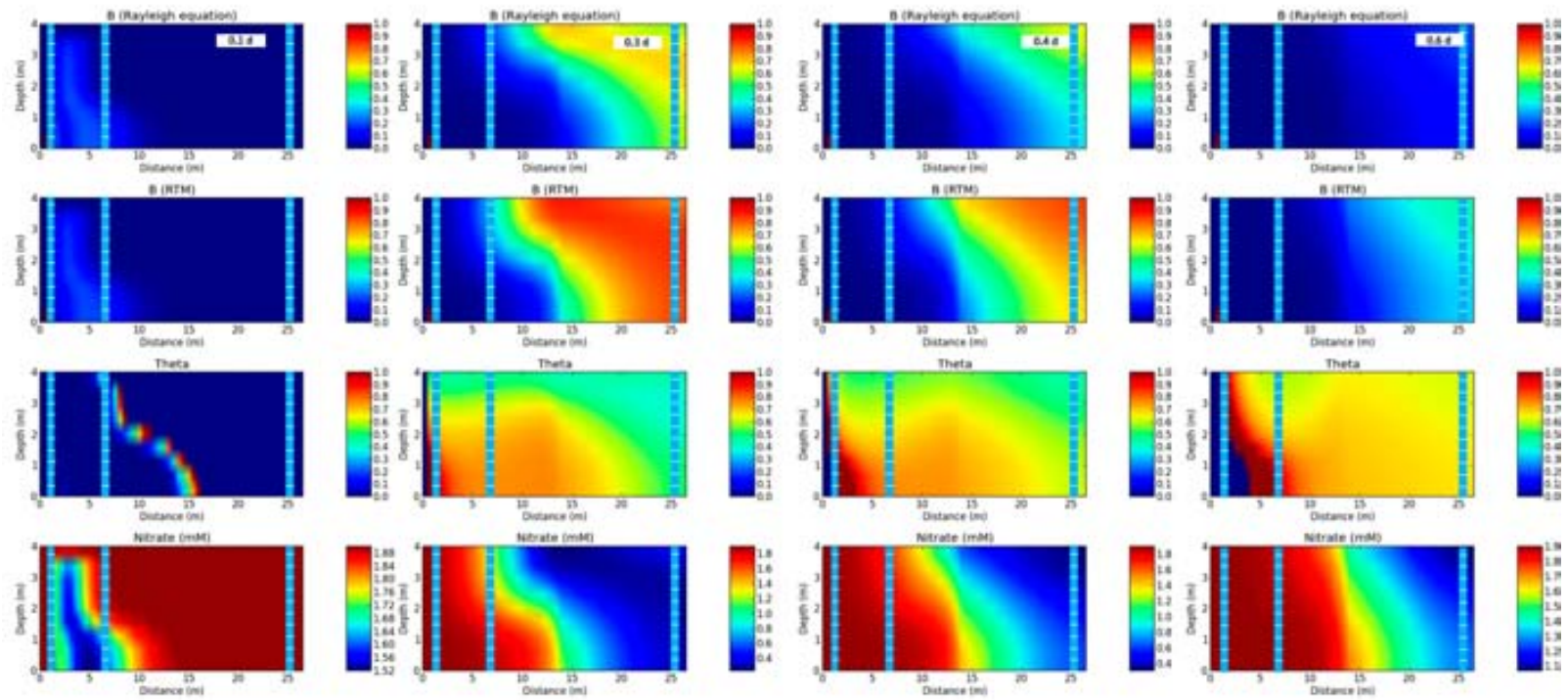
Figure 3.9 Evolution of the extents of Enhanced *in situ* Biodenitrification calculated using the Rayleigh equation and the RTM; theta value and nitrate evolution.

Figure 3.9 also shows that different parts of the clean groundwater plume are underestimated to different degrees. In general, the core of the clean groundwater plume was underestimated less (60-80%) than the fringes (90-100%). This may occur because the fringes were affected more by hydrodynamic dispersion and mixing than the core of the plume. This was also observed by van Breukelen and Prommer (2008). The underestimations observed in this study are greater than those in other studies (Abe and Hunkeler, 2006; Lutz et al., 2013; van Breukelen and Prommer, 2008), most likely because of the higher dispersivity coefficients in the study site.

As a result, and as was described by van Breukelen and Prommer (2008), it is recommended that the extent of biodenitrification as calculated with the Rayleigh equation is based on monitoring points located downgradient along the plume's central axis as far from the plume fringes as possible.

3.5   Conclusions

In this chapter it was developed a field scale 2D reactive transport model in a fractured aquifer that considers biogeochemical processes as well as isotope fractionation to enable better planning, characterization, monitoring, and optimization of Enhanced *in situ* Biodenitrification (EIB). The reactive transport model was based on the upscaling of previous batch models that used groundwater and the core material from the same experimental site. The microbiological processes were upscaled based on adjustments of the half-saturation and decay constants. Most of the modified microbiological parameters did not differ by more than one order of magnitude, indicating that the initial batch values were a good approximation for the initial field scale modeling. In contrast, the calcite precipitation constant was larger than in the batch experiments. This difference was attributed to different conditions between the lab and the field, whereas in lab, sediment was deposited in reactor limiting the growth of calcite precipitation, in field there was more contact between the groundwater and the solid matrix through the microfractures. Although assumed the hydraulic properties of the media were assumed to be constant over time, a decrease in porosity due to calcite precipitation of less than 3% was quantified. Biofilm growth did not change considerably, and degassing in the media was complete. It is important to note that this decrease in porosity due to calcite precipitation was produced exclusively as a result of a slug injection of an organic carbon source. More research is needed to evaluate the reversibility of the changes in

hydraulic properties to optimize injection strategies or to evaluate the addition of other substances (e.g., changes in the external organic carbon source) to minimize problems related to changes in the hydraulic properties.

The incorporation of isotope fractionation into the model allowed us to evaluate the overall model consistency. Compared to the batch scale, where denitrification produced significant changes, δ^{13}C-DIC was mainly affected by the natural background variations, and changes due to enhanced bioremediation were not noticeable at the field scale. The Rayleigh equation underestimated the extent of biodenitrification mainly at the fringes between the purified cleaned and polluted groundwater. Despite this underestimation, the extents of biodenitrification were qualitatively similar in both the RTM and Rayleigh approaches. This indicates that from a practical point of view and considering its conservative behavior, the Rayleigh equation can be applied to EIB as an easy initial step to evaluate the extent of EIB.

CHAPTER 4

Modeling long term Enhanced *in situ* Biodenitrification from column experiments: Insight in how feeding strategy affect hydraulic properties[*]

4.1   Introduction

The most common configuration of Enhanced *in situ* Biodenitrification at the field scale is the daisy configuration (Hamon and Fustec, 1991; Janda et al., 1988; Jechlinger et al., 1998; Khan and Spalding, 2003; Khan and Spalding, 2004; Mercado et al., 1988), based on the combination of multiple injection wells and a single central extraction well (Figure 1.2). The distance between the injection and extraction well is calculated considering the capture zone of the latter, the groundwater velocity and the residence time necessary to degrade nitrate. In general, a residence time of two days is sufficient for complete denitrification (Bates and Spalding, 1998).

The injection of an organic carbon creates a bioactive zone of denitrification. It has been observed from scanning electron microscopy that microorganisms in groundwater grow in micro-colonies or aggregates being heterogeneously distributed within the pores (Dupin and McCarty, 2000; Hand et al., 2008; Rittmann, 1993; Vandevivere and Baveye, 1992) rather than in a continuous and homogenous biofilm which is more characteristic to high load nutrients flow such as wastewater

---

[*] Chapter based on Rodríguez-Escales, P., Folch, A., van Breukelen, B.M., Vidal-Gavilan, G., Sánchez-Vila, 2014. Modeling long term Enhanced *in situ* Biodenitrification from column experiments: insight in how different feeding strategies affect hydraulic properties. Submitted to Water Resources Research.

treatments (Rittmann, 1993). These biomass 'plugs' induce bioclogging (Dupin and McCarty, 2000; Hand et al., 2008). The electron donor injection strategy has to account for biomass growth and nitrate degradation in order to properly evaluate bioclogging risk, considered the most common problem of enhanced bioremediation practices (Dupin and McCarty, 2000).

Bioclogging results in changes in aquifer hydraulic properties: porosity, hydraulic conductivity, and dispersivity (Taylor and Jaffé, 1990; Taylor et al., 1990; Thullner et al., 2008). Consequently, the residence times between injection and extraction wells can become modified, influencing the capacity for nitrate bioremediation. With the objective of managing bioclogging, different authors have introduced the electron donor in discrete pulses into the aquifer rather than continuously to limit biomass growth (Devlin and Barker, 1996; Gierczak et al., 2007; Khan and Spalding, 2004; Peyton, 1996; Semprini et al., 1990). Nevertheless, little is known about how the frequency of injection pulses affects biofilm growth and nitrate degradation.

 Reactive transport modeling (RTM) can facilitate the prediction of the clogging risk coupled to denitrification. RTM offers the possibility of exploring a variety of remediation strategies such as injection duration, injection rates, and reactant concentrations (Herold et al., 2011). Despite there are several models that describe denitrification processes (Chen and MacQuarrie, 2004; Kinzelbach et al., 1991; Lee et al., 2009; Rodríguez-Escales et al., 2014a; Rodríguez-Escales et al., 2014b), no long term studies have yet been performed on the effect of feeding strategies on bioclogging of porous media.

One of the most important challenges of RTM of a long term enhanced bioremediation application is how to incorporate the temporal changes of hydraulic properties due to biomass growth into the model. Despite several studies evaluated how hydrological parameters change in response to biomass growth (Frankenberger et al., 1979; Holm et al., 1997; Taylor et al., 1990; Vandevivere and Baveye, 1992), it is not clear how these changes are interrelated (Thullner, 2010). Most of these studies focused on porosity and hydraulic conductivity alterations (Taylor et al., 1990), while only some focused on dispersivity and spatial changes in hydraulic parameters (Taylor and Jaffé, 1990). A potential consequences of temporal and spatial variations in hydraulic parameters might even lead to a transition from Fickian to anomalous (non-Fickian) transport (Seymour et al., 2004), with significant implication for the actual model to be used to interpret experiments on biodenitrification.

Different approaches have been developed to describe anomalous (i.e., non-Fickian) transport. Amongst them, a widely used one is the multirate mass transfer (MRMT) model (Haggerty and Gorelick, 1995; Lawrence et al., 2002), representing the porous medium as composed of a mobile (aqueous bulk phase) and a suite of interacting immobile regions (biofilms) that coexist at any given point in the domain. Mobile and immobile regions transfer solute mass proportionally to the difference in their concentrations. When only one immobile region is considered (single rate), the model is equivalent as a dual porosity (van Genuchten and Wagenet, 1989). Analysis of conservative breakthrough curves (BTCs) by dual porosity models have already been used to describe changes of hydraulic properties due to biofilm growth (Seifert and Engesgaard, 2007). Nevertheless, there is no work that evaluates the induced heterogeneity of biofilm growth through MRMT models as compared to a standard (single porosity) advection-dispersion models. Only Seymour et al. (2004) showed that a Continuous Time Random Walk model was suitable to describe transport in a soil where biofilm was observed.

Considering all aspects involved when modeling EIB, this chapter is aimed to: 1) evaluate if biomass growth during EIB column experiments may promote the transition from Fickian to anomalous (non Fickian) transport, by comparing the experimental BTCs at different times; and 2) develop a model capable of reproducing different feeding injection frequencies (daily and weekly) in a long term experiment of EIB and relate injection frequency to biomass growth and bioclogging risk.

4.2   Materials and methods

4.2.1 Column experiment and initial conditions

The experimental data used in this chapter was obtained from Vidal-Gavilan et al. (2014). The experiment consisted of a glass cylindrical column (70 cm length, 8 cm inner diameter) filled with unconsolidated sediment from a sandy alluvial aquifer (located in Argentona, NE Spain) (Figure 4.1). Obtained groundwater was forced to flow from the bottom to the top of the column. Both the inflow and outflow were controlled by pumps set at the same flow-rate to reduce instabilities. A total of eight sampling ports were established: one at the inflow reservoir, six across the length of the glass column (at 6, 16, 26, 36, 46 and 56 cm from inlet), and one at the outflow. Over the duration of the experiment different spatial nitrate profiles were measured.

Groundwater was obtained from an existing large-diameter well located at the Argentona site. The well was always purged prior to sampling. A total of three 25-L containers were used to store the input water of the experiment, filled up at different days (August 2011, December 2011, and April 2012). No forced deoxygenation was performed, so the filled groundwater was oxic. The experiment ran for 10 months (342 days) at aquifer temperature (15ºC) while a control experiment without carbon substrate addition was run for 2 months to check for the potential effect of natural denitrification which was not observed.

Ethanol was added as an external organic carbon source through four injectors located 16 cm from the inlet. It was added in a solution mixed with the input water. Different feeding strategies were tested during the experiments (Table 4.1) with two periods without feeding. The first one was between day 150 and 175 due to hydraulic problems with the pump, so that no flow was supplied. The second one was between days 286 and 311 and it was carried out to evaluate the resilience of the system without feeding; thus, water without supplemented organic carbon was applied during that period.
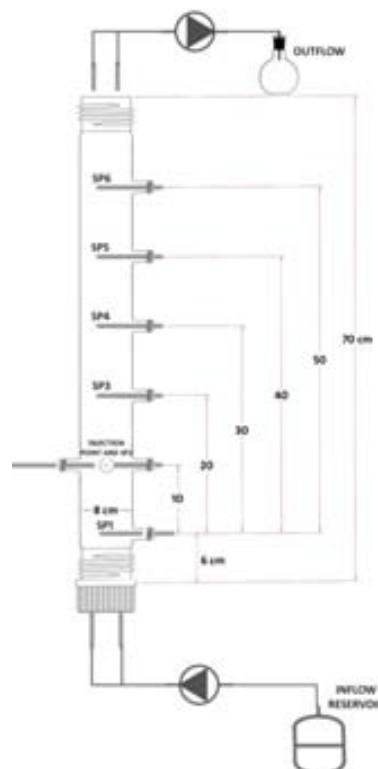
Figure 4.1 Experimental flow-through system and sampling points, figure based on Vidal-Gavilan et al. (2014).

Two bromide tracer tests were performed; one at the beginning of the experiments before any feeding and the other after 342 days of periodic injection of nutrients. The tracer tests were conducted under continuous flow with a constant concentration of bromide (Br = 1.45-2.23 mM, respectively). The bromide breakthroughs were monitored at the outflow point located at the end of the column. All analytical details are explained in Vidal-Gavilan et al. (2014).

Table 4.1 Different strategies tested during experiment. Ethanol concentration was corrected considering nitrate concentration from groundwater.

Feeding strategy	Feeding frequency	Average C:N	Ethanol injected (mM ethanol)	Days of experiment
I	Weekly	2.5	261-292	1-98
II	Daily	2.5	15-35	99-205*
III	Daily	1.5	17	206-252
IV	Daily	1	014	253-342**

4.3   Model construction

4.3.1   Evaluation of the heterogeneity: Single Rate Mass Transfer Model

As a first step, the hydraulic properties of the column were determined by modeling the BTCs from the bromide tracer tests at the beginning and at the end of the feeding period. This was initially performed by fitting the traditional one-dimensional advection-dispersion equation (ADE) with the CXTFIT code (Toride et al., 1999). The BTC from the second experiment was interpreted with STAMMT-L v.3.0 (Haggerty, 2009), allowing obtaining the corresponding parameters for the single rate mass transfer model (SRMT), thus introducing the effect of induced heterogeneity by biofilm growth. The general equation describing the concentration of species i in the mobile zone, $c_{m,i}$, for the SRMT model is described as:

$$\varphi_m \frac{\partial c_{m,i}}{\partial t} = -q\nabla c_{m,i} + \varphi_m \nabla (D\nabla c_{m,i}) - \Gamma_i \tag{4.1}$$

where D is the dispersion tensor, q is the Darcy's velocity, ϕ_m is the porosity corresponding to the mobile zone, and Γ_i is the source-sink term controlling the mass transfer of species i between the mobile (m) and the immobile regions (im) (see e.g., Willmann et al. (2010)):

$$\Gamma_i = \alpha \phi_{im} \left(c_{m,i} - c_{im,i} \right) \tag{4.2}$$

where α and ϕ_{im} are respectively the inverse of the characteristic waiting time [T^{-1}] and the porosity associated to the immobile region, and $c_{im,i}$ denotes concentration of species *i* in the immobile region. The actual total porosity is $\phi_t = \phi_m + \phi_{im}$. A significant parameter characterizing the shape of the BTC is the ratio of porosities given by:

$$\beta = \frac{\phi_{im}}{\phi_m} = \frac{\phi_t}{\phi_m} - 1 \tag{4.3}$$

An additional relevant parameter is the biofilm volume (Λ) which would correspond to a strictly diffusion layer developed in the column by assuming that there is a direct correspondence between biofilm growth and mobile porosity reduction:

$$\Lambda = \varphi_{im} V_c \tag{4.4}$$

where V_c represents the total volume [L^3] of the column.

4.3.2   Long-term EIB model

The PHT3D model code (v. 2.17) (Prommer and Post, 2010) was used to simulate the evolution of groundwater hydrochemistry during enhanced biodenitrification in the column. This model couples the transport simulator MT3DMS (Zheng and Wang, 1999) and the geochemical model PHREEQC-2 (Parkhurst and Appelo, 1999), by means of a sequential split-operator technique.

In a first step, the reactive processes relevant at the conceptual model stage were integrated into a site-specific PHT3D reaction module. Since this module uses the original PHREEQC-2 database syntax, arbitrary equilibrium and non-equilibrium reaction networks can be defined using the model described in Chapter 2 and 3. Kinetic reactions such as ethanol degradation and bacterial growth/decay, not being part of the standard database, were incorporated into the module in the form of simple BASIC routines (Equations 2.1-2.3 (Chapter 2)).

Biomass was assumed to be attached to the solid matrix and thus immobile. For equilibrium reactions, the reaction constants were used directly as provided by the PHREEQC-2 standard database. For all transport simulations the third-order Total Variation Diminishing (TVD) solution was used to compute dispersive transport. Moreover, the model considered the dual domain mass transfer between immobile (biofilm) and mobile (solution) phases, a feature recently incorporated in PHT3D. The 70 cm column was numerically discretized into 70 elements of 1 cm length. The time discretization was selected to satisfy Peclet and Courant number criteria.

4.4   Results and discussion

4.4.1 Evaluation of induced heterogeneity by biofilm growth

The BTCs from the two tests using bromide as tracers, performed at days 0 and 342 of
the column denitrification experiment are presented in Figure 4.2, together with the
best fits obtained either with code CTXFIT or STAMMT-L (the actual fitted parameters
are listed in Table 4.2). It was found that total porosity values during the 342 days of
experimental duration are statically not different, with the best estimate just
reducing from 0.33 to 0.32, and estimate intervals largely overlapping (Table 4.2).
Contrarily, there was a remarkable increase in the dispersivity coefficient (mean
values from 0.48 to 3.43 cm, see Table 4.2). Note the flow velocity remained constant
during the experiment. Then, the system was forced to increase the dispersivity as
pointed by formulations of Taylor and Jaffé (1990) that described the inversely
proportional relationship between changes in mobile porosity and dispersivity in a
column experiment colonized by biofilm. In short, while total porosity remained
basically constant, a portion of it seemed to change properties and become immobile.
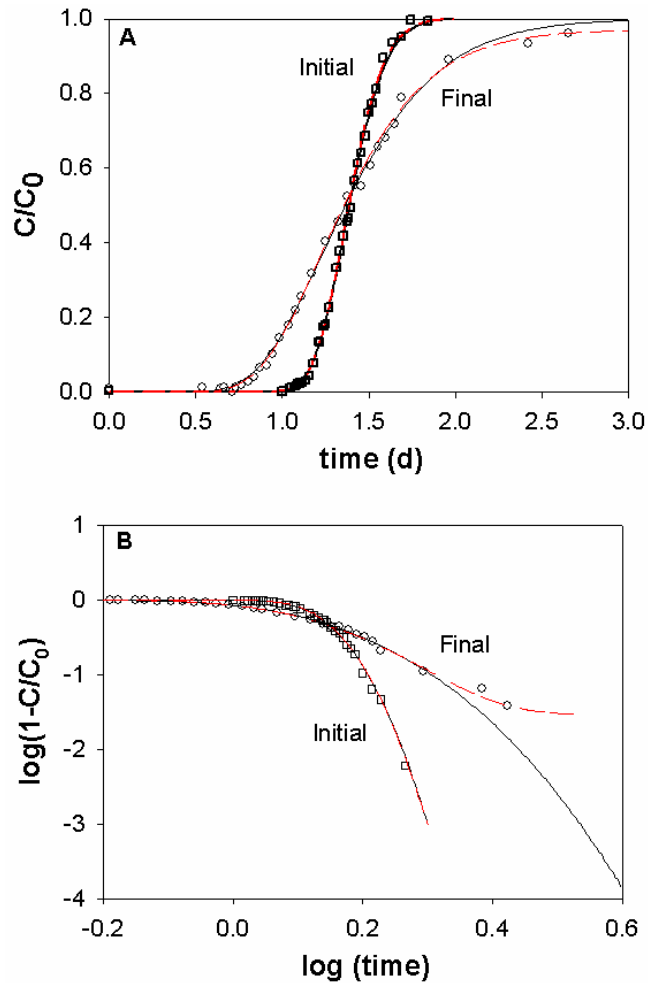
Figure 4.2 Model fittings using the ADE (CTXFIT, black lines) and a single rate mass transfer model (STAMMT-L, red dashed lines). Circles (○) are related to experimental values of initial tracer test (day 0), whereas square symbols (□) correspond to the BTC at day 342.

This process was interpreted as biofilm colonizing the sandy media of the column. This produced an increase of micro-colonies that induced a more irregular surface of the solid particles (Rittmann, 1993) and consequently, heterogeneity in the pore distribution within the porous media increased (Seifert and Engesgaard, 2007). The first consequence was the reported increase in dispersivity. Other studies have also reported significant changes in dispersivity during bioremediation experiments (a factor 2 to 8 during 2-7 weeks; (Arnon et al., 2005; Bielefeldt et al., 2002b; Hill and Sleep, 2002; Seifert and Engesgaard, 2007; Sharp et al., 1999; Taylor and Jaffé, 1990; Taylor et al., 1990). The increase in dispersivity between early and late tests could be as high as 10-100 folds (Taylor and Jaffé, 1990; Bielefeldt et al., 2002a).

Table 4.2 Evolution of hydraulic properties due to biofilm growth.

	Porosity	Dispersivity	Mass transfer parameter (α, d^{-1})	Immobile porosity
Initial	0.331 ± 0.016	0.485 ± 0.006	0	0
End	0.321 ± 0.017	3.430 ± 1.787	0.022	0.0109

Nevertheless, the most relevant feature was a conceptual model change. Whereas the traditional ADE equation was capable of properly fitting the initial BTC, it failed to provide a good fit of the tail of the final BTC. This phenomenon was also observed in some previous works (e.g. Taylor and Jaffé, 1990; Sharp et al., 1999). The fitting of the BTC was thus considerably improved applying a SRMT model (Figure 4.2).

This modification in transport behavior was also attributed to the enhanced heterogeneity caused by biofilm growth. In the SRMT model, the hand calibrated α parameter (α = 0.022 d^{-1}) represents the inverse of the characteristic residence time of diffusive transport of bromide through the immobile phase (being equal to 45 days). Moreover, the β value (β = 0.033) (determined by STAMMT-L) represents the proportion of the void volume occupied by the biofilm (3.33%). Notice that this value is very similar to the theoretical one (3.32%) reconstructed from the estimated values for mobile and immobile porosities assuming all changes are caused by biofilm growth (Equation 4.3). Additionally, the biofilm volume is estimated from Equation 4.4, being 38.8 cm^3 for the whole column. Nevertheless, how this volume was distributed within the column is unknown. Moreover, this volume also incorporated all the extracellular polysaccharide substances (EPS) which are inherently forming the biofilm. Also note that the determined volume does not account for micro colonies and free biomass.

As traditionally shown in the analysis of BTCs, the ADE is capable of fitting reasonably well a large portion of the curve, only failing to give a proper fitting at the receding tail. Indeed, it fitted perfectly until 90% of tracer recovery, and when the traditional ADE achieved complete recovery, experimental values were around 97% (see Figure 4.2). This indicates that using the traditional ADE causes an intrinsic absolute error of less than 3% in nitrate and ethanol concentrations in EIB applications. It is also important to take into account that this effect was observed after 342 days of experiment, but it could not be evaluated at intermediate times. Moreover, the non-Fickian behavior was associated to a long-term experiment in a 1D column with flow controlled by peristaltic pump. As pointed by Thullner (2010), biofilm colonization is intrinsically different in 1D and 2D or 3D media. Therefore more research is needed to evaluate the error associated with biofilm colonization of porous media in real 3D

media. For all these reasons in the subsequent analysis of the effect of feeding strategies it will be used to ignore that the impact of mass transfer between mobile and immobile domain, and apply the ADE equation.

4.4.2   Long-term modeling of EIB with different organic carbon injections

Daily and weekly feeding strategies carried out in the column experiments were modeled using the transport parameters obtained from fitting the previous tracer experiments with the ADE in order to account for the evolution of the concentrations of nitrate, ethanol, and biomass as a function of time. Since Table 4.2 displays two dispersivity values taken at different times, but the evolution in time could not be assessed (no tests at intermediate times), the column experiments (342 d) are modeled using the two dispersivity values reported in the table by assuming that they lasted the full duration of the experiment, thus providing the two limiting cases that would include the real case. The actual data and the model fittings are shown in Figure 4.3.

The microbiological parameters (manually fitted) used to obtain the best fitting (see Table 4.3) resulted in values that compare reasonably well with some reported in the literature. These values were not modified in the two dispersivity scenarios previously reported. The lowest value of dispersivity (0.48 cm) resulted in a good fitting of the experimental data during the weekly feeding strategy (see Figure 4.3). This indicates that during the first part of the experiment (100 days), dispersivity did not change significantly. This result could be masked because measurements were taken at the end of the column and probably most of the biomass growth and the subsequent change in dispersivity took place around the injection point (Kildsgaard and Engesgaard, 2001), associated to high nutrient concentrations. This result contrasts with other works based on column experiments (Bielefeldt et al., 2002a; Seifert and Engesgaard, 2007; Taylor and Jaffé, 1990), where dispersivity increased faster than in the experiment. For example, Seifert and Engesgaard (2007) in an experiment using acetate and oxygen as electron acceptor, calculated an increase of dispersivity from 0.33 cm to 1.1 cm in 64 days in a continuously feeding system. On the other hand, Bielefeldt et al. (2002b) observed a 20-60 fold increase of dispersivity in 15 days in clean sand also for a continuously feeding system. Their experiment was based up on propylene glycol degradation using nitrate as electron acceptor.

Table 4.3 Estimated values in this work.

Parameter	Unit	This work	Literature	Reference [a]
k_{max}	(mol C-etanol/mol-C-biomass d^{-1})	3.8×10^1	1×10^1; 1.1×10^1; 2×10^1; 1.08×10^2	1,2,3,4
$K_{sat,nit}$	(M)	1×10^{-5}	1.6×10^{-6}; 3.2×10^{-6}; 1.2×10^{-5}; 1.8×10^{-4}	1,3,2,4
$K_{sat,eth}$	(M)	1×10^{-4}	8.3×10^{-6}; 1.7×10^{-4}; 6.6×10^{-4}; 7.3×10^{-2}	1,2,3,4
b	(d^{-1})	5×10^{-2}	6×10^{-2}; 1.5×10^{-1}; 2×10^{-1}	2,4,3

[a] References are 1, Chen and MacQuarrie (2004); 2, Lee et al., (2009); 3, Kinzelbach et al., (1991); 4, Rodríguez-Escales et al., (2014b).
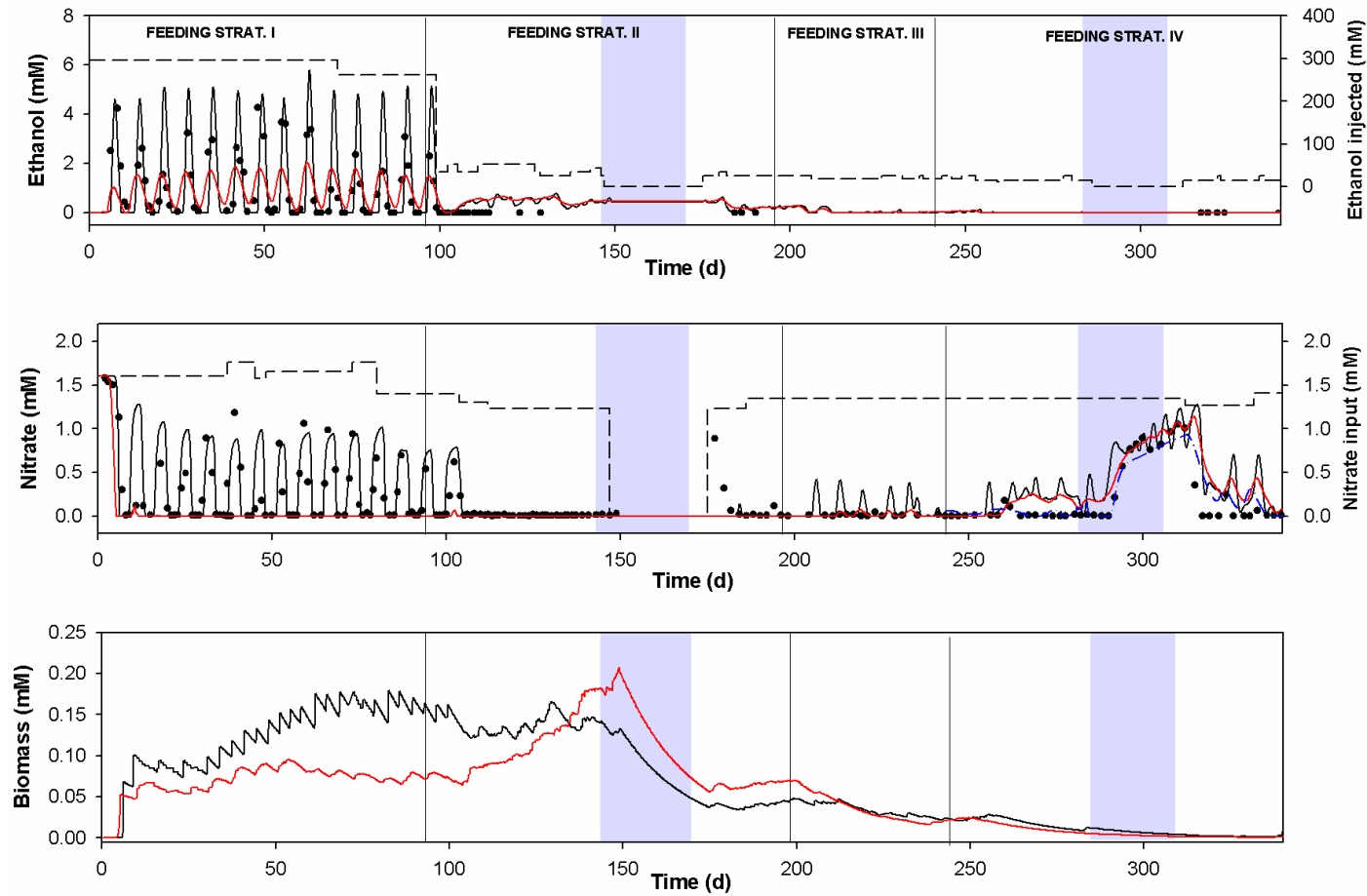
Figure 4.3 Results of the EIB models considering different injection strategies at the outflow of the column. The black and the red solid lines were obtained with dispersivity values of 0.48 and 3.43 cm, respectively, considering an ADE equation. The dashed-dotted blue line corresponds to a model using a dispersivity value of 3.43 cm and a dual model mass transfer.

Then, comparing this work with the literature, it would seem that a weekly strategy feeding is limiting the increase of dispersivity. This hypothesis was confirmed by spatial profiles of nitrate. In Figure 4.4 it is presented the spatial shapes of the nitrate concentration at different times within the weekly feeding strategy (left column). Data was best fitted by a traditional reactive transport model assuming a dispersivity of 0.48 cm, while a dispersivity of 3.43 cm provided a very bad fitting (visual inspection, no error measurement was computed).
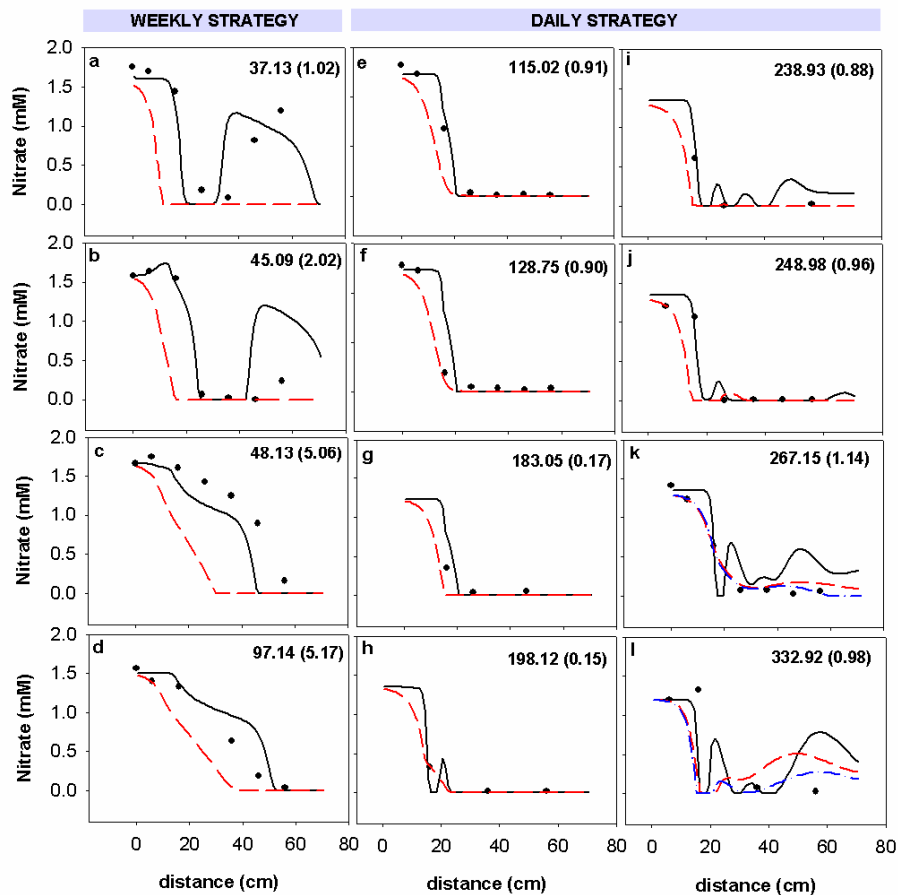
Figure 4.4 Nitrate vertical profiles during the experiment. Numbers represents the days where samples were taken in order to reconstruct the vertical profiles, whereas number in brackets reflect the elapsed time since the last injection period. The black and the red solid lines were obtained with dispersivity values of 0.48 and 3.43 cm, respectively, considering an ADE equation. The dashed-doted blue line corresponds to a model using a dispersivity value of 3.43 and dual mass transfer.

During the daily feeding strategy, starting after day 99, a best fit was obtained by using a larger dispersivity value (3.43 cm), both for nitrate time-series (Figure 4.3) as

well as for spatial nitrate profiles (Figure 4.4). Consequently, the increase in dispersivity seems triggered by the changes in the feeding strategy from discrete (weekly) to more-or-less continuous (daily). Despite it is observed a seven-fold increase in dispersivity, this was less significant than other values reported in the literature applicable for a fully continuous feeding strategy (Bielefeldt et al., 2002a; Seifert and Engesgaard, 2007; Taylor and Jaffé, 1990). The differences can be explained because the injection in this experiment was once per day rather than fully continuous. The results confirm that the feeding frequency is a key operational parameter that affects hydraulic parameters and thereby controls the transport of substances during EIB.

In the scenarios with the lowest C:N ratios (strategies III and IV), both experimental data and modelled results showed that nitrate and ethanol were completely consumed inside the column. This meant that the source of organic carbon was used optimally, because it was not detected at the outlet of the column (opposite to that observed in strategy I), thus indicating full consumption. Note the increase in dispersivity resulted in enhanced spreading of the injected ethanol enabling a more efficient substrate use and thereby avoiding the presence of high elevated carbon levels.

Nevertheless, to evaluate the success of the different injection strategies, it is important to consider the stress produced to the biomass population. In Figure 4.3, it is observed that when the carbon load was decreased (strategies III and IV), the modeled biomass diminished. However, nitrate remained undetected, indicating that observed denitrification was partially linked biomass decay (endogenous respiration) meaning that there was not enough external carbon to maintain the elevated biomass population. Moreover, these low C:N strategies were not sustainable in time because active biomass became negligible. Therefore, it is recommend to only apply low C:N strategies when the system had reached maturity and/or when an important risk of clogging exists.

Inspecting the last days of the experiment (during feeding strategy IV) it is noticed that traditional RTM using a high dispersivity value did not properly fit the experimental data (see Figure 4.3). This is attributed to the development of a biofilm which induced diffusive layer behavior. The incorporation of a dual transport model into the traditional reactive model resulted in an improved fitting of the modeled results to the experimental data (Figure 4.3, blue dashed-dotted line in the nitrate concentration curve). The parameters used, equal for all mobile species, were taken

from the dual porosity model reported in Table 4.2. The fact that the dual porosity model was only applicable to this particular feeding strategy could indicate that until this point, diffusive transport through the biofilm layer could be neglected, but that this transport became significant in strategy IV. Two main reasons are attributed for the increasing importance of this process: 1) with time a biofilm layer developed under a daily feeding strategy, and 2) diminishing ethanol in feeding injection caused that ethanol concentrations in the mobile phase were lower than those in the immobile phase (which is coherent with a characteristic diffusion time of 45 days). Consequently, an ethanol concentration gradient between the immobile and mobile phases was created, the Γ term (Equation 4.2) became positive and acted as a source of ethanol in the mobile phase (Equation 4.1). Therefore, it would seem that in the reported experimental conditions a dual domain mass transfer model could be neglected when the C:N ration was not severely reduced and at the first stages of the experiment whenever feeding strategies were not continuous.

4.5　Conclusions

Enhanced *in situ* Biodenitrification performed in a 70 cm long column experiment promoted the transition from Fickian to anomalous transport. This transition was well characterized using a single rate mass transfer model applied to two BTCs of conservative bromide tracer tests performed at the beginning and at the end of the experiment. This change was further illustrated by the significant increase of dispersivity from 0.48 to 3.43 cm. The immobile porosity has been also determined (3.33% of the total porosity) which was attributed to biofilm formation where compounds are exclusively transported by diffusion, explaining how a small reduction in mobile porosity results in such a significant increase in dispersivity over time.

Furthermore, a long term experiment of EIB has been modeled using different injection strategies. The traditional RTM fitted well the experimental data until the feeding strategy was changed after 252 days. Nevertheless, a subsequent change in the feeding strategy implied the need to consider a dual domain model to provide a proper fitting of the concentration curves both in space and in time. This effect was associated to the presence of a diffusive layer becoming increasingly relevant with time, linked to the considerable decrease in ethanol concentration in the feeding solution. At this point, a negative concentration gradient was created and the diffusive layer acted as a source of ethanol for the mobile phase.

During the weekly supply strategy (first 100 days), the RTM fitted well using a low dispersivity value (0.48 cm), whereas during the daily strategy, it fitted better with a larger value (3.43 m). This behavior is attributed to the change in injection feeding strategy, from weekly to daily, after day 100. In this way, this work has shown that besides other parameters (nutrient loading, flow rate, or grain size), injection frequency is a significant operational parameter that can affect hydraulic parameters (porosity, dispersivity), in particular in case of more continuous (in time) feeding strategies. This finding promotes field EIB application because a larger dispersivity value offers the possibility to enhance spreading of injected solutes and to limit the organic carbon loss. This is coupled to the changes in hydraulic conductivity that could be observed around the injection wells. Then, depending of the hydraulic properties of the geological media where the EIB is carried out, a specific feeding strategy should be chosen and tested before it is applied in the field.

Finally, reducing the C:N ratio allowed for the optimization of ethanol injection into the system and avoided its spillage through the column outlet. Nevertheless, the results of the modelled biomass showed that these strategies were not sustainable in time because biomass was completely depleted. Using these strategies is recommended when an EIB system reaches maturity and when an important risk of clogging exists.

CHAPTER 5

Conclusions

In this thesis, an integrated model has been developed that considers microbiological, hydrogeochemical, and isotopic processes and improves upon existing biodenitrification models. The conceptual relationships among all processes were developed at the batch scale, and the integrated model was applied at the field scale under a complex hydrogeology (fractured aquifer). Moreover, a long-term model that reproduced different scenarios with modification of hydraulic properties due to biofilm growth was developed at the column scale. The main conclusions based on the results obtained at various scales in different scenarios are described as follows.

The kinetic microbiological parameter values obtained at the batch scale are a good approximation for use as initial parameter values for field-scale modeling. In the case of EIB, the modified parameter values were related to the availability of nutrients, which were considerably higher at batch than at field scale (saturation half constants) and the adaptation of the microbial community to the environment which was lower at batch than at field scale (biomass decay constant). In all cases, the modifications were less than one order of magnitude.

The integration of microbiological and water-rock interactions allows identification and quantification of the carbonate mineral (calcite) dissolution/precipitation induced by denitrification. The induced dissolution or precipitation of calcite depends on the imbalanced proton consumption and CO_2 production resulting from denitrification.

With ethanol, calcite precipitation was enhanced, whereas with glucose, calcite dissolution was observed. The calcite precipitation rate constant was modified considerably from the batch to field scale (incremented fifty times, from 1×10^{-10} to 5×10^{-9}). This difference was attributed to different conditions between the lab and the field; whereas in lab, sediment was deposited in reactor limiting the growth of calcite precipitation, in field there was more contact between the groundwater and the solid matrix through the microfractures. Moreover, in this thesis, the reduction of porosity due to calcite precipitation was quantified; at the field scale and over two days, the porosity was reduced by 3% in a site with low porosity (10^{-4}). Additional research is needed to evaluate how specific organic substrates can be used to minimize the risk of clogging (e.g., change to use of glucose when significant bioclogging occurs). Moreover, the reversibility of porosity changes should be evaluated once EIB was stopped.

The incorporation of isotope fractionation in EIB models allows clear differentiation of nitrate concentration changes due to degradation and merely dilution. However, the Rayleigh equation underestimated the extent of EIB around 60-80%. This underestimation was focused primarily at the fringes between the cleaned and still polluted groundwater. Despite this underestimation, the extents of biodenitrification were qualitatively similar in both the RTM and Rayleigh approaches. This result indicates that from a practical point of view and with consideration of its conservative behavior, the Rayleigh equation can be applied to EIB as a simple initial step for evaluating the extent of EIB.

The inclusion of δ^{13}C-DIC in EIB models is important because this isotope is affected by all main EIB processes, thereby enabling an overall check of model consistency. Both calibrated enrichment factors (+8‰ for ethanol and +17‰ for glucose degradation) indicated that the heavy isotope reacted faster than the light isotope (inverse fractionation). This inverse fractionation could indicate that the denitrifiers used the TCA cycle for oxidation. Nevertheless, additional research is required to understand certain processes involved in isotopic fractionation, such as how metabolic pathways result in inverse or normal fractionation. Compared with the batch scale in which denitrification produced significant changes, the low δ^{13}C-DIC changes at the field scale were masked by temporal variations of its background value.

Enhanced *in situ* Biodenitrification promoted the transition from normal to anomalous non-Fickian transport in a column experiment with flow controlled via a peristaltic pump. This transition was illustrated by the significant increase of dispersivity from

0.48 cm to 3.43 cm and was well characterized with a single-rate mass transfer model of two breakthrough curves from different tracer tests (at the beginning and at the end of the experiment). In this transition, traditional RTM with adapted hydraulic properties reproduced the long-term experiment over 242 d. After this period, it was necessary to incorporate dual mass transfer to the model to fit the experimental results. Additional research is required for prediction of the transition from normal to anomalous non-Fickian transport. Additionally, it would be of interest to evaluate how immobile porosity was modified through time (in order to know if traditional RTM could be used) and what organic carbon substrates to use to reduce biofilm growth.

In addition to other parameters (such as nutrient loading or grain size), injection frequency is an important parameter that can modify the dispersivity, which becomes higher when injections are more continuous in time. Reducing the C:N ratio during EIB allowed the efficient ethanol use in the system because it was not detected at the outlet of the column experiment, thus indicating full consumption. Nevertheless, the results of the modelled biomass showed that these strategies were not sustainable in time because biomass was completely depleted. Therefore, it is recommend using these strategies when an EIB system reaches maturity and when an important risk of clogging exists.

Overall, this thesis has contributed to the knowledge and quantification of all processes involved in Enhanced *in situ* Biodenitrification using numerical models. The developed models can aid in improving the design, planning, monitoring and optimization of this technology at the field scale.

CHAPTER 6

References

Abe, Y., Hunkeler, D., 2006. Does the Rayleigh equation apply to evaluate field isotope data in contaminant. Environ. Sci. Technol., 40(5): 1588-96.

ACA, 2007. Evolució i estat de les aigües subterrànies de Catalunya. In: Niñerola, J.M., Iglesias, M., Frailes, J., Floría, E., Garrido, T. (Editors).

Almeida, J.S., Reis, M.A., Carrondo, M.J., 1995. Competition between nitrate and nitrite reduction in denitrification by *Pseudomonas fluorescens.* Biotechnol. Bioeng., 46(5): 476-84.

Alvarez, P., Anid, P., Vogel, T., 1994. Kinetics of toluene degradation by denitrifying aquifer microorganisms. J. Environ. Eng., 120(5): 1327-1336.

André, L., Pauwels, H., Dictor, M.C., Parmentier, M., Azaroual, M., 2011. Experiments and numerical modelling of microbially-catalysed denitrification reactions. Chem. Geol., 287(3–4): 171-181.

Aravena, R., Robertson, W.D., 1998. Use of multiple isotope tracers to evaluate denitrification in groundwater: Study of nitrate from a large-flux septic system plume. Ground Water, 36(6): 975-982.

Arnon, S., Adar, E., Ronen, Z., Yakirevich, A., Nativ, R., 2005. Impact of microbial activity on the hydraulic properties of fractured chalk. J. Contam. Hydrol., 76(3-4): 315-36.

Baker, A., 2003. Land use and water quality. Hydrol. Process., 17(12): 2499-2501.

Barbieri, M. et al., 2011. Microcosm experiments to control anaerobic redox conditions when studying the fate of organic micropollutants in aquifer material. J. Contam. Hydrol., 126(3–4): 330-345.

Bates, H.K., Spalding, R.F., 1998. Aquifer denitrification as interpreted from *in situ* microcosm experiments. J. Environ. Qual.(1): 174-182.

Bekins, B.A., Warren, E., Godsy, E.M., 1998. A comparison of zero-order, first-order, and monod biotransformation models. Ground Water, 36(2): 261-268.

Beller, H.R., 2005. Anaerobic, nitrate-dependent oxidation of U(IV) oxide minerals by the chemolithoautotrophic *Bacterium Thiobacillus* denitrificans. Appl. Environ. Microbiol., 71(4): 2170-2174.

Bielefeldt, A., Illangasekare, T., Uttecht, M., LaPlante, R., 2002a. Biodegradation of propylene glycol and associated hydrodynamic effects in sand. Water Res., 36(7): 1707-1714.

Bielefeldt, A., McEachern, C., Illangasekare, T., 2002b. Hydrodynamic changes in sand due to biogrowth on Naphthalene and decane. J. Environ. Eng., 128(1): 51-59.

Blair, N. et al., 1985. Carbon isotopic fractionation in heterotrophic microbial metabolism. Appl. Environ. Microbiol., 50(4): 996-1001.

Bohdziewicz, J., Bodzek, M., Wąsik, E., 1999. The application of reverse osmosis and nanofiltration to the removal of nitrates from groundwater. Desalination, 121(2): 139-147.

Boisson, A. et al., 2013. Reaction chain modeling of denitrification reactions during a push–pull test. J. Contam. Hydrol., 148(0): 1-11.

Busenberg, E., Plummer, L.N., 1982. The kinetics of dissolution of dolomite in CO_2-H_2O systems at 1.5 to 65ºC and 0 to 1 atm P_{CO2}. Am. J. Sci., 282(1): 34.

Button, D.K., Robertson, B., Gustafson, E., Zhao, X., 2004. Experimental and theoretical bases of specific affinity, a cytoarchitecture-based formulation of nutrient collection proposed to supercede the Michaelis-Menten paradigm of microbial kinetics. Appl. Environ. Microbiol., 70(9): 5511-5521.

Béranger, S., Sleep, B., Sherwood Lollar, B., Brown, A., 2006. Isotopic fractionation of tetrachloroethene undergoing biodegradation supported by endogenous decay. J. Environ. Eng., 132(7): 725-735.

Calderer, M. et al., 2010a. Denitrification in presence of acetate and glucose for bioremediation of nitrate-contaminated groundwater. Environ. Technol., 31(7): 799-814.

Calderer, M., Jubany, I., Pérez, R., Martí, V., de Pablo, J., 2010b. Modelling enhanced groundwater denitrification in batch micrococosm tests. Chem. Eng. J., 165(1): 2-9.

Carrey, R., Otero, N., Soler, A., Gómez-Alday, J.J., Ayora, C., 2013. The role of Lower Cretaceous sediments in groundwater nitrate attenuation in central Spain: Column experiments. Appl. Geochem., 32(0): 142-152.

Cey, E.E., Rudolph, D.L., Aravena, R., Parkin, G., 1999. Role of the riparian zone in controlling the distribution and fate of agricultural nitrogen near a small stream in southern Ontario. J. Contami. Hydrol., 37(1–2): 45-67.

Champ, D.R., Gulens, J., Aackson, R.E., 1979. Oxidation–reduction sequences in ground water flow systems. Can. J. Earth Sci., 16(1): 9.

Chen, D.J.Z., MacQuarrie, K.T.B., 2004. Numerical simulation of organic carbon, nitrate, and nitrogen isotope behavior during denitrification in a riparian zone. J. Hydrol., 293(1–4): 235-254.

Clement, T.P., Peyton, B.M., Skeen, R.S., Jennings, D.A., Petersen, J.N., 1997. Microbial growth and transport in porous media under denitrification conditions: experiments and simulations. J. Contam. Hydrol., 24(3–4): 269-285.

Coffin, R.B., Velinsky, D.J., Devereux, R., Price, W.A., Cifuentes, L.A., 1990. Stable carbon isotope analysis of nucleic acids to trace sources of dissolved

substrates used by estuarine bacteria. Appl. Environ. Microbiol., 56(7): 2012-20.

Copper, H.H.J., Jacob, C.E., 1946. A generalized graphical method for evaluating formation constants and summarazing well field-history. Eos Trans., AGU, 27(4): 8.

Dawes, E.A., Ribbons, D.W., 1964. Some aspects of the endogenous metabolism of bacteria. Bacteriol. Rev., 28: 126-49.

Della Rocca, C., Belgiorno, V., Meriç, S., 2007. Overview of *in situ* applicable nitrate removal processes. Desalination, 204(1–3): 46-62.

Devlin, J.F., Barker, J.F., 1996. Field investigation of nutrient pulse mixing in an *in situ* biostimulation experiment. Water Resour.Res., 32(9): 2869-2877.

Doherty, J., 2005. PEST: model independent parameter estimation. Watermark Numerical Computing, fifth edition of user manual.

Dupin, H.J., McCarty, P.L., 2000. Impact of colony morphologies and disinfection on biological clogging in porous media. Environ. Sci. Technol., 34(8): 1513-1520.

Elmidaoui, A. et al., 2003. Selective nitrate removal by coupling electrodialysis and a bioreactor. Desalination, 153(1–3): 389-397.

Elsner, M., 2010. Stable isotope fractionation to investigate natural transformation mechanisms of organic contaminants: principles, prospects and limitations. J. Environ. Monitor., 12(11): 2005-2031.

European Environment Agency, E., 2007. Present concentration of nitrate in groundwater bodies in European countries, 2003.

Fan, A.M., Steinberg, V.E., 1996. Health implications of nitrate and nitrite in drinking water: an update on methemoglobinemia occurrence and reproductive and development toxicity. Regul. Toxicol. Pharmacol., 23(1 Pt 1): 35-43.

Fernàndez-Garcia, D., Illangasekare, T.H., Rajaram, H., 2005. Differences in the scale-dependence of dispersivity estimated from temporal and spatial moments in chemically and physically heterogeneous porous media. Adv. Water Resour., 28(7): 745-759.

Fernández-Nava, Y., Marañón, E., Soons, J., Castrillón, L., 2008. Denitrification of wastewater containing high nitrate and calcium concentrations. Bioresou. Technol., 99(17): 7976-7981.

Frankenberger, W.T., Troeh, F.R., Dumenil, L.C., 1979. Bacterial effects on hydraulic conductivity of soils 1. Soil Sci. Soc. Am. J.(2): 333-338.

Galloway, J.N., 1998. The global nitrogen cycle: changes and consequences. Environ. Pollut., 102(1, Supplement 1): 15-24.

Galloway, J.N., 2000. Nitrogen mobilization in Asia. Nutr. Cyc. Agroecosyst., 57(1): 1-12.

Galloway, J.N., Schlesinger, W.H., Levy, H., Michaels, A., Schnoor, J.L., 1995. Nitrogen fixation: anthropogenic enhancement-environmental response. Global Biogeochem. Cy., 9(2): 235-252.

Gelhar, L.W., 1986. Stochastic subsurface hydrology from theory to applications. Water Resour. Res., 22(9S): 135S-145S.

Gelhar, L.W., Welty, C., Rehfeldt, K.R., 1992. A critical review of data on field-scale dispersion in aquifers. Water Resour. Res., 28(7).

Gierczak, R., Devlin, J.F., Rudolph, D.L., 2007. Field test of a cross-injection scheme for stimulating in situ denitrification near a municipal water supply well. J. Contam. Hydrol., 89(1–2): 48-70.

Goevert, D., Conrad, R., 2008. Carbon isotope fractionation by sulfate-reducing bacteria using different pathways for the oxidation of acetate. Environ. Sci. Technol., 42(21): 7813-7817.

Gomez, M.A., Galvez, J.M., Hontoria, E., González-López, J., 2003. Influence of ethanol concentration on biofilm bacterial composition from a denitrifying submerged filter used for contaminated groundwater. J. Biosci. Bioeng., 95(3): 245-251.

Grischek, T., Hiscock, K.M., Metschies, T., Dennis, P.F., Nestler, W., 1998. Factors affecting denitrification during infiltration of river water into a sand and gravel aquifer in Saxony, Germany. Water Res., 32(2): 450-460.

Gómez, M.A., González-López, J., Hontoria-García, E., 2000. Influence of carbon source on nitrate removal of contaminated groundwater in a denitrifying submerged filter. J. Hazard. Mater., 80(1–3): 69-80.

H Bosch, H.M., Rosefield, A.B., Huston, R., Shipman, H.R., Woodward., F.L., 1950. Methemoglobinemia and Minnesota well supplies. J. Am. Water Works Assoc., 42: 9.

Haggerty, R., 2009. STAMMT-L version 3.0. User Manual Document Version 3.0-UM-0., Oregon State University.

Haggerty, R., Gorelick, S., 1995. Multiple-Rate Mass Transfer for modeling diffusion and surface reactions in media with pore-scale heterogeneity. Water Resour. Res., 31(10): 2383-2400.

Hall, J.A., Kalin, R.M., Larkin, M.J., Allen, C.C.R., Harper, D.B., 1999. Variation in stable carbon isotope fractionation during aerobic degradation of phenol and benzoate by contaminant degrading bacteria. Org. Geochem., 30(8, Part 1): 801-811.

Hamon, M., Fustec, E., 1991. Laboratory and field study of an *in situ* groundwater denitrification reactor. Res. J. of the Water Pollut. C., 63(7).

Hand, V.L., Lloyd, J.R., Vaughan, D.J., Wilkins, M.J., Boult, S., 2008. Experimental studies of the influence of grain size, oxygen availability and organic carbon availability on bioclogging in porous media. Environ. Sci. Technol., 42(5): 1485-91.

Haugen, K.S., Semmens, M.J., Novak, P.J., 2002. A novel in situ technology for the treatment of nitrate contaminated groundwater. Water Res., 36(14): 3497-3506.

He, B. et al., 2011. Assessment of global nitrogen pollution in rivers using an integrated biogeochemical modeling framework. Water Res., 45(8): 2573-2586.

Hell, F., Lahnsteiner, J., Frischherz, H., Baumgartner, G., 1998. Experience with full-scale electrodialysis for nitrate and hardness removal. Desalination, 117(1–3): 173-180.

Herold, M., Greskowiak, J., Ptak, T., Prommer, H., 2011. Modelling of an enhanced PAH attenuation experiment and associated biogeochemical changes at a former gasworks site in southern Germany. J. Contam. Hydrol., 119(1–4): 99-112.

Hill, D.D., Sleep, B.E., 2002. Effects of biofilm growth on flow and transport through a glass parallel plate fracture. J. Contam. Hydrol., 56(3-4): 227-46.

Holm, J., Engesgaard, P.K., Høgh Jensen, K., Henze, M., Albrechtsen, H.-J., 1997. Effects of biomass growth on the hydrodynamic properties of groundwater aquifers, EOS, vol. 78, no. 46.

Horan, N.J., 1990. Biological wastewater treatment systems. Theory and Operations. Chichester: John Wiley.

Hosono, T., Tokunaga, T., Tsushima, A., Shimada, J., 2014. Combined use of $\delta^{13}C$, $\delta^{15}N$, and $\delta^{34}S$ tracers to study anaerobic bacterial processes in groundwater flow systems. Water Res., 54(0): 284-296.

Hunkeler, D. et al., 2004. Effect of source variability and transport processes on carbon isotope ratios of TCE and PCE in two sandy aquifers. J. Contam. Hydrol., 74(1–4): 265-282.

IGME, 2009. Las aguas subterráneas. Un recurso natural del subsuelo.

Inskeep, W.P., Bloom, P.R., 1985. An evaluation of rate equations for calcite precipitation kinetics at p_{CO2} less than 0.01 atm and pH greater than 8. Geochim. Cosmochim. Acta, 49(10): 2165-2180.

IPCC, 2007. Climate change 2007: synthesis report.

Istok, J.D., Humphrey, M.D., Schroth, M.H., Hyman, M.R., O'Reilly, K.T., 1997. Single-well, "Push-Pull" test for *in situ* determination of microbial activities. Ground Water, 35(4): 619-631.

Janda, V., Rudovský, J., Wanner, J., Marha, K., 1988. *In situ* denitrification of drinking water. Water Sci. Technol., 20(3): 4.

Jechlinger, G., Eilb, W., Martinell, R., 1998. Denitrification the Swedish way. World Water Environ. Eng., 21(2): 2.

Jensen, D.L., Boddum, J.K., Tjell, J.C., Christensen, T.H., 2002. The solubility of rhodochrosite ($MnCO_3$) and siderite ($FeCO_3$) in anaerobic aquatic environments. Appl. Geochem., 17(4): 503-511.

Jin, Q., Bethke, C.M., 2003. A new rate law describing microbial respiration. Appl. Environ. Microbiol., 69(4): 2340-2348.

Jin, Q., Bethke, C.M., 2005. Predicting the rate of microbial respiration in geochemical environments. Geochim. Cosmochi. Acta, 69(5): 1133-1143.

Jin, Q., Roden, E.E., Giska, J.R., 2012. Geomicrobial kinetics: extrapolating laboratory studies to natural environments. Geomicrobiol. J., 30(2): 173-185.

Karanasios, K.A., Vasiliadou, I.A., Pavlou, S., Vayenas, D.V., 2010. Hydrogenotrophic denitrification of potable water: A review. J. Hazard. Mater., 180(1–3): 20-37.

Karlsen, R.H., Smits, F.J.C., Stuyfzand, P.J., Olsthoorn, T.N., van Breukelen, B.M., 2012. A post audit and inverse modeling in reactive transport: 50 years of artificial recharge in the Amsterdam water supply dunes. J. Hydrol., 454–455(0): 7-25.

Khan, I.A., Spalding, R.F., 2003. Development of a procedure for sustainable *in situ* aquifer denitrification. Remediation Journal, 13(2): 53-69.

Khan, I.A., Spalding, R.F., 2004. Enhanced *in situ* denitrification for a municipal well. Water Res., 38(14–15): 3382-3388.

Kildsgaard, J., Engesgaard, P., 2001. Numerical analysis of biological clogging in two-dimensional sand box experiments. J. Contam. Hydrol., 50(3–4): 261-285.

Killingstad, M.W., Widdowson, M.A., Smith, R.L., 2002. Modeling enhanced *in situ* denitrification in groundwater. J. Environ. Eng., 128: 14.

Kinzelbach, W., Schäfer, W., Herzer, J., 1991. Numerical modeling of natural and enhanced denitrification processes in aquifers. Water Resour. Res., 27(6): 1123-1135.

Knowles, R., 1982. Denitrification. Microbiol. Rev., 46(1): 43-70.

Kornaros, M., Lyberatos, G., 1998. Kinetic modelling of pseudomonas denitrificans growth and denitrification under aerobic, anoxic and transient operating conditions. Water Res., 32(6): 1912-1922.

Korom, S.F., 1992. Natural denitrification in the saturated zone: A review. Water Resour. Res., 98(6).

Kouznetsova, I. et al., 2010. Biological reduction of chlorinated solvents: Batch-scale geochemical modeling. Adv. Water Reour., 33(9): 969-986.

Lawrence, A.E., Sanchez-Vila, X., Rubin, Y., 2002. Conditional moments of the breakthrough curves of kinetically sorbing solute in heterogeneous porous media using multirate mass transfer models for sorption and desorption. Water Resour. Res., 38(11): 1248.

Lee, E.J., Kim, M., Kim, Y., Lee, K.-K., 2009. Numerical and field investigation of enhanced *in situ* denitrification in a shallow-zone well-to-well recirculation system. Ecol. Modell., 220(19): 2441-2449.

Lee, M.-S., Lee, K.-K., Hyun, Y., Clement, T.P., Hamilton, D., 2006. Nitrogen transformation and transport modeling in groundwater aquifers. Ecol. Modell., 192(1–2): 143-159.

Li, L., Benson, C.H., Lawson, E.M., 2006. Modeling porosity reductions caused by mineral fouling in continuous-wall permeable reactive barriers. J. Contam. Hydrol., 83(1–2): 89-121.

Liu, C., Zachara, J.M., Qafoku, N.P., Wang, Z., 2008. Scale-dependent desorption of uranium from contaminated subsurface sediments. Water Resour. Res., 44(8): W08413.

Lutz, S.R., van Meerveld, H.J., Waterloo, M.J., Broers, H.P., van Breukelen, B.M., 2013. A model-based assessment of the potential use of compound-specific stable isotope analysis in river monitoring of diffuse pesticide pollution. Hydrol. Earth Syst. Sci., 17(11): 4505-4524.

MacQuarrie, K.T.B., Sudicky, E.A., 2001. Multicomponent simulation of wastewater-derived nitrogen and carbon in shallow unconfined aquifers: I. Model formulation and performance. J. Contami. Hydrol., 47(1): 53-84.

MacQuarrie, K.T.B., Sudicky, E.A., Robertson, W.D., 2001. Numerical simulation of a fine-grained denitrification layer for removing septic system nitrate from shallow groundwater. J. Contam. Hydrol., 52(1–4): 29-55.

Mastrocicco, M., Colombani, N., Salemi, E., Castaldell, G., 2011. Reactive modelling of denitrification in soils with natural and depleted organic matter. Water, Air, Soil Pollut., 222(1-4): 10.

Matott, L.S., Rabideau, A.J., 2008. Calibration of subsurface batch and reactive-transport models involving complex biogeochemical processes. Adv. Water Resour., 31(2): 269-286.

Matějů, V., Čižinská, S., Krejčí, J., Janoch, T., 1992. Biological water denitrification—A review. Enzyme and Microbial Technology, 14(3): 170-183.

McAdam, E.J., Judd, S.J., 2007. Denitrification from drinking water using a membrane bioreactor: Chemical and biochemical feasibility. Water Res., 41(18): 4242-4250.

McCarty, P.L., 1975. Stoichiometry of biological rates. Prog. Water. Technol., 7(1): 157-172.

McMahon, P.B., Dennehy, K.F., Sandstrom, M.W., 1999. Hydraulic and geochemical performance of a permeable reactive barrier containing zero-valent iron, Denver Federal Center. Ground Water, 37(3): 396-404.

Meier, P.M., Carrera, J., Sánchez-Vila, X., 1998. An evaluation of Jacob's Method for the interpretation of pumping tests in heterogeneous formations. Water Resour. Res., 34(5): 1011-1025.

Melander, L., Saunders, W.H., 1980. Reaction rates of isotopic molecules, New York, 331 pp.

Mengis, M. et al., 1999. Multiple Geochemical and Isotopic Approaches for Assessing Ground Water NO_3^- Elimination in a Riparian Zone. Ground Water, 37(3): 448-457.

Mengis, M., Walther, U., Bernasconi, S.M., Wehrli, B., 2001. Limitations of Using $\delta^{18}O$ for the Source Identification of Nitrate in Agricultural Soils. Environ. Sci. Technol., 35(9): 1840-1844.

Menkouchi Sahli, M.A. et al., 2006. Technical optimization of nitrate removal for groundwater by ED using a pilot plant. Desalination, 189(1–3): 200-208.

Mercado, A., Lbhaber, M., Soares, I.M., 1988. *In situ* biological groundwater denitrification: concepts and preliminary field tests. Water Sci. Technol., 20(3): 12.

Mook, W.G., 2000. Environmental isotopes in the hydrological cycle. Principles and applications. Volume I. Introduction: Theory, Methods, Review, UNESCO/IAEA, Vienna.

Nagpal, S., Chuichulcherm, S., Livingston, A., Peeva, L., 2000. Ethanol utilization by sulfate-reducing bacteria: An experimental and modeling study. Biotechnol. Bioeng., 70(5): 533-543.

Noiriel, C., Steefel, C.I., Yang, L., Ajo-Franklin, J., 2012. Upscaling calcium carbonate precipitation rates from pore to continuum scale. Chem. Geol., 318–319(0): 60-74.

Oenema, O. et al., 1998. Leaching of nitrate from agriculture to groundwater: the effect of policies and measures in the Netherlands. Environ. Pollut., 102(1, Supplement 1): 471-478.

Organisation for Economic Co-operation and Development, O., 2008. Environmental performance of agriculture in OECD countries since 1990.

Orozco, A.M.F., Contreras, E.M., Zaritzky, N.E., 2010. Cr(Vi) reduction capacity of activated sludge as affected by nitrogen and carbon sources, microbial acclimation and cell multiplication. J. Hazard. Mater., 176(1–3): 657-665.

Otero, N., Torrentó, C., Soler, A., Menció, A., Mas-Pla, J., 2009. Monitoring groundwater nitrate attenuation in a regional system coupling hydrogeology with multi-isotopic methods: The case of Plana de Vic (Osona, Spain). Agr. Ecosyst. Environ., 133(1–2): 103-113.

Palandri, J.L., Kharaka, Y.K., 2004. A compilation of rate parameters of water-mineral interaction kinetics interaction for application to geochemical modeling, U.S. GEOLOGICAL SURVEY.

Parkhurst, D.L., Appelo, C.A.J., 1999. User's guide to PHREEQC (version 2) - a computer program for speciation, reaction-path, 1D-transport, and inverse geochemical calculations., U.S. GEOLOGICAL SURVEY.

Parkhurst, D.L., Kipp, K.L., Charlton, S.R., 2010. PHAST Version 2—A program for simulating groundwater flow, solute transport, and multicomponent geochemical reactions.

Peyton, B.M., 1996. Improved biomass distribution using pulsed injections of electron donor and acceptor. Water Res., 30(3): 756-758.

Pirt, S.J., 1965. The maintenance energy of bacteria in growing cultures. Proc. R. Soc. Lond. B. Biol. Sci., 163(991): 224-31.

Porges, N., Jasewicz, L., Hoover, S., 1956. Principles of biological oxidation. In biological treatment of sewage and industrial wastes. Reinhold. Publ., New York.

Prommer, H., Post, V., 2010. A reactive multicomponent transport model for saturated porous media. User's Manual. v2.10.

Puig, R., Folch, A., Menció, A., Soler, A., Mas-Pla, J., 2013. Multi-isotopic study (^{15}N, ^{34}S, ^{18}O, ^{13}C) to identify processes affecting nitrate and sulfate in response to local and regional groundwater mixing in a large-scale flow system. Appl. Geochem., 32(0): 129-141.

Reddy, K.J., Lin, J., 2000. Nitrate removal from groundwater using catalytic reduction. Water Res., 34(3): 995-1001.

Ricardo, A.R., Carvalho, G., Velizarov, S., Crespo, J.G., Reis, M.A.M., 2012. Kinetics of nitrate and perchlorate removal and biofilm stratification in an ion exchange membrane bioreactor. Water Res., 46(14): 4556-4568.

Richard, Y.R., 1989. Operating Experiences of Full-Scale Biological and Ion-Exchange Denitrification Plants in France. Water Environ. J., 3(2): 154-167.

Rittmann, B.E., 1993. The significance of biofilms in porous media. Water Resour. Res., 29(7): 2195-2202.

Rittmann, B.E., McCarty, P.L., 2001. Environmental biotechnology : principles and applications. McGraw-Hill, cop. 2001.

Rivett, M.O., Buss, S.R., Morgan, P., Smith, J.W.N., Bemment, C.D., 2008. Nitrate attenuation in groundwater: A review of biogeochemical controlling processes. Water Res., 42(16): 4215-4232.

Robertson, W.D., Blowes, D.W., Ptacek, C.J., Cherry, J.A., 2000. Long-term performance of *in situ* reactive barriers for nitrate remediation. Ground Water, 38(5): 689-695.

Robertson, W.D., Cherry, J.A., 1997. Long-tern performance of the Waterloo denitrification barrier. Land Contamination and Reclamation, 5(3): 5.

Rodríguez-Escales, P., Folch, A., Vidal-Gavilan, G., van Breukelen, B., 2014a. Modelling biogeochemical processes and isotope fractionation of enhanced *in situ* biodenitrification in a fractured aquifer. Submitted to Water Research.

Rodríguez-Escales, P., van Breukelen, B., Vidal-Gavilan, G., Soler, A., Folch, A., 2014b. Integrated modeling of biogeochemical reactions and associated isotope fractionations at batch scale: A tool to monitor enhanced biodenitrification applications. Chem. Geol., 365(0): 20-29.

Rust, C.M., Aelion, C.M., Flora, J.R.V., 2000. Control of pH during denitrification in subsurface sediment microcosms using encapsulated phosphate buffer. Water Res., 34(5): 1447-1454.

Saitoh, S., Iwasaki, K., Yagi, O., 2003. Development of a most-probable-number method for enumerating denitrifying bacteria by using 96-well microtiter plates and an anaerobic culture system. Microbes Environ., 18(4): 210-215.

Sauty, J.-P., 1980. An analysis of hydrodispersive transfer in aquifers. Water Resour. Res., 16(1): 145-158.

Schepers, J.S., Varvel, G.E., Watts, D.G., 1995. Nitrogen and water management strategies to reduce nitrate leaching under irrigated maize. J. Contam. Hydrol., 20(3–4): 227-239.

Schipper, L.A., Barkle, G.F., Hadfield, J.C., Vojvodic-Vukovic, M., Burgess, C.P., 2004. Hydraulic constraints on the performance of a groundwater denitrification wall for nitrate removal from shallow groundwater. J. Contam. Hydrol., 69(3–4): 263-279.

Schipper, L.A., Vojvodic-Vukovic, M., 2001. Five years of nitrate removal, denitrification and carbon dynamics in a denitrification wall. Water Res., 35(14): 3473-7.

Schipper, L.A., Vojvodić-Vuković, M., 2000. Nitrate removal from groundwater and denitrification rates in a porous treatment wall amended with sawdust. Ecol. Eng., 14(3): 269-278.

Schnobrich, M.R., Chaplin, B.P., Semmens, M.J., Novak, P.J., 2007. Stimulating hydrogenotrophic denitrification in simulated groundwater containing high dissolved oxygen and nitrate concentrations. Water Res., 41(9): 1869-1876.

Schoeman, J.J., Steyn, A., 2003. Nitrate removal with reverse osmosis in a rural area in South Africa. Desalination, 155(1): 15-26.

Seifert, D., Engesgaard, P., 2007. Use of tracer tests to investigate changes in flow and transport properties due to bioclogging of porous media. J. Contam. Hydrol., 93(1–4): 58-71.

Semprini, L., Roberts, P.V., Hopkins, G.D., McCarty, P.L., 1990. A field evaluation of *in-situ* biodegradation of chlorinated ethenes: Part 2, results of biostimulation and biotransformation experiments. Ground Water, 28(5): 715-727.

Seymour, J.D., Gage, J.P., Codd, S.L., Gerlach, R., 2004. Anomalous fluid transport in porous media induced by biofilm growth. Phys. Rev. Lett., 93(19): 198103.

Shahbazi, P., Vaezi, F., Mahvi, A.H., Naddaffi, K., Rahmani, A.R., 2010. Nitrate removal from drinking water by point of use ion exchange. J. Res. Health Sci., 10(2): 91-7.

Sharp, R.R., Cunningham, A.B., Komlos, J., Billmayer, J., 1999. Observation of thick biofilm accumulation and structure in porous media and corresponding hydrodynamic and mass transfer effects. Water Sci. Technol., 39(7): 195-201.

Smith, R.L., Miller, D.N., Brooks, M.H., Widdowson, M.A., Killingstad, M.W., 2001. *In situ* stimulation of groundwater denitrification with formate to remediate. Environ. Sci. Technol., 35(1): 196-203.

Soares, M., Braester, C., Belkin, S., Abeliovich, A., 1991. Denitrification in laboratory sand columns: Carbon regime, gas accumulation and hydraulic properties. Water Res., 25(3): 325-332.

Soares, M.I.M., 2000. Biological denitrification of groundwater. Water Air Soil Poll, 123(1-4): 183-193.

Soares, M.I.M., Belkin, S., Abeliovich, A., 1989. Clogging of microbial denitrification sand columns - gas- bubbles or biomass accumulation. Zeitschrift Fur Wasser Und Abwasser Forschung-Journal for Water and Wastewater Research, 22(1): 20-24.

Spalding, R.F., Exner, M.E., 1993. Occurrence of nitrate in groundwater—A Review. J. Environ. Qual.(3): 392-402.

Steefel, C.I., DePaolo, D.J., Lichtner, P.C., 2005. Reactive transport modeling: An essential tool and a new research approach for the Earth sciences. Earth Planet. Sc. Lett., 240(3–4): 539-558.

Straub, K.L., Benz, M., Schink, B., Widdel, F., 1996. Anaerobic, nitrate-dependent microbial oxidation of ferrous iron. App. Environ. Microbiol., 62(4): 1458-1460.

Stuart, M.E., Gooddy, D.C., Bloomfield, J.P., Williams, A.T., 2011. A review of the impact of climate change on future nitrate concentrations in groundwater of the UK. Sci. Total Environ., 409(15): 2859-2873.

Sánchez-Vila, X., Carrera, J., Girardi, J.P., 1996. Scale effects in transmissivity. J. Hydrol., 183(1–2): 1-22.

Tang, G. et al., 2013. U(VI) Bioreduction with emulsified vegetable oil as the electron donor – model application to a field test. Environ. Sci. Technol., 47(7): 3218-3225.

Tartakovsky, B., Millette, D., Delisle, S., Guiot, S.R., 2002. Ethanol-sitimulated bioremediation of nitrate-contaminated grounwater. Ground Water Monit. R., 22(1): 9.

Taylor, S.W., Jaffé, P.R., 1990. Biofilm growth and the related changes in the physical properties of a porous medium: 3. Dispersivity and model verification. Water Resour. Res., 26(9): 2171-2180.

Taylor, S.W., Milly, P.C.D., Jaffé, P.R., 1990. Biofilm growth and the related changes in the physical properties of a porous medium: 2. Permeability. Water Resour. Res., 26(9): 2161-2169.

Thullner, M., 2010. Comparison of bioclogging effects in saturated porous media within one- and two-dimensional flow systems. Ecol. Eng., 36(2): 176-196.

Thullner, M., Kampara, M., Richnow, H.H., Harms, H., Wick, L.Y., 2008. Impact of bioavailability restrictions on microbially induced stable isotope fractionation. 1. Theoretical calculation. Environ. Sci. Technol., 42(17): 6544-6551.

Tong, Y., He, Z., 2013. Nitrate removal from groundwater driven by electricity generation and heterotrophic denitrification in a bioelectrochemical system. J. Hazard. Mater., 262(0): 614-619.

Toride, N., Leij, F.J., van Genuchten, M.T., 1999. The CXTFIT code for estimating transport parameters from laboratory or field tracer experiments.

Torrentó, C. et al., 2011. Enhanced denitrification in groundwater and sediments from a nitrate-contaminated aquifer after addition of pyrite. Chem. Geology., 287(1–2): 90-101.

UN, 1996. Country Population Statistics and Projections 1950–2050, Report.

UN, 2004. World Population to 2300.

USEPA, 2013. Wastewater treatment fact sheet: external carbon sources for nitrogen removal. In: Agency, U.S.E.P. (Editor).

van Breukelen, B.M., 2007. Quantifying the degradation and dilution contribution to natural attenuation of contaminants by means of an open system rayleigh equation. Environ. Sci. Technol., 41(14): 4980-4985.

van Breukelen, B.M., Griffioen, J., Röling, W.F.M., van Verseveld, H.W., 2004. Reactive transport modelling of biogeochemical processes and carbon isotope geochemistry inside a landfill leachate plume. J. Contam. Hydrol., 70(3–4): 249-269.

van Breukelen, B.M., Prommer, H., 2008. Beyond the Rayleigh equation: Reactive Transport Modeling of isotope fractionation effects to improve quantification of biodegradation. Environ. Sci. Technol., 42(7): 2457-2463.

van Breukelen, B.M., Rolle, M., 2012. Transverse hydrodynamic dispersion effects on isotope signals in groundwater chlorinated solvents' plumes. Environ. Sci. Technol., 46(14): 7700-7708.

van Rijn, J., Tal, Y., Barak, Y., 1996. Influence of volatile fatty acids on nitrite accumulation by a *Pseudomonas*. Appl. Environ. Microbiol., 62(7): 2615-20.

VanBriesen, J., 2002. Evaluation of methods to predict bacterialyield using thermodynamics. Biodegradation, 13(3): 171-190.

Vandenbohede, A., Louwyck, A., Lebbe, L., 2008. Identification and reliability of microbial aerobic respiration and denitrification kinetics using a single-well push–pull field test. J. Contam. Hydrol., 95(1–2): 42-56.

Vandevivere, P., Baveye, P., 1992. Saturated hydraulic conductivity reduction caused by aerobic bacteria in sand columns. Soil Sci. Soc. Am. J.(1): 1-13.

Vavilin, V.A., 2013. Estimating changes of isotopic fractionation based on chemical kinetics and microbial dynamics during anaerobic methane oxidation: apparent zero- and first-order kinetics at high and low initial methane concentrations. Antonie van Leeuwenhoek, 103(2): 375-383.

Veraart, A.J. et al., 2014. Denitrification in restored and unrestored Danish streams. Ecol. Eng., 66(0): 129-140.

Vidal-Gavilan, G., Carrey, R., Solanas, A.M., Soler, A., 2014. Feeding strategies for groundwater enhanced biodenitrification: chemical, microbiological and isotopic assessment of a 1D-flow-through experiment. Submitted to Science of the Total Environment.

Vidal-Gavilan, G., Folch, A., Otero, N., Solanas, A.M., Soler, A., 2013. Isotope characterization of an in situ biodenitrification pilot-test in a fractured aquifer. Appl. Geochem., 32(0): 153-163.

Vitoria, L., Otero, N., Soler, A., Canals, À., 2004. Fertilizer characterization: Isotopic Data (N, S, O, C, and Sr). Environ. Sci. Technol., 38(12): 3254-3262.

Volkmer, B.G. et al., 2005. Influence of nitrate levels in drinking water on urological malignancies: a community-based cohort study. Br. J. Urol. Int., 95(7): 972-976.

Volokita, M., Abehovich, A., Soares, M.I.M., 1996. Denitrification of groundwater using cotton as energy source. Water Sci. .Technol., 34(1–2): 379-385.

Wakida, F.T., Lerner, D.N., 2005. Non-agricultural sources of groundwater nitrate: a review and case study. Water Res., 39(1): 3-16.

Walton, G., 1951. Survey of literature relating to infant methemoglobinemia due to nitrate-contaminted water. Am J Public Health Nations Health., 41: 10.

Ward, M.H. et al., 2005. Workgroup report: Drinking-water nitrate and health--recent findings and research needs. Environ. Health Perspect., 113(11): 1607-14.

White, D., 2000. The Physiology and biochemistry of prokaryotes, New York [etc.] : Oxford University Press.

WHO, 2010. Ingested nitrate and nitrite and cyanobacterial peptide toxins.

Willmann, M., Carrera, J., Sanchez-Vila, X., Silva, O., Dentz, M., 2010. Coupling of mass transfer and reactive transport for nonlinear reactions in heterogeneous media. Water Resour. Res., 46(7): W07512.

Xu, M., Eckstein, Y., 1995. Use of weighted least-squares method in evaluation of the relationship between dispersivity and field scale. Ground Water, 33(6): 905-908.

Zhang, J. et al., 2014. Effect of phosphate rock on denitrification in a nitrate-polluted groundwater remediation system. Desalination and Water Treatment: 1-11.

Zhang, Y., Angelidaki, I., 2013. A new method for *in situ* nitrate removal from groundwater using submerged microbial desalination–denitrification cell (SMDDC). Water Res., 47(5): 1827-1836.

Zheng, C., Wang, P.P., 1999. MT3DMS: A modular three-dimensional multispecies model for simulation of advection, dispersion and chemical reactions of contaminants in groundwater systems. Documentation and User's Guide, Contract Reo. SERDP-99-41. U.S. Army Eng. Res. and Dev. Cent., Vicksburg, Miss.

Zhou, Q., Liu, H.H., Molz, F.J., Zhang, Y., Bodvarsson, G.S., 2007. Field-scale effective matrix diffusion coefficient for fractured rock: results from literature survey, J. Contam. Hydrol., Netherlands, pp. 161-87.

Zumft, W.G., 1997. Cell biology and molecular basis of denitrification. Microbiol. Mol. Biol. Rev., 61(4): 533-616.

APPENDIX 1

Table of selected models with parameters and their values

Table A. 1. Selection of models of EIB and natural attenuation of nitrate with the processes considered and the involved parameters including their values.

	Source	Aquifer type	Processes considered	Electron donor used	Parameters					
					Y_h (mol C-cel mol C-OC^{-1})	Q (mol C-OC-mol nitrate^{-1})	K_{max} Mol C-OC mol C-cell^{-1} d^{-1}	b d^{-1}	K_{satoc} mol C-OC l^{-1}	$K_{sat,\,nit}$ mol nitrate l^{-1}
BATCH	Calderer (2010)	-	Aerobic respiration Nitrate respiration Microbial growth and decay	Glucose	0.48	2.84	10.20	0.44	6.2×10^{-4}	3.6×10^{-5}
BATCH	Mastrocicco (2011)	-	Nitrate respiration Microbial growth and decay	Acetate	0.35	1.25	0.05	-	1×10^{-3}	1×10^{-4}
BATCH	Killingstad et al. (2002)	-		Natural organic matter	0.19	-	7.36	0.01	2.2×10^{-5}	1.4×10^{-5}
BATCH	Kornaros and Lyberatos (1998)	-	Aerobic respiration Nitrate respiration Microbial growth and decay	Glutamate	0.61	1.05	3.93	-	2.5×10^{-4}	5.5×10^{-5}
COLUMN	Clement et al. (1997)	-	Nitrate respiration Microbial growth and decay	Acetate	0.20	0.96	4.63	0.06	4.1×10^{-5}	1.1×10^{-5}
FIELD	Killingstad et al. (2002)	Sedimentary			0.19	-	3.42	0.01	2.2×10^{-5}	1.4×10^{-5}
FIELD	Lee et al. (2009)	Sedimentary	Nitrate respiration Microbial growth and decay	Natural organic matter			11.11	0.06	1.7×10^{-4}	1.2×10^{-5}
FIELD	Chen and MacQuarrie (2004)	Sedimentary	Nitrate respiration Geochemical interaction Isotope geochemistry	Natural organic matter	0.05	-	10	0	8.3×10^{-6}	1.6×10^{-6}
FIELD	Kinzelbach et al. (1991)	Sedimentary	Nitrate respiration Microbial growth and decay	Hydrocarbon (aliphatic and aromatic)	0.2	-	20	0.2	4.2×10^{-5}	3.2×10^{-6}
				RANGE	**(0.05-0.61)**	**(0.96-2.84)**	**(0.05-20)**	**(0-0.44)**	**(8.3×10^{-6}-1×10^{-3})**	**(1×10^{-4} - 1.6×10^{-6})**

APPENDIX 2.1

Carrey, R.; **Rodríguez-Escales P.;** Otero, N.; Ayora, C.; Soler, A.; Gómez-Alday, J.J. (2014). Nitrate attenuation potential of hypersaline lake sediments in central Spain: Flow-through and batch experiments.

APPENDIX 2.2

Rodríguez-Escales P.; Sayara T.; Vicent T.; Folch A. (2012). Influence of Soil Granulometry on Pyrene Desorption in Groundwater Using Surfactants. Water, Air, &Soil Pollution 223: 125-123. DOI:10.1007/s11270-011-0844-3

APPENDIX 2.3

Rodríguez-Escales P.; Borràs E.; Sarrà M.; Folch A. (2013). Effect of soil granulometry and the type of surfactant on desorption of a PAH mixture and its biodegradation by *Trametes versicolor*. Water, Air, & Soil Pollution 224 (2). DOI: 10.007/s11270-012-1422-z

APPENDIX 3

List of contributions to scientific meetings

CONFERENCE: **EGU**
TITLE: Integrated modeling of Enhanced *in situ* Biodenitrification in a fractured
aquifer: biogeochemistry and isotope geochemistry.
AUTHORS: **Rodríguez-Escales P;** van Breukelen B. M; Vidal-Gavilan G; Soler A.; Folch A
TYPE OF PRESENTATION: Poster
PUBLICATION: Abstract
PLACE AND DATE: Vienna (Austria), April 2014

CONFERENCE: **Applied Isotope Geochemistry 10 (AIG-10)**
TITLE: Biogeochemical and isotopical fractionation models: a tool for control
Enhanced *in situ* Biodenitrification.
AUTHORS: **Rodríguez-Escales P;** van Breukelen B. M; Vidal-Gavilan G.; Soler A.; Folch A
TYPE OF PRESENTATION: Poster
PUBLICATION: Abstract
PLACE AND DATE: Budapest (Hungary), September 2013

CONFERENCE: **Goldschmidt**
TITLE: Modeling of Enhanced *in situ* Biodenitrification in fractured aquifer:
biogeochemical interactions and isotope fractionation.
AUTHORS: **Rodríguez-Escales P;** van Breukelen B. M; Vidal-Gavilan G.; Soler A.; Folch A
TYPE OF PRESENTATION: Oral Presentation

PUBLICATION: Abstract
PLACE AND DATE: Firenze (Italy), August 2013

CONFERENCE: **12th International UFZ-Deltares Conference on Groundwater-Soil-Systems and Water Resource Management. Aqua-Consoil 2013.**
TITLE: Biogeochemical and isotopical fractioantion models: a tool for control Enhanced *in situ* Biodenitrificaction applications.
AUTHORS: **Rodríguez-Escales P;** van Breukelen B. M; Vidal-Gavilan G.; Soler A.; Folch A
TYPE OF PRESENTATION: Oral Presentation
PUBLICATION: Abstract
PLACE AND DATE: Barcelona (Spain), April 2013

CONFERENCE: **12th International UFZ-Deltares Conference on Groundwater-Soil-Systems and Water Resource Management. Aqua-Consoil 2013.**
TITLE: Desorption and biodegradation of PAHs in soil and groundwater: granulometry and surfactants as a key control parameters.
AUTHORS: Vicent T.; **Rodríguez-Escales P.;** Borràs E.; Sarrà M.; Folch A.
TYPE OF PRESENTATION: Poster
PUBLICATION: Proceeding
PLACE AND DATE: Barcelona (Spain), April 2013

CONFERENCE: **5th European Conference on Permeable Reactive Barriers & Reactive Zones (PRB/RZ-2012)**
TITLE: Modeling biological, geochemical and isotopic processes during enhanced denitrification using two different sources of organic carbon in batch experiments.
AUTHORS: **Rodríguez-Escales P;** van Breukelen B. M; Vidal-Gavilan G; Soler A.; Folch A.
TYPE OF PRESENTATION: Oral presentation
PUBLICATION: Abstract
PLACE AND DATE: Barcelona (Spain), September 2012

CONFERENCE: **5th European Conference on Permeable Reactive Barriers & Reactive Zones (PRB/RZ-2012)**
TITLE: How granulometry and surfactants affect desorption and biodegradation (*T. Versicolor*) of PAHs in soil and groundwater
AUTHORS: **Rodríguez-Escales P.;** Borràs E.; Vicent T.; Sarrà M.; Folch A.
TYPE OF PRESENTATION: Poster
PUBLICATION: Abstract
PLACE AND DATE: Barcelona (Spain), September 2012